EXPERIMENTAL ASSESSMENT AND NUMERICAL VALIDATION OF THE THERMAL PERFORMANCE OF CONCRETE WALLS

BY

WALEED AHMED YASLAM AL-AWSH

A Thesis Presented to the

DEANSHIP OF GRADUATE STUDIES

KING FAHD UNIVERSITY OF PETROLEUM & MINERALS

DHAHRAN, SAUDI ARABIA

In Partial Fulfillment of the
Requirements for the Degree of

MASTER OF SCIENCE

In

CIVIL ENGINEERING

April 2019

KING FAHD UNIVERSITY OF PETROLEUM & MINERALS

DHAHRAN 31261, SAUDI ARABIA

DEANSHIP OF GRADUATE STUDIES

This thesis, written by **WALEED AHMED YASLAM ALAWSH** under the direction of his thesis advisor and approved by his thesis committee, has been presented and accepted by the Dean of Graduate Studies, in partial fulfillment of the requirements for the degree of **MASTER OF SCIENCE IN CIVIL ENGINEERING.**

Prof. Omar S. Baghabra Al-Amoudi
(Advisor)

Dr. Mohammed A. Al-Osta
(Co-Advisor)

Dr. Salah U. Al-Dulaijan
Department Chairman

Dr. Tawfik A. Saleh
(Member)

Prof. Salam A. Zummo
Dean, Graduate Studies

Prof. Mohammed Maslehuddin
(Member)

17/6/2019
Date

Dr. Salah U. Al-Dulaijan
(Member)

This humble work is dedicated to:

My parents, brothers, sisters, wife and son

for their support

ACKNOWLEDGMENTS

All praise be to Allah, SubhaanaHu wata'aala, for giving me the chance, patience, health and knowledge, to complete this work with success.

My heartfelt gratitude is given to my beloved parents, brothers, sisters, wife and son, who always supported me with their love, patience and constant prayers. May Allah bless them and give them Paradise.

I would like to express my gratitude to King Fahd University of Petroleum & Minerals and the Department of Civil and Environmental Engineering for providing me the opportunity to pursue my master degree. Special thanks are directed to my thesis advisor, Prof. Omar S. Baghabra Al-Amoudi, for his tremendous effort, help and feedback during my research period. I express my deepest thank to my co-advisor, Dr. Mohammed Al-Osta, for his extensive guidance during my MS research. Also, I appreciate the support of my committee members, Dr. Tawfik Saleh, Prof. Mohammed Maslehuddin and Dr. Salah Al-Dulaijan, for their guidance, motivation and help during my thesis.

Further, I would like to thank the Saudi Readymix Concrete Company, Arab Recycling Company Ltd., Saudi Rubber Products Co. and the Advanced Concrete Products, Ltd., for providing all the necessary materials during the experimental work.

Special thanks and appreciation are to Dr. Naef Qasem for helping me in the Fluent software and his continuous support during my modeling part in this research.

I would like to thank my KFUPM and Hadhrami colleagues at KFUPM for their motivation, friendship and help. May Allah bless them and reward them Paradise. I am grateful for my colleague, Ahmed Al-Tamimi, for extending his MSc. thesis work.

I would like to extend my appreciation to Sheikh Eng. Abduallah Ahmed Bugshan and Hadhramout Establishment for Human Development for providing me a scholarship to complete my MS degree at KFUPM. May Allah bless them and support their initiatives.

TABLE OF CONTENTS

LIST OF TABLES

LIST OF FIGURES

LIST OF ABBREVIATIONS

A: Surface area of the main heater, m^2.

AR: Aspect ratio.

BC: Boundary condition.

C: Control block.

CA: Coarse aggregate.

°C: Degrees in centigrade (Celsius).

d_d: Thickness of dummy specimen, m.

d_b: Thickness of test specimen, m.

EPS: Expanded polystyrene.

FA: Fine aggregate.

HB: Hollow block.

HR: Hollow ratio.

I: Main heater current, mA.

K_p: Thermal conductivity of dummy sample (W/m.K).

K_b: Thermal conductivity of masonry block sample (W/m.K).

°K: Degrees in Kelvin.

LDPE Low-density polyethylene.

N: Correction factor of the instrument.

PL: Perlite.

Q: Total Heat flow in main heater, W.

Q_1: Heat flow through dummy sample, W.

Q_2: Heat flow through test sample, W.

RU: Crumb tires rubber.

SP: Super-plasticizer.

T_i: Average interior surface temperature of hollow block, °C.

$T_{h,d}$: Heated surface of dummy sample, °C.

$T_{c,d}$: Cold surface of dummy specimen, °C.

$T_{h,b}$: Heated surface of masonry block specimen, °C.

$T_{c,b}$: Cold surface of masonry block specimen, °C.

V: Main heater voltage, mV.

V_{cube}: Volume of cube, m^3.

W_d: Oven-dry weight of specimen, kg.

W_s: Saturated weight of specimen, kg.

ABSTRACT

Full Name: Waleed Ahmed Yaslam Alawsh

Thesis Title: Experimental Assessment and Numerical Validation of The Thermal Performance of Concrete Walls

Major Field: Civil Engineering - Structures

Date of Degree: April 2019

The main objective of this research was to produce concrete walls (blocks, mortar and plaster) that could reduce the heat transfer through the exterior building walls in order to minimize the electricity consumption by reducing the air conditioning demand. Therefore, new medium-weight concrete blocks with low thermal conductivity and acceptable compressive strength were manufactured using the following four insulated materials: Recycled low density polyethylene (LDPE), expanded polystyrene beads (EPS), vermiculite (VL) and volcanic scoria aggregate (VS) that are cheap and available in the Saudi market. In addition, three types of insulation mortar and plaster were produced using crushed crumb-rubber (RU), perlite powder (PL) and vermiculite (VL). Furthermore, finite element modelling (FEM) was developed using ANSYS package to verify the experimental test of Guarded Hot Plate (ASTM C177) and demonstrate the compatibility between the numerical solution and experimental results. The model was also used to calculate the temperature change between the exterior and interior surfaces of the walls of the different blocks and insulation plaster and mortar types and the result were compared with the control masonry wall.

The experimental results were based on two criteria: Thermal conductivity (ASTM C177 and C518-04) and compressive strength (ASTM C129 and C270) for block and cement mortar, respectively. The results proved that the thermal conductivity of VS, EPS, LDPE

and VL blocks were reduced by about 26.1, 19.4, 17.0, and 16.7%, respectively, as compared to the control block. However, the results showed that the reduction in compressive strength was 51, 47, 39, and 37% for VS, VL, LDPE, and EPS blocks, respectively, as compared to the control block. For the mortar, the experimental results proved that the thermal conductivity of insulation mortar was reduced significantly by about 57, 47 and 36% for vermiculite, perlite and rubber, respectively, as compared to the control mortar. Further, the reduction in strength was 78, 63 and 36% for vermiculite, rubber and perlite, respectively, as compared to the control mortar. Although the reduction in strength was very high, none of the samples went beyond the threshold values of 3.45 and 5.40 MPa for block and mortar, respectively.

The data of Guarded Hot Plate were analyzed and validated using FEM (Fluent package in ANSYS workbench). The agreement between the experimental data and the modeling results was in the range of the accuracy error, which may be considered as an excellent validation. The optimal wall (VL block plus 15% VL mortar and plaster) improved the thermal resistance by about 290% when compared to the conventional concrete blocks. This improvement could reduce the energy consumption from 118.43 to 30.35 KWh/m^2 (about 3.9 times of reduction) annually. This optimal wall is proposed to be used in the domestic (private) and industrial and public buildings instead of the traditional walls.

ملخص الرسالة

الاسم الكامل: وليد أحمد يسلم العوش

عنوان الرسالة: التقييم التجريبي والتحقق العددي للأداء الحراري للجدران الخرسانية

التخصص: هندسة مدنية – انشاءات

تاريخ الدرجة العلمية: أبريل 2019

يهدف هذا البحث إلى إنشاء حائط خرساني (طوب ومونة ولياسة إسمنتية) يمكنه تقليل انتقال الحرارة من أجل تقليل استهلاك الكهرباء وذلك من خلال تقليل استخدام التكييف. ولذلك، تم تصنيع طوب خرساني بإضافة مواد بلاستيكية ثانوية ومعاد تدويرها والتي تعتبر خفيفة الوزن وذات موصلية حرارية منخفضة، وتقييم مدى كفاءة هذا الطوب مقارنةً مع الطوب الموجود في السوق المحلية. لذلك، تم استخدام أربعة أنواع من المواد لتصنيع هذا الطوب ذو الموصلية الحرارية المنخفضة وهي: حبات البوليسترين (EPS) ، والبولي ايثيلين منخفض الكثافة المعاد تدويره (PE) والفيرميكولايت (VL) والصخور البركانية (VS). وبالإضافة إلى ذلك، هنالك ثلاثة أنواع من المونة الاسمنتية تم إنتاجها باستخدام النفايات والمواد الرخيصة المتوفرة في أسواق المملكة العربية السعودية. وقد أُستخدم ثلاثة مواد ذات موصلية توصيلة حرارية منخفضة لأنتاج هذه الأنواع من المونة الاسمنتية العازلة وهي مسحوق الإطارات المطاطية (RU)، ومسحوق البيرلايت (PL) والفيرميكولايت (VL). علاوة على ذلك، تم تطوير نموذج محاكاة للواقع بإستخدام طريقة العناصر المحدودة (FEM) بإستخدام برنامج ANSYS لتقييم الاختبار التجريبي لجهاز صفيحة التسخين المحميَّة (Guarded Hot Plate) وأظهرت النتائج مدى التوافق الكبير بين الحل العددي والعمل التجريبي، بالأضافة إلى حساب مقدار التغير في درجة الحرارة بين السطح الخارجي والسطح الداخلي من الجدار الذي تم إنشائه باستخدام الطوب والمونة والليلسة ذات الموصلية الحرارية المنخفضة ومقارنة النتائج مع الجدار الأساسي والذي لايحتوي على أي مواد عازلة .

استندت النتائج التجريبية إلى معيارين أساسيين وهما: الموصلية الحرارية (ASTM C177 و C518) وقوة الضغط (ASTM C129 و C270) للطوب الخرساني والمونة الاسمنتية على التوالي. أثبتت النتائج أن الموصلية الحرارية للطوب VS و EPS و LDPE و VL تم خفضها بحوالي 26.1 و 19.4 و 17.0 و 16.7٪ على التوالي، مقارنة مع الطوب الخرساني التي لاتحتوي على اي مواد عازلة. كما أظهرت النتائج انخفاضاً كبيراً في قوة الضغط بمقدار 51 ، 47 ، 39 ، و 37٪ للطوب VS، VL، LDPE ، و EPS، على التوالي ، مقارنة مع الطوب العادي. أما بالنسبة للمونة الاسنتية، فأن التجارب أثبتت أن الموصلية الحرارية للمونة قد انخفضت بشكل ملحوظ بحوالي 57 و 47 و 36٪ بالنسبة للفيرموكولايت والبيرلايت والمطاط ،

على التوالي، مقارنة مع المونة الاصلية. وكان الانخفاض في القوة يقدر ب 78 و 63 و 36 ٪ للفيرميكولايت والمطاط والبيرلايت ، على التوالي ، مقارنة مع المونة الاصلية التي لاتحتوي على اي مواد عازلة. وعلى الرغم من أن الانخفاض في القوة كان كبيراً للغاية، إلا أن أياً من هذه العينات لم تتجاوز الحد الادنى من قوة الضغط المسموح بها وهي 3.45 MP للطوب الخرساني و 5.40 MPa للمونة الاسمنتية.

تم تحليل نتائج أختبار صفيحة التسخين المحمية والتحقق من صحتها بإستخدام برنامج محاكي للواقع (برنامج Fluent)، وكان هنالك توافقاً كبيراً بين النتائج التجريبية ونتائج المحاكاة وكان مقدار التباين بين القراءتين ضمن نطاق الخطأ المسموح به. وكان الجدار الأمثل في هذا البحث (طوب VS بالإضافة إلى المونة والليّاسة الاسمنتية التي تحتوي على 15% من الفيرموكيولايت) قد حسّن المقاومة الحرارية بحوالي 290٪ مقارنة بالكتل الخرسانية التقليدية. ويمكن أن تقلل هذه المقاومة الحرارية العالية من استهلاك الطاقة من 118.43 إلى 30.35 كيلو واط ساعة / م^2 (أي بحوالي 3.9 ضعفاً من التخفيض) سنويًا. ولذلك، يوصى إستخدام هذا الجدار في المنشآت العامة والخاصة بدلاً من الجدران التقليدية.

CHAPTER 1
INTRODUCTION

1.1 Overview

With the steady growth of population and increasing demand for energy in Saudi Arabia, the need to conserve energy is becoming more and more pressing and demanding. The excessive usage of electricity, in particular, represents a major concern, and the Saudi Energy Efficiency Center (known as KAFAA) has recently been established with the principal and strategic objective of regulating and reducing the consumption of energy [1].

Due to the prevailing hot and sometimes humid climate in most of the major cities in Saudi Arabia, air conditioning accounts for nearly three-quarters of the electricity consumption in residential buildings nationwide, and buildings, in general, consume three-quarters of all the energy generated within the country [2].

As in many other countries around the world, the population of Saudi Arabia (KSA) is growing steadily and its demand for energy is increasing. In KSA, the demand for electricity has been rising since 2000. The peak electricity demand increased from 20 GW in 2000 to 60 GW in 2017 and it is projected to exceed 70 GW by the year 2020 [3].

In December 2017, the Saudi Electricity Company has increased the tariff of electricity consumption for all categories of service from 0.12 SR/kwh to 0.25 SR/kwh on the average [4]. Although it still remains below the tariff for many other countries, the Saudi Electric Company spent at least SR 380 billions in investments during the period 2009-2017 to cover the electricity consumption [5].

The electricity consumption has been increased noticeably during the last decade. In last the five years, the building sector has consumed about 76% of the total electricity and the energy demand has increased by 10% annually [2]. Many coastal areas in Saudi Arabia can be very hot and humid especially during the summer months when the air day temperature may reach 45^{o}C or even higher [6]. Extremely hot climate combined with low energy tariff of the region are considered the main factors behind the growth of domestic electricity consumption due to air conditioning. For instance, the air conditioning consumes around 71% of the total electricity in the hot climate like Jeddah. For the milder climate like Abha, the electricity consumption for cooling estimates by about 40% of the total electricity consumption [2]. In Dammam, the air conditioning consumes around 67% of the total electricity consumption [2]. Other important factors such as increasing wealth, population growth, and energy efficiency are considered as minor factors for energy dissipation [3]. Therefore, the air-conditioning becomes compulsory to supply thermally comfortable indoor environment. Consequently, the electricity demand will increase.

The oil and natural gas resources are excessively consumed in the power stations in Saudi Arabia. In 2008, the total energy consumption of oil reached to about 800 million barrels and it is expected to be doubled in 2030 [5]. This excessive consumption will reduce the Saudi oil export to the world, which will negatively affect to the Saudi economy.

The ambient air temperature in some regions in Saudi Arabia could reach to 45°C during summer days and the exterior concrete surfaces of the building, such as the external wall and roof surfaces, could reach up to 80°C if they are directly exposed to sunlight [3,5]. If the exterior envelope temperature is 80°C and the desirable indoor temperature is 25°C, the temperature difference between the interior and exterior surfaces of the masonry

building is around 55°C. Because of this large difference in temperature, the consumption of electricity will be increased in order to provide a comfortable indoor air. Since fossil fuel is the main source for the energy generation in Saudi Arabia, the increased fuel consumption will certainly increase the air pollution due to the increase in the emission of CO_2. To reduce the electricity consumption, the air condition should be minimized by reducing the heat flow from outer to inner surfaces of the building. Since one-third of the energy loss occurs through the walls and one-third through the roof [9], double skin walls with insulating materials will contribute to some extent in decreasing the heat flow to the inside envelope but there is an urgent need to use insulation materials that will help reduce the energy consumption [10]. Therefore, the main goal of this research was to produce a new hollow concrete blocks with higher thermal resistance by using insulation materials in the concrete mix.

In order to maintain comfortable indoor temperatures while reducing the amount of electricity needed for air conditioning, information about the thermal properties and cost-effective building materials are necessary. Most of the thermal load is transferred through the building walls and constitutes a considerable proportion of the total thermal flow. Therefore, the choice of optimal building materials might considerably decrease this thermal transmission load and make it possible to cool the buildings using less energy, by keeping the temperature indoors low despite the intense heat outdoors.

The most common building material used in construction in Saudi Arabia is concrete in the form of blocks. Blocks that are hollow can be modified to tune their thermal conductivity, so that they have better thermal insulation properties and transmit less heat.

1.2 Motivation

This research was intended to investigate the thermal behavior and mechanical properties of normal and lightweight concrete blocks produced using cheaper insulation materials that are available in Saudi Arabia. As the main motivation for the research was to mitigate the sharp rise in energy and electricity consumption, the ultimate goal of this project was to develop guidelines for producing energy-saving and cost-effective concrete blocks for usage in the construction industry. This project would also develop new insulation mortar with low thermal conductivity by adding three type of recycling and by-product materials in the mix proportion. The results developed in this research would contribute to the development of new concrete blocks and mortar that have superior thermal insulation properties and can be used to construct a wide range of energy-efficient and sustainable structures in hot climates.

1.3 Objectives

The main objective of this research was to produce concrete blocks and mortar with lower thermal conductivity and self-weight using lightweight (LW) insulation materials with acceptable bearing strength.

The specific objectives of the proposed research were as follows:

1 Selecting the optimum dosage of the LW materials to produce insulation blocks and mortar;

2 Studying the thermal and mechanical properties of these blocks and compare the results with ASTM standards;

3 Examining the thermal and mechanical properties of the insulation mortar and compare the results with ASTM standards;

4 Developing a finite element model (using Fluent package in ANSYS workbench) to verify the experimental test results of Guarded Hot Plate instrument; and

5 Reporting appropriate recommendations for using the best type of insulation block and mortar based on modeling different walls using different insulated blocks and mortars.

1.4 Thesis Organization

This MS Thesis consists of six chapters. Each chapter in this thesis presents the details of the work done, including literature review, experimental work for blocks and mortars, and numerical work for FEM modelling. The thesis was structured as follows: CHAPTER 1 presents the introduction and motivation for the thesis and the main objectives. CHAPTER 2 reports the literature review that is related to this work. CHAPTER 3 presents the methodology and experimental program of this research. CHAPTER 4 presents the experimental results for insulation blocks and mortars in terms of compression, thermal conductivity, absorption and density tests and the results were summarized in charts and tables. In addition, the 33% improvement in reducing the heat transfer in walls (as a result of using the insulating blocks and mortar) is presented in CHAPTER 4. CHAPTER 5 reports the thermal performance of walls built using insulation hollow blocks and mortar (using ANSYS program) to select the best type. CHAPTER 6 concludes and summarizes all the findings and results of all chapters and gives recommendations for future work.

CHAPTER 2

LITERATURE REVIEW

The most common material used to construct building walls in eastern Saudi Arabia is concrete in the form of blocks, mortar and plaster. Concrete block can have either solid or hollow cores. The concrete blocks with hollow cores use less material and have lower total thermal conductivity than the solid ones thereby making them the preferred choice, both economically and environmentally, for the prevailing hot and humid climates. However, casting hollow concrete blocks is more demanding than casting solid blocks, and a more cost-effective way of reducing the thermal conductivity of concrete blocks is by introducing air gaps using lightweight aggregates [11]. The normal cement plaster may also reduce the heat flow from outer to inner envelope wall due to increasing the wall thickness which leads to increase the thermal resistance of masonry wall. Lightweight aggregates can be made of processed natural materials, processed by-products, or unprocessed materials [12]. When lightweight aggregates are used to make lightweight concrete or insulation mortar and plaster, the resulting blocks, mortars and plasters are less dense and give better thermal insulation, but they also display poorer mechanical properties [13].

In this chapter, the previous work which dealt with the insulation mortar, plaster and block, was displayed. Then, the literature for FEM modeling to evaluate the thermal performance was reported.

2.1 Cement Mortar with Insulation Materials

Several studies were conducted to enhance the insulation of buildings by reducing the thermal conductivity using different materials and techniques. Further, many researchers used vermiculite, perlite and rubber to produce thermally efficient mortars.

Zulkifeli and Saman [14] evaluated experimentally the effect of fire on perlite cement mortar. The sand was replaced by perlite with the contents of 10, 20, 30, and 40% by volume. The mortars were exposed to high temperatures of 200, 400, 700 and 1000°C. The compressive strength was reduced with increasing the perlite content, particularly for low temperature exposure, while the performance was improved in high temperature. This improvement could be due to the hydrothermal reaction of silica in perlite and sand due to the rising of temperature during hydration reaction [14, 15].

Lanzón & García-Ruiz [16] studied the influence of perlite on fresh and hardened state of cement mortar. Water absorption, workability and mechanical strength were reported. The outcomes indicated that the water absorption and mechanical strength were reduced, while the workable life increased from 2 h 31 min to 5 h 45 min.

Xu et al [17] produced a new type of rubber and perlite mortar modified by SBR latex and polyester. Thermal and mechanical properties were studied. The experimental results showed that the amount of rubber and perlite have a major influence on compressive strength and thermal conductivity. With increasing the rubber and perlite dosages, the compressive strength and thermal conductivity decreased. The reduction in compressive strength was 25-65%, as compared to the control mortar. The reduction of thermal conductivity was 6-12% and 30-35% for rubber and perlite, respectively.

Meshgin et al. [18] used recycled tires rubber as insulation material in cement mortar with additive materials. Two different sizes of rubber particles were used in four mix groups. The study indicated that adjusting the size of rubber particles had a slight effect on the mechanical and thermal properties. Two mix proportions with fine and course rubber were prepared. The resulted strengths were 6.93 and 7.55 MPa for fine and coarse rubber particles, respectively, at 28 days, while the k-values were 0.364 and 0.323 W/m.K.

Turgut and Yesilata [19] produced lightweight concrete blocks with low cost and good thermal performance by using a crumb rubber as a fine aggregate. The replacement ratio of sand and crumb rubber were taken as a volumetric ratio instead of weighted ratio because the crumb rubber has higher volume content compared to sand. The percentage of improvement of thermal insulation was 5-11% depending on the amount of rubber used.

Zukowski and Haese [20] studied the effectiveness of perforated masonry unit filled with perlite insulation material in reducing the heat transfer. The thermal properties of the sample block were evaluated from measurements and numerical simulation. The authors suggested using an equivalent heat capacity of 855.1 J/kg.K, equivalent heat conductivity of 0.09 W/m.K and equivalent density of 653.15 kg/m^3 for these building materials.

Budaiwi et al. [21] investigated the effect of temperature on thermal conductivity of several insulation materials used in Saudi Arabia. The most sensitive material for temperature was polyethylene while polystyrene was the least. In Dhahran, polyethylene exhibited 17% increase in thermal conductivity during the hot month of August.

Coz Dıaz et al.[22] studied the effect of different lightweight concrete blocks with three different mortar properties on thermal conductivity. The three mortar types had thermal

conductivity equal 1.4, 1, 0.3 W/m.K. Finite element model was used to find out the accurate solution of heat transfer equation for five different hollow concrete block walls. From the analysis, it was reported that when the thermal conductivity varied from 1.4 to 1 and 0.3 W/m.K, the equivalent thermal conductivity of wall could reduce from 327 to 320 and 305 W/m.K, respectively.

2.2 Concrete Masonry Blocks with Insulation Materials

During the last few decades, a significant amount of relevant research has been conducted on materials that can be used in concrete blocks. For example, based on experimental testing, Moufti et al. [23] investigated scoria from a quarry in Harrat Rahat, western Saudi Arabia, for industrial utilization. The results showed that the use of scoria as a heat-insulating material satisfied the ASTM C330 requirements for lightweight aggregate, absorption and alkalinity content. Therefore, scoria could be harnessed in the manufacturing of building blocks. It was concluded that the use of scoria in construction was essential to reduce the energy due to heating and air-conditioning.

Ling and Teo [24] studied the contribution of waste expanded polystyrene beads (EPS) and waste rice husk ash (RHA) on compressive strength, density, and water absorption in concrete blocks. Solid bricks of 21.5×10.25×6.5 cm were prepared in this work with different dosages of RHA and EPS. One dosage of EPS was replaced with fine aggregate by volume for all mixes, while different dosages of RHA (5, 10, 15, 20% by volume) were replaced with cement as a cementitious pozzolanic material. The results showed that the mix with 15% of RHA achieved the highest compressive strength with an increase of about 25%, as compared with a control mix.

Al-Hazmy [25] examined the most common masonry hollow blocks from a thermal point of view using Fluent software. Three types of masonry walls were studied with different configurations. The cavities were filled with air or polystyrene. The numerical results showed that cavities with air filled contributed significantly in reducing the thermal flow. Further, polystyrene bars decreased the heat transfer by 36%.

Al-Hadhrami and Ahmad [26] evaluated the thermal performance of eleven types of block walls used in Saudi Arabia (two of them were concrete blocks and others were clayey blocks). The two concrete walls built by hollow concrete blocks one with cavities filled by perlite and another with air. The thermal resistivity increased when hollow blocks were filled by perlite from 0.205 m^2.K/W to 0.409 m^2.K/W and the thermal conductivity was reduced from 0.976 W/m.K to 0.489 W/m.K.

Park and Chilsholm [27] studied the thermal conductivity of the concrete with polystyrene aggregate instead of normal aggregate. Six mix designs of concrete were made. Three of them were classified according to their density: 600 (P600), 800 (P800) and 1000 (P1000) kg/m^3, and the other three (PF600), (PF800) and (PF1000) were classified according to the amount of fly ash, which was used as an additive material to the mix for the same densities. The thermal conductivity of P600, PF600, P800, PF800, P1000 and PF1000 were obtained as 0.134, 0.132, 0.219, 0.216, 0.308 and 0.292 W/m.^{o}C, respectively. The results indicated that adding a fly ash to concrete had a small effect on thermal conductivity.

Yang et al. [28] developed a new type of the concrete hollow blocks to improve the thermal conductivity and impermeability of the walls. The block was made from cement, cobble or

crushed stone and sand. As reported by the authors, the new compound blocks tended to reduce the thermal conductivity and permeability.

Al-Jabri et al. [29] investigated the lightweight concrete block with insulation materials in the hot climate region. Polystyrene beads, vermiculite and cement kiln dust (CKD) were used to produce the blocks. Polystyrene and vermiculite were used as lightweight aggregates while CKD was used as additive material (partial replacement of cement). Two types of blocks were produced: polystyrene block and vermiculite block. The compressive strength and thermal conductivity of the two types of blocks were compared with ordinary concrete blocks and thermal insulation block like (PolyBlock2), as shown in Figure 2.1. The thermal conductivity of blocks of polystyrene (PolyBlock1), vermiculite, PolyBlock2 and ordinary concrete block types were 0.626, 0.76, 0.616 and 1.60 W/m.^{o}C, respectively, while the compressive strength of these blocks was obtained as 3.3, 2.2, 10.2 and 10 MPa. Furthermore, the results indicated that the addition of CKD up to 15 % had a negligible effect the thermal performance and reduction in compressive strength.

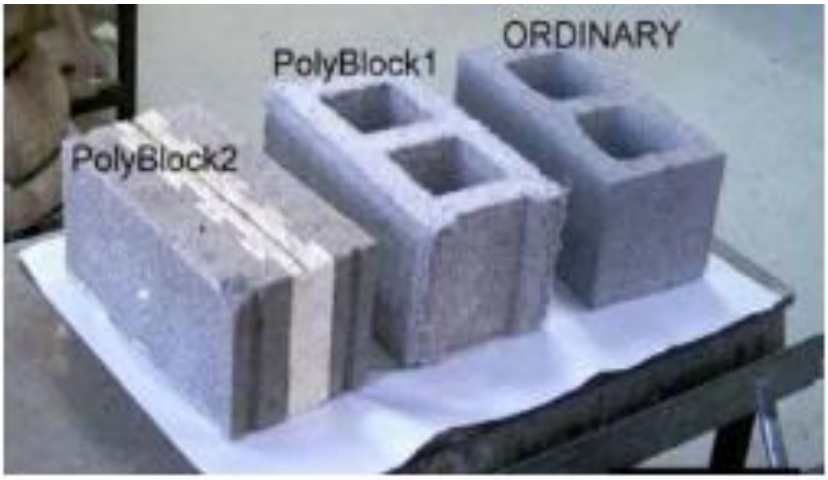

Figure 2.1: Different types of blocks [29].

Unal et al. [30] produced concrete blocks with diatomite of various aggregate sizes and different amounts of cement contents. Since the diatomite has low density and high pore volume, the thermal insulation of block has been dramatically improved and the best thermal conductivity coefficient was 0.23–0.233 W/m.K.

Hossain [31] investigated the potential use of volcanic scoria as fine and coarse aggregates to produce lightweight concrete with other lightweight aggregates. The properties of developed concrete were investigated by carrying out comprehensive sequences of tests on its strength, density, workability, drying shrinkage, water permeability and air content. The viability of using scoria as a heat-insulating material was also investigated. The results showed that scoria concrete satisfied the requirements of ASTM C332 for the insulating concrete which was ranging between (0.15 to 0.4 W/m.K). The block was ranging between (0.15 to 0.22 W/m.K) , therefore, it could be used in the buildings to save the energy.

Çelik et al. [32] produced lightweight solid bricks (50×100×100 mm) by mixing perlite, Carboxymethylcellulose (CMC), coal dust (powder) and water without cement, sand or aggregate. The brick was prepared by using different amounts of colemanite [it is mineral material and its formula $Ca_2B_6O_{11}.5(H_2O)$] (0–20% by mass) at different temperatures (200–400^{o}C). The best result was when the colemanite was equal to 10% after heat treatment at 400^{o}C. The thermal conductivity coefficient of this brick was around 0.12 W/m.K which is lower than other commercial lightweight bricks. Further, other physico-mechanical properties of the produced bricks displayed improvement as compared to other commercial lightweight bricks.

Çelik [33] reproduced the same blocks with the same mixed materials (perlite, CMC, coal dust and water) and same geometric shape. The blocks were prepared by using sodium borate and potassium borate instead of colemanite. The thermal conductivity coefficient of this block was 0.09- 0.123 W/m.K, which is lower than the commercial clay blocks.

Xu et al., [34] produced lightweight hollow concrete blocks by adding expanded polystyrene beads (EPS) as a lightweight aggregate to the mix proportion. Three dosages of EPS (15, 20, and 25% by volume of total mix) were used as aggregate replacement in the mixes. The compressive strength, density, and stress-strain behavior were examined to select the optimal mix. The optimal mixture was selected to manufacture the hollow blocks. The compressive strength of hollow masonry block was 3.2 MPa. The results showed that the dosage of EPS had the major effect on the compressive strength.

Sayadi et al [35] evaluated the compressive strength, thermal conductivity, and fire resistance of foamed concrete (FC) and expanded polystyrene foamed concrete (PFC). The expanded polystyrene (EPS) beads were replaced as lightweight aggregate by volume from all components. The PFC had low thermal conductivity ranging from 0.0848 to 0.1566 W/m.K with densities ranging from 150 to 400 kg/m^3. However, the compressive strength was very low ranging from 0.08 to 0.29 MPa. The best fire resistance was gained for the sample with higher cement and lower EPS due to the amorphous silica in the cement paste [35].

Singh and Garg [36] evaluated the strength, setting time, porosity and water absorption on different contents of vermiculite in the blocks product from fluorogypsum binder. The reduction on compressive strength in the 28 days was 41.9%, 48.3%, 60.3% and 64%, with

the content of 5%, 7.5%, 10% and 15% vermiculite, respectively, while the water absorption in the 7 and 28 days, which was tested only for the optimum quantity of vermiculite (10%), was 18.2 and 19.8%, respectively.

2.3 Finite Element Modelling (FEM) for Masonry Hollow Blocks

Arendt et al. [37] examined the effect of cavities concentration (i.e. hollow ratio or recess) in hollow blocks on the dynamic and static thermal parameters using semi-analytical method. The dynamic thermal analysis of hollow block with the optimum recess shape was conducted to minimize the amount of convection and radiation interchange. The optimum thermal parameters of hollow blocks were gotten by the ratios of the total cavities to the gross area of the block in the range of 30 to 45% for low thermal conductivity and 45 to 65% for higher thermal conductivity, though the latter was impossible to make technologically because the thickness of webs and ribs of block will be very thin and thus will be very weak and will be broken easily .

Coz Díaz et al. [38] conducted analytical and numerical studies to find out the optimum block using FEM. The conduction, convection and radiation phenomena were considered in this work for four types of blocks with different thermal conductivities. Based on the thermal analysis, the best candidate block was taken and then a wall was made of these blocks. The simulation was conducted using FEM for fifteen configurations and temperature distribution. In addition, FEM was used to find out the accurate solution for heat transfer equation of LW concrete hollow block walls.

Baig and Antar [39] evaluated the heat leak/thermal resistance numerically for different air cavities in concrete blocks. The results proved that rearrangement of the cavities increases

the thermal resistance significantly up to 17.65% without affecting the strength of the block. Additional, reducing the thickness of the solid material increases the thermal resistance due to decrease the thermal bridges of the solid part.

Coz Dıaz et al. [40] showed a new methodology to enhance the thermal performance of walls made of block with large cavities. 3-D analysis for the walls was conducted using finite element model to find out the optimum block with multi-cavities from a thermal point of view. The heat transfer equation with the accurate solution was found out and the non-linearity was attributed to the presence of radiation inside the cavities of the block. Moreover, the thermal optimization of the walls with different geometry was developed using FEM. It was observed that the heat flow depended on the thermal conductivity of the material as well as the size and distribution of the cavities.

Zhou et al. [7] assessed experimentally and numerically (using ABAQUS program) the thermal performance for gypsum layer inside the concrete wall panel. Three types of the sandwich layers were arranged in this experiment with 65-mm thickness, namely, concrete layer, solid gypsum layer, and gypsum layer with voids. The results showed that the wall panel with gypsum decreases the heat transfer of building envelopes by about 1.1^{o}C.

Del Coz Díaz et al. [41] investigated numerically the effect of the holes in multi-holed blocks using FEM. Three types of lightweight blocks with large and tiny cavities were modelled. It was reported that the variation of the size and shape of recesses affected the thermal conductivity. In other words, when the width of recesses was increased, the thermal resistance of block increased. Moreover; an increase in the length/width ratio of the cavities

tends to reduce the radiation emissivity phenomenon, thereby leading to get a better thermal resistance.

Oluwole et al. [10] examined the cavities influence on heat conduction through interlocking and conventional blocks using MATLAB. The results proved that the interlocking blocks with the 4 staggered cavities increase the thermal resistance significantly. In contrast, increasing the number of cavities more than four did not have a positive effect. For conventional blocks, the staggered cavities did not achieve the thermal conductivity advantage but the blocks with four cavities were considered effective in thermal insulated blocks. Increasing the number of holes more than four in the conventional blocks achieved the minimal thermal resistance.

Al-Tamimi et al. [42] have recently developed FEM for a hollow block masonry wall with filling the cavities by insulation materials. Three types of mortar were used to join the blocks (ordinary, LW and insulation mortars). The insulation and LW mortars reduced the temperature by 1.30 and 0.60°C, respectively, as compared to ordinary mortar. The effect of mortar was reduced with increasing the thermal conductivity of cavity insulation material.

Li *et al.* [43] studied numerically the reduction of heat transfer through walls using finite volume method. Clay hollow block with five cavity rows and each row had five cavities were used to build the wall. Expanding polystyrene board (EPS) was used to fill in the cavities with different ratios and location (the filled started from the external row cavities) to obtain the best filling effect of the EPS. Results showed the average decrement rates of low EPS filling ratio (20%) had more influence on inner surface heat flow by 21.19%, as

compared to other filling ratios (40, 60, 80 and 100%) which were (33.62, 40.79, 43.24 and 45.78%). In addition, the external filled cavities had higher decrement rates of inner surface heat flow by about (10.9-5.3%) than internal cavities of blocks under the all ratios (20-80%).

Kant *et al.* [44] simulated the thermal performance of hollow building block filled with phase change materials (PCM) using COMSOL software. Three types of commercial PCM (Capric acid, Paraffin and RT-25) were used to fill the blocks with three cylindrical cavities. The study showed the Capric acid efficiency was more effective, as compared with other two types of PCM. The maximum heat flux reduction was 8.31, 6.07 and 3.61% for Capric acid, Paraffin and RT-25, respectively.

Martínez *et al.* [45] investigated experimentally and numerically the thermal behavior for different types of concrete block (normal and medium density). Six different geometries were fabricated and the cavities of each geometry were filled with different insulated materials (extruded cardboard, expanded polystyrene and polyurethane foam). The best geometry reduced the thermal resistance (R-value) by 153 and 114% for normal and medium weight concrete blocks, as compared to the control block. Further, the best filled material was the polyurethane foam and the redaction in R-value was 323% for normal concrete block and 403% for medium concrete block, as compared to the referenced block.

Zhai *et al.,* [46] studied numerically the thermal insulation efficiency of a sintered coal gangue self-insulation block (SCGSB) and compared its performance with ordinary clay block. Blocks with staggered small rectanglular cavities and two different thickness were simulated using ANSYS software. In addition, two types of mortar (ordinary cement and

special mortar) were used in this study. The results proved that SCGSB with cement mortar and same thickness could save 50% energy, as compared with clay block, whereas the SCGSB with the special mortar and 240 mm thickness could save energy up to 65%, as compared with clay block with the cement mortar.

CHAPTER 3

EXPERIMENTAL PROGRAM

3.1 Introduction

In this research, the experimental program was basically planned to cover all the details about the selection of materials, concrete mix design, trials of masonry blocks and mortar, casting process, curing and testing of the samples. In consonance with the motivation of this research, the four lightweight materials for blocks and the three for mortar, which are obtainable locally available in the Saudi market and are very cheap, were utilized to develop thermally effective masonry blocks and mortar. The following three types of insulation materials were used to replace sand to create insulation mortar and plaster with low thermal conductivity (k-value): fine crumb tires-rubber (RU), perlite powder (PL) and granules vermiculite (VL). Approximately 58% of the mortar volume is sand, hence, it has the largest volume in the mortar components and also it is considered as a filling material in the mix design of mortar and plaster [47]. Therefore, replacing the sand by insulation materials will absolutely reduce the k-value of mortar and plaster. Furthermore, four materials [i.e. expanded polystyrene beads (EPS), vermiculite, recycling low density polyethylene (LDPE) and volcanic scoria aggregate (VS)] were used for the development of energy efficient blocks in combination with ordinary Portland cement.

The experimental program for this MS thesis is divided into three parts. The first part included the selection of the insulation materials and other concrete mix design components. The second part was devoted for the mix design and the trials that were

conducted until the proper “optimum” mix (for each light-weight material) was satisfied. This part was preceded by conducting many trial mixes whereby the insulated materials were used to replace coarse, fine and combined aggregates. In this part, there are the following two main phases:

Phase 1: Producing insulated blocks: Insulation materials (ESP, SA, LDPE and VL) with different contents were used to replace coarse and fine aggregates in the mix of the hollow concrete blocks.

Phase 2: Producing insulated mortar: Three replacement materials (RU, PL and VL) were used in the mortar mix to replace coarse and fine aggregates.

In the third part, compressive strength, thermal conductivity, absorption and density were experimentally measured to investigate the influence of the additive (i.e. light-weight) materials on these properties for both masonry block units and mortar mixes.

3.2 Essential Materials

3.2.1 Cement

Ordinary Portland (Type I) cement was used in the project. It was manufactured by the Saudi Cement Company. This type of cement is the most widely used by the construction industry in Saudi Arabia [48]. The properties of cement are: specific gravity 3.15, thermal conductivity 0.44 W/m.K, and melting point 1450^{o}C [49]. All the properties satisfied ASTM C 150 requirements [50]. Table 3.1 summarizes the chemical composition of this type of cement.

Table 3.1: Chemical composition of Type I cement

Component	Weight %
CaO	64.35
SiO_2	22.00
Al_2O_3	5.64
Fe_2O_3	3.80
K_2O	0.36
MgO	2.11
Na_2O	0.19
Equivalent alkalis	0.33
SO_3	2.10
Loss on ignition	0.70
C_3S	55.00
C_2S	19.00
C_3A	10.00
C_4AF	7.00
Blaine fineness (m^2/kg)	370

3.2.2 Coarse and Fine Aggregates

Crushed limestone rocks were used as the coarse aggregate in this research, which was brought from the Advanced Concrete Products, Ltd. Company, Dammam. The two sizes (9.53 and 4.76 mm) of course aggregate, which are used in factory blocks, were used in the mix. The fine aggregate used in this work was a local sand, which is widely available in Saudi Arabia. Fig. 3.1 shows both the coarse and fine aggregates used in this research. Their specific gravity was 2.60 and 2.53, while their water absorption was 1.10 and 0.6%, respectively. A typical chemical composition of limestone and sandstone aggregates is shown in Table 3.2

Coarse Aggregate #3/8 in (9.53 mm) Coarse Aggregate #3/16 in (4.76 mm) Fine Aggregate (Sand)

Figure 3.1: Sizes of fine and coarse aggregate

Table 3.2: Chemical composition of limestone and sandstone aggregate [51]

Constituent	Limestone (Weight %)	Sand (Weight %)
SiO_2	4.29	90.79
Al_2O_3	0.20	2.51
Fe_2O_3	0.23	0.84
MgO	0.44	0.54
CaO	52.5	1.46
Na_2O	0.03	0.25
K_2O	0.087	0.51
TiO_2	<0.1	0.19

3.2.3 Mixing Water

Generally, drinkable water is satisfactory to be used in concrete as a mixing or curing water. The normal tap water available in the Concrete Laboratory at KFUPM is considered as a sweet water. Therefore, it was used for casting and curing all the concrete blocks and mortars specimens.

3.3 Replacement Materials

In this research, four materials were utilized in mix proportion of masonry blocks to replace coarse and fine aggregates. In addition, three materials were used as replacement materials

for sand in the cement mortar mix design. All these materials are cheap and available in the Saudi markets. The sources of replacement materials are presented in Tables 3.3 and 3.4

Table 3.3: Replacement materials of the masonry blocks

Type of material	Materials	Abbreviation
Industrial	Expanded polystyrene beads	EPS
	Low density polyethylene	LDPE
Natural	Vermiculite	VL
	Scoria aggregate	SA

Table 3.4: Replacement materials of cement mortar

Type of material	Materials	Abbreviation
Industrial	Crumb Tires Rubber	RU
Natural	Vermiculite	VL
	Perlite	PL

3.3.1 Polystyrene Beads

Polystyrene beads are light-weight plastic foamed material formed of hydrogen and carbon atoms [29]. They are manufactured from natural gas and petroleum by-products [52]. They are manufactured by subjecting the small expandable beads to steam, which changes the thermoplastic small polystyrene beads to a softened state. Adding bowing agent and rising steam pressure expand the beads to the final density required. The expansion could reach upto 40 times of their original volume [53]. Nowadays, the physical properties of polystyrene (i.e. frost proof, fire resistance, good vapor diffusion, insect and vermin proof, and lack of toxic components) have been improved [53]. The class of the polystyrene beads used in this work is B1 Flame [54]. This type of beads retards the flame and has less smoke and short burning time, as compared to B2 [54]. Other properties of the polystyrene beads

are [53]: a density around 16 kg/m^3, water absorption 1.5% by weight, thermal conductivity 0.036 W/m.K, thermal resistance 1.4 m^2.K/W, and diameter of beads ranging from 5 to 3 mm, as shown in Fig. 3.2.

Figure 3.2: Expanded polystyrene beads

3.3.2 Low-Density Polyethylene (LDPE)

LDPE is a first grade of polyethylene group, which is made from a monomer ethylene. Recycled LDPE from the plastic industry was used in this work. LDPE recycled granules were resulting from an uncomplicated process of plastic packs (plastic bags and garbage bags) [55]. In the recycling plant, the plastic was collected, separated, washed, and heated at an approximate temperature of 60 ºC, and crushed into small granules [56]. The density of LDPE, which was used in this work, was 860 kg/m^3. Other properties of the LDPE are thermal conductivity 0.3 W/m.K, water absorption (7.4%) [56], and diameter of granules was ranging from 3 to 2 mm, as shown in Fig. 3.3.

Figure 3.3: Low-density polyethylene (3-2 mm)

3.3.3 Vermiculite (VL)

Vermiculite is a phyllosilicate mineral with flakes structure, and it is to some degree comparable to mica. Vermiculite can be expanded from15 to 30 times of its original volume when heated at (650-950 ^{o}C). The resultant expansion can change its properties resulting into low bulk density, low thermal conductivity, high water absorption and high melting temperature point [57]. The vermiculite aggregates used in this research have a bulk density of about 80 kg/m^3. Other properties of vermiculite were a thermal conductivity of 0.06 W/m.K, water absorption of 530 % by weight, a melting point of 1330 ^{o}C [49] and specific gravity of 0.12 [58]. The other chemical composition and physical properties are shown in Tables 3.5 and 3.6. The diameter of small vermiculite granules was ranging from 2.8 to < 0.5 mm and the typical sieve analysis is shown in Table 3.7 and Figure 3.4.

Table 3.5: Chemical composition of vermiculite*

Materials	Weight (%)
Silicon (as SiO_2)	38.93
Magnesium (as MgO)	22.03
Aluminum (as Al_2O_3)	8.99
Potassium (as K_2O)	5.43
Iron (as Fe_2O_3)	8.45
Calcium (as CaO)	3.62
Titanium (as TiO_2)	1.10
Fluorine (as F)	0.59

*The chemical and physical properties were brought from supplier company

Table 3.6: Physical properties of vermiculite*

Melting Point (°C)	1330
Specific Heat (1kJ/kg.K)	1.08
Specific Gravity	0.5
Moh's Hardness (Crude)	1-2
pH (ISO 787-9)	7 - 8
% Loss at 105°C (Product)	< 1.5
% Loss at 1000°C (Product)	< 6
Water retention	530%
Air porosity	24-44
Cationic exchange capacity (me/100g)	Approx. 75
Incombustibility	1039 ºC

*The chemical and physical properties were brought from supplier company

Table 3.7: Typical sieve analysis of vermiculite

Sieve Aperture (mm)	Retained (%)
2.8	5
2.0	20
1.0	42
0.5	28
<0.5	5

Figure 3.4: Vermiculite granules (2.8- <0.5 mm)

3.3.4 Volcanic Scoria Aggregate (VS)

Scoria is a lightweight aggregate obtained from volcanic basaltic rocks in western Saudi Arabia. These rocks cover about 180000 km^2 distributed between 13 separate lava fields

called Harrats [23]. The trapped air inside the scoria makes the concrete lighter and better insulator. Scoria can be used in many industrial applications such as producing lightweight concrete, a source of natural pozzolan to manufacture supplementary cementitious materials, a thermal insulation material and other architectural applications [23].

In this work, scoria was used with two sizes of coarse lightweight aggregate (4.76 and 9.52 mm) and used to replace the same sizes of normal coarse aggregates (limestone aggregate), as shown in Figure 3.5. A typical chemical composition of scoria aggregate is shown in Table 3.8.

Coarse Aggregate #3/8 in (9.52 mm)

Coarse Aggregate #3/16 in (4.76 mm)

Figure 3.5: Sizes of scoria aggregate

Table 3.8: Chemical composition of scoria aggregate [23]

Constituent	Weight %
SiO_2	64.35
Al_2O_3	22.00
Fe_2O_3	5.64
MgO	3.80
CaO	0.36
Na_2O	2.11
K_2O	0.19
TiO_2	0.33
Loss on ignition	2.10

3.3.5 Fine Crumb Rubber Particles (RU):

Tire-rubber is manufactured using more than hundred raw materials including raw rubber, and compound ingredients. About 50% of these materials are chemical components [59]. A chemical composition of the tires rubber is listed in Table 3.9.

The fine crumb rubber was provided by the Saudi Rubber Products Co., Dammam. These crush rubbers can be supplied in large quantities with different sizes to be used in asphalt. In this thesis, the fine crushed rubber was used as a replacement of sand. The rubber particles were fine with particle size of 0.6 to 2 mm, as shown in Figure 3.6. Its specific gravity was 1.12, with almost no absorption [60] and the thermal conductivity was 0.243 W/m.K [61].

Table 3.9: Chemical composition of tires [59].

Materials	Weight %
Rubber	46.00
Carbon black	22.00
Metal	20.70
Textile	5.50
Zinc oxide	1.50
Sulfur	1.00
Additives	6.25

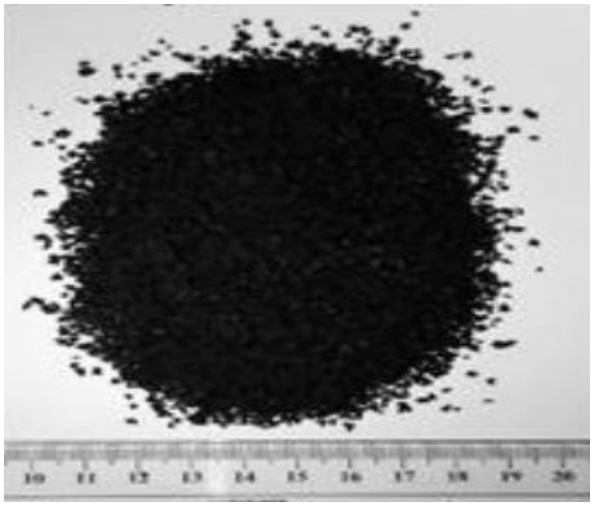

Figure 3.6: Fine crumb rubber particles

3.3.6 Perlite Powder (PL):

The perlite aggregate is a lightweight, porous, fire-resistant material, which has significant thermal and sound insulation properties [62]. The perlite aggregate meets ASTM C-332 Group 1, used to manufacture insulated lightweight blocks or concrete. The perlite used in this research was acquired from the Arabian Vermiculite Industries Co. in the first Industrial Area in Dammam as a raw natural perlite material. The chemical composition of the perlite powder is shown in Table 3.10 [63]. The thermal conductivity, specific gravity and absorption of the perlite powder was 0.04-0.06 W/m.K, 0.15 and 100% , respectively [58, 63]. The perlite powder is shown in Fig. 3.7.

Table 3.10: Chemical composition of perlite powder [63]

Materials	Weight (%)
Si	33.80
AL	7.20
K	3.50
Na	3.40
Ca	0.60
Mg	0.60
Trace	0.20

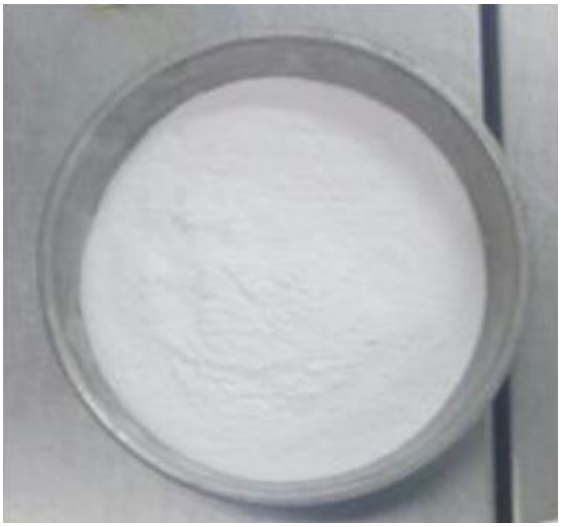

Figure 3.7: Graded sizes of perlite powder

3.4 Experimental Program of Blocks

For EPS beads, LDPE, vermiculite and scoria, a preliminary program was initially conducted to determine the optimum dosage of EPS, LDPE, VL and VS to produce the insulation concrete blocks. Therefore, three cubes (100 mm^3) of lightweight concrete were initially cast for each mix design as a trial mix in the laboratory.

3.4.1 Mix Preparation for the Trial Mixes

A series of trial mixes were prepared in order to obtain the optimal mix proportions for each type of the insulation materials. EPS, LDPE and VS were used to replace the coarse aggregate while VL was used to replace either the coarse or fine aggregate with the principal objective of satisfying the compressive strength of 3.45 MPa (as required by ASTM C-129) to be classified as non-load bearing walls. Since testing of blocks in compression is cumbersome and time consuming, our preliminary investigation indicated that a minimum compressive strength of 6 MPa for 100-mm cubes would satisfy the ASTM C-129 requirement.

In EPS series, 13 trial mixes were cast by adding different proportions of EPS to the mix components, as shown in Table 3.11. The EPS was used to replace the coarse aggregate by volume in three groups because it was difficult to be replaced by weight, as was observed during the preliminary work as well as in the literature review [23, 26, 28, 33-34]. In the first group, the EPS beads were used to replace the coarse aggregate of size (4.76 mm), which is of the same size of EPS beads. In the second group, the EPS beads were used to replace the coarse aggregate of size (9.52 mm). In the third group, the EPS beads were used to replace both size (4.76 and 9.52 mm).

In LDPE series, 8 trial mixes were conducted in three groups. LDPE was used to replace the coarse aggregate size (4.76 mm) by weight for all groups (G1, G2 and G3) and CA/TA ratio was 76.5, 66.5 and 60 for G1, G2, and G3, respectively. It was varied to increase the cement paste due to the increase of the sand in the mix, as shown in Table 3.12.

Table 3.11: Trial mix proportion of polystyrene (EPS) replacements (by volume)

Mix number	Percentage [CA/TA (%)]	Size replacement	Cement (%)	Water (%)	Superplasticizer (%)	Coarse aggregate		Fine aggregate	Replacement by volume	Density (kg/m^3)	Average 28-days compressive strength (MPa)
						CA 3/8 (%)	CA 3/16 (%)	Sand (%)	EPS beads (%)		
CM	76.5	---	6.2	11.5	0.2	43.5	13.0	17.6	---	1883	12.16
G1-TM1	60	3/16 (4.79 mm)	6.2	11.4	0.2	34.0	---	29.9	10.0	1827	10.92
G1-TM2	65	3/16 (4.79 mm)	6.2	11.4	0.2	36.9	---	26.2	11.0	1815	9.78
G1-TM3	70	3/16 (4.79 mm)	6.2	11.5	0.2	39.8	---	22.5	12.0	1795	8.33
G1-TM4	76.5	3/16 (4.79 mm)	6.2	11.7	0.2	43.5	---	17.6	13.0	1786	7.08
G1-TM5	70	3/16 (4.79 mm)	6.2	11.5	0.2	38.7	---	22.5	13.0	1775	6.46
G2-TM1	60	3/8 (9.52 mm)	6.2	11.4	0.2	23.9	10.2	29.9	10.0	1835	11.01
G2-TM2	65	3/8 (9.52 mm)	6.2	11.4	0.2	25.9	11.0	26.2	11.0	1809	9.44
G2-TM3	70	3/8 (9.52 mm)	6.2	11.5	0.2	27.9	11.9	22.5	12.0	1798	8.57
G2-TM4	76.5	3/8 (9.52 mm)	6.2	11.7	0.2	30.5	13.0	17.6	13.0	1768	6.04
G3-TM1	60	3/8 & 3/16	6.2	11.4	0.2	29.0	5.1	29.9	10.0	1841	11.51
G3-TM2	65	3/8 & 3/16	6.2	11.4	0.2	31.4	5.5	26.2	11.0	1821	10.93
G3-TM3	70	3/8 & 3/16	6.2	11.5	0.2	33.8	5.9	22.5	12.0	1768	6.56
G3-TM4	76.5	3/8 & 3/16	6.2	11.7	0.2	37.0	6.5	17.6	13.0	1453	3.48

Table 3.12: Trial mix proportion of low density of polyethylene (LDPE) replacements (by weight)

Mix number	Percentage [CA/TA (%)]	Size replacement	Cement (kg)	Water (kg)	Superplasticizer (ml)	Coarse aggregate		Fine aggregate	Replacement by weight (Kg)		Density (kg/m^3)	Average 28-days compressive strength (MPa)
						CA 3/8 (kg)	CA 3/16 (kg)	Sand (kg)	LDPE (kg)	LDPE (%)		
CM	76.	---	195	115	3	1132	338	451	---	---	1883	12.16
G1-TM1	76.5	3/16	195	111	3	877	262	389	127	10	1721	5.18
G1-TM2	76.5	3/16	195	110	3	775	231	363	178	15	1532	2.39
G1-TM3	76.5	3/16	195	108	3	684	204	342	222	20	1443	2.12
G2-TM1	66.5	3/16	195	111	3	748	223	553	127	10	1740	5.31
G2-TM2	66.5	3/16	195	109	3	655	196	518	178	15	1694	3.22
G2-TM3	66.5	3/16	195	108	3	572	171	486	222	20	1588	2.29
G3-TM1	60	3/16	195	112	3	757	226	704	74	7	1875	7.50
G3-TM2	60	3/16	195	111	3	708	211	681	102	10	1821	6.21

For the volcanic scoria (VS) in Table 3.13, 9 trial mixes were conducted in two groups. VS was used to replace all the coarse aggregate (both sizes of 4.76 and 9.52 mm) by weight for both groups (G1 and G2). The CA/TA ratio was varied until the optimum mix was achieved (i.e., compressive strength greater than 6 MPa). In the second group, the cement content was increased to assess the improvement in the compressive strength. However, the best mix was found to be G1-TM5 because it had a compressive strength greater than 6 MPa, as well as an acceptable density and low cost (low cement content).

Table 3.13: Trial mix proportion of volcanic scoria (VS) replacements (by weight)

Mix number	percentage (CA/TA)	Size replacement	cement (kg)	water (kg)	Superplasticizer (ml)	Coarse Aggregate		Fine Aggregate	Replacement by weight (Kg)		Density (kg/m^3)	Average 28-days compressive strength
						CA 3/8 (kg)	CA 3/16 (kg)	Sand (kg)	CA 3/8 (kg)	CA 3/16 (kg)		
CM	76.5	---	195	115	3	1132	338	451	---	---	1883	12.16
G1-TM1	65	3/8 & 3/16	195	192	3	---	---	455	651	194	1314	3.04
G1-TM2	60	3/8 & 3/16	195	188	3	---	---	533	616	184	1402	3.82
G1-TM3	55	3/8 & 3/16	195	183		---	---	615	579	173	1484	5.52
G1-TM4	50	3/8 & 3/16	195	178	3	---	---	701	540	161	1656	5.88
G1-TM5	45	3/8 & 3/16	195	173	3	---	---	792	499	149	1725	6.70
G1-TM6	40	3/8 & 3/16	195	167	3	---	---	888	456	136	1788	6.76
G2-TM1	50	3/8 & 3/16	250	200	3	---	---	659	508	152	1772	11.98
G2-TM2	45	3/8 & 3/16	250	195		---	---	744	469	140	1802	12.23
G2-TM3	40	3/8 & 3/16	250	190	3	---	---	835	428	128	1845	15.50

For VL series, 28 trial mixes were conducted in three groups. The VL was used to replace the fine aggregate by weight in the first two groups and it was used to replace coarse aggregates in the third group. In first group, the aim was to minimize the fine aggregate (sand) by varying the CA/TA ratio and increasing the replacement ratio (VL/FA). In the second group, six mixes were cast (using mix number G1-TM16 in Table 3.14) in two ways. In the first three mixes, the mixing procedure was in the traditional way (all components were mixed together in the mixer then adding the water gradually with continued mixing), while in the second three mixes, the VL was put on the gross water of the mix and was left to fully saturate for one day then all the components were mixed together. The results show that the second way gave better compressive strength than the traditional way. In third group, the second way of mixing was used and the cement content was increased to get acceptable strength. Table 3.14 shows all the trial proportions of vermiculite concrete mixes.

Table 3.14: Trial mix proportion of vermiculite (VL) replacements (by weight)

Mix number	Percentage (CA/TA)	Size replacement	Cement (kg)	Water (kg)	Superplasticizer (ml)	Coarse aggregate		Fine aggregate	Replacement by weight (Kg)		Density (kg/m^3)	Compressive strength (MPa) 28-days
						CA 3/8 (kg)	CA 3/16 (kg)	Sand (kg)	VL (kg)	VL (%)		
CM	76.5	---	195	115	3	1132	338	451	---	---	1883	12.16
G1-TM1	76.5	FA (sand)	195	220	3	1031	308	370	41	10	2009	7.06
G1-TM2	76.5	FA (sand)	195	266	3	987	295	335	59	15	1928	4.23
G1-TM3	76.5	FA (sand)	195	308	3	946	283	302	75	20	1862	3.23
G1-TM4	76.5	FA (sand)	195	315	3	930	278	278	93	25	1743	2.82
G1-TM5	85	FA (sand)	195	302	3	1060	317	170	73	30	1833	2.81
G1-TM6	85	FA (sand)	195	328	3	1033	308	154	83	35	1835	3.04
G1-TM7	85	FA (sand)	195	352	3	1007	301	138	92	40	1796	2.75
G1-TM8	90	FA (sand)	195	303	3	1123	335	89	73	45	1864	3.02
G1-TM9	90	FA (sand)	195	320	3	1104	330	80	80	50	1846	1.32
G1-TM10	90	FA (sand)	195	336	3	1085	324	70	86	55	1829	1.08
G1-TM11	90	FA (sand)	195	352	3	1067	319	62	92	60	1860	2.75
G1-TM12	93	FA (sand)	195	305	3	1159	346	40	74	65	1867	2.81
G1-TM13	93	FA (sand)	195	317	3	1145	342	34	78	70	1815	3.07
G1-TM14	93	FA (sand)	195	340	3	1118	334	22	87	80	1731	2.42
G1-TM15	95	FA (sand)	195	303	3	1186	354	8	73	90	1806	2.84
G1-TM16	95	FA (sand)	195	320	3	1166	348	---	80	100	1762	2.04
G2-TM1	95	FA (sand)	225	323	3	1103	329	---	75	100	1734	2.49
G2-TM2	95	FA (sand)	250	334	3	1064	318	---	75	100	1729	2.29
G2-TM3	95	FA (sand)	275	345	4	1025	306	---	75	100	1727	2.72
G2-TM4	95	FA (sand)	225	323	3	1103	329	---	75	100	1920	4.51
G2-TM5	95	FA (sand)	250	334	3	1064	318	---	75	100	1889	4.12
G2-TM6	95	FA (sand)	275	345	4	1025	306	---	75	100	1914	4.38
G3-TM1	76.5	CA	225	320	3	829	248	354	75	6.5	1941	4.05
G3-TM2	76.5	CA	250	331	3	798	238	341	75	6.7	1959	5.31
G3-TM3	76.5	CA	275	344	4	766	229	329	75	7.0	1983	6.58
G3-TM4	76.5	CA	225	283	3	881	370	263	60	5.0	1959	5.87
G3-TM5	76.5	CA	250	290	3	856	256	359	58	5.0	2098	6.58
G3-TM6	76.5	CA	275	298	4	831	248	349	57	5.0	1983	6.77

All the concrete blocks in this study were cast in a mold that was designed in a previous study [48], as shown in Figure 3.8. The wooden box's size was (400 x 200 x 200 mm) and three set of polystyrene boards were fixed inside the wooden box to form the cavities in the block. The polystyrene boards and wooden box were pre-oiled and fixed at the base of mold. The concrete mix was poured manually using tamping steel rod in three layers (Fig. 3.9). The block was covered by plastic sheet and left to dry out in the laboratory atmosphere for 24 hours (23 ± 2°C). Then, the wooden box was removed carefully and the block was cured in sweet water for 6 days. After the 7th day, the polystyrene boards were removed and returned back to the water tank until the date of testing.

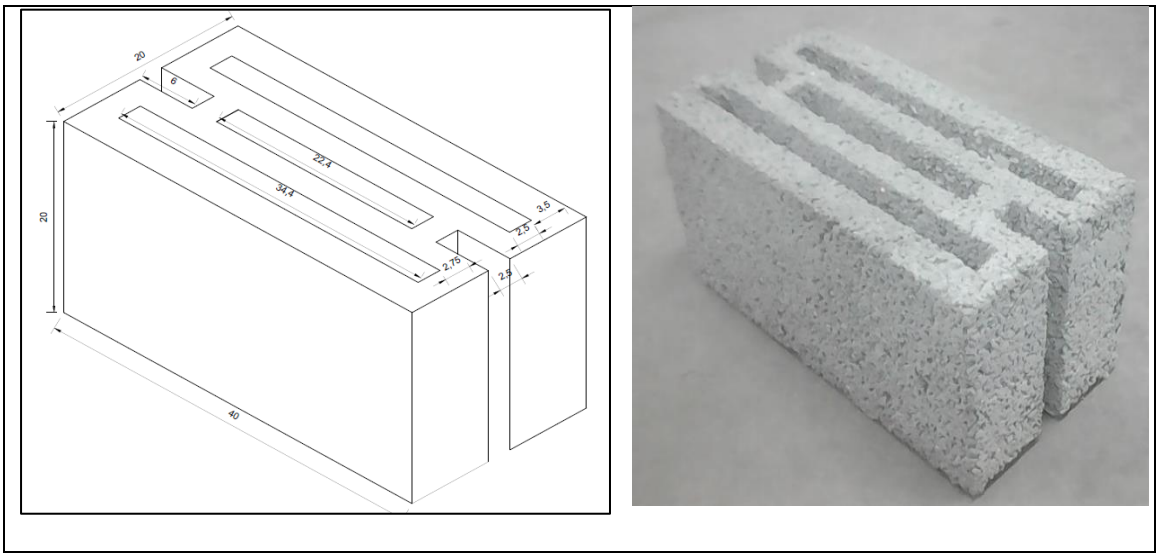

Figure 3.8: Geometry of the block

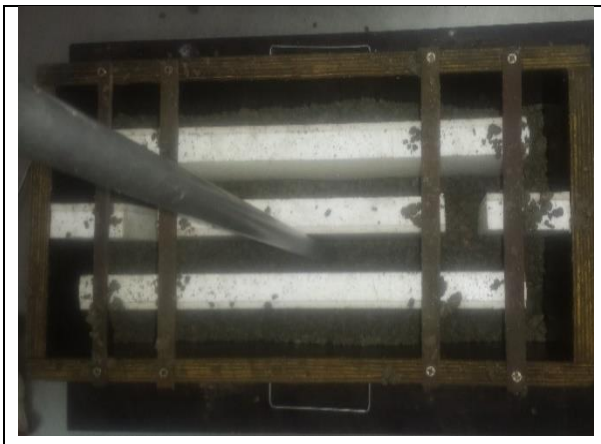

1- Pouring the mix manually using tamping rod

2- Demolding the wood box

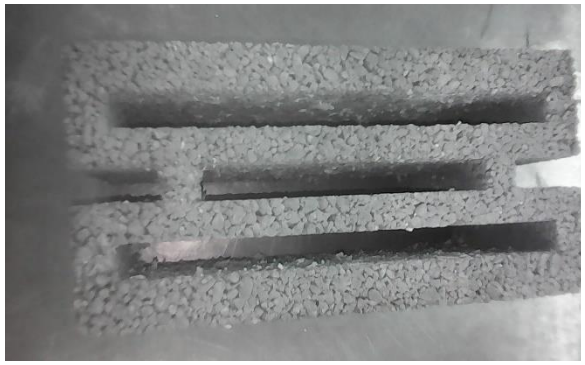

3- Removing the polystyrene boards

4- Capping the loading bearing surfaces

Figure 3.9: Steps for cast and preparing for compressive test

3.4.2 Testing the Properties of Hollow Blocks

After the necessary curing period, the cubes and the hollow blocks were dried out, weighed and prepared for the following tests:

3.4.2.A Compressive Strength Test

Concrete cubes (with 100 mm size) were used to assess the compressive strength after 7 days of water curing according to ASTM C 39. A hydraulic compressive testing machine (MATEST) with a capacity about 3000 kN was used to test all the cubes samples. Compressive loading was automatically applied at a rate of 0.50 kN/s until the cube failure.

The value of the surface bearing area was input into the machine to get the compressive strength in (MPa).

For the concrete, 100-mm cubes were tested for all the 58 mixes (13 for ESP, 8 for LDPE, 28 for VL and 9 for VS) and three cubes were tested for each mix in order to get better results by taking the average (i.e., the total number of cubes tested for the block mixes was 174).

The compressive strength test of the blocks was conducted according to ASTM C140 [64]. The blocks were first dried out and weighted to calculate the dry weight of the block. After that, they were capped using a special high strength cement mortar to ensure uniform pressure distribution. Rigid steel plates were placed at the top and the bottom of block surfaces to distribute the load regularly over the cross-sectional area of the block, see Figure 3.10. The load was applied regularly at a rate 0.3 kN/s until failure. The failure load was recorded and divided by the net area of the block, which is normal to the load, to calculate the strength at failure.

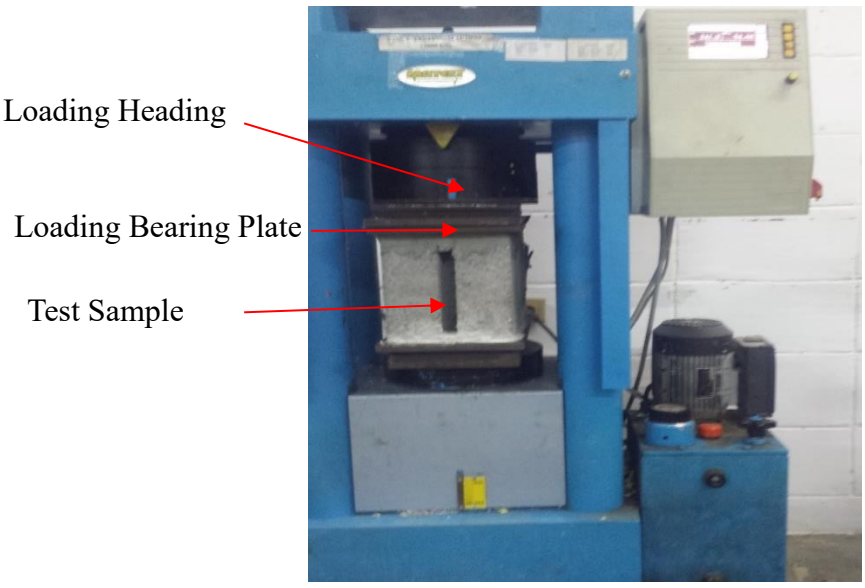

Figure 3.10: Compression test for hollow concrete blocks

3.4.2.B Thermal Performance

The thermal performance of concrete blocks was assessed using the Guarded Hot Plate (Fig. 3.11). It measures the equivalent thermal conductivity of the blocks under steady-state condition that satisfies ASTM C-177 [65].

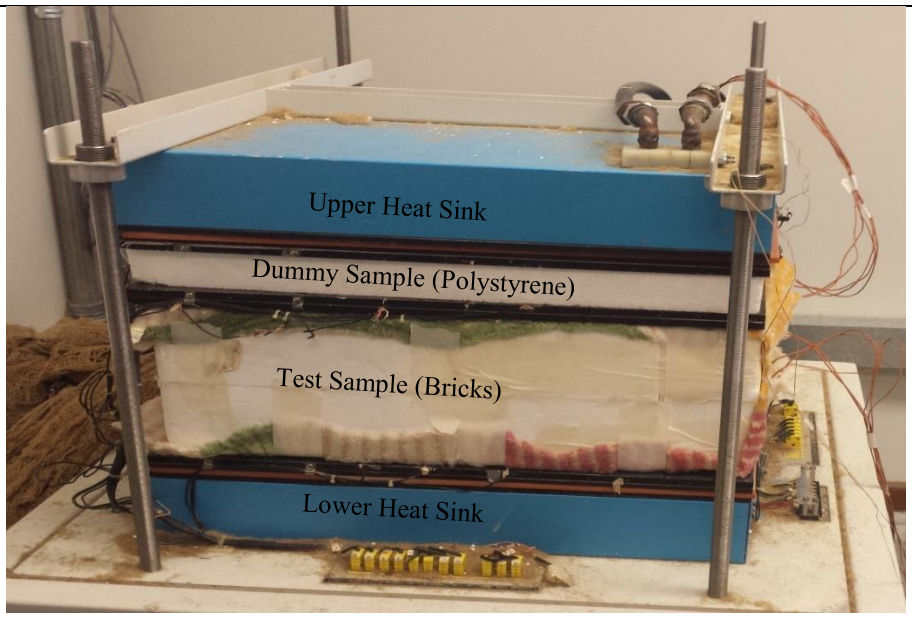

The main part of guarded hot plate instrument

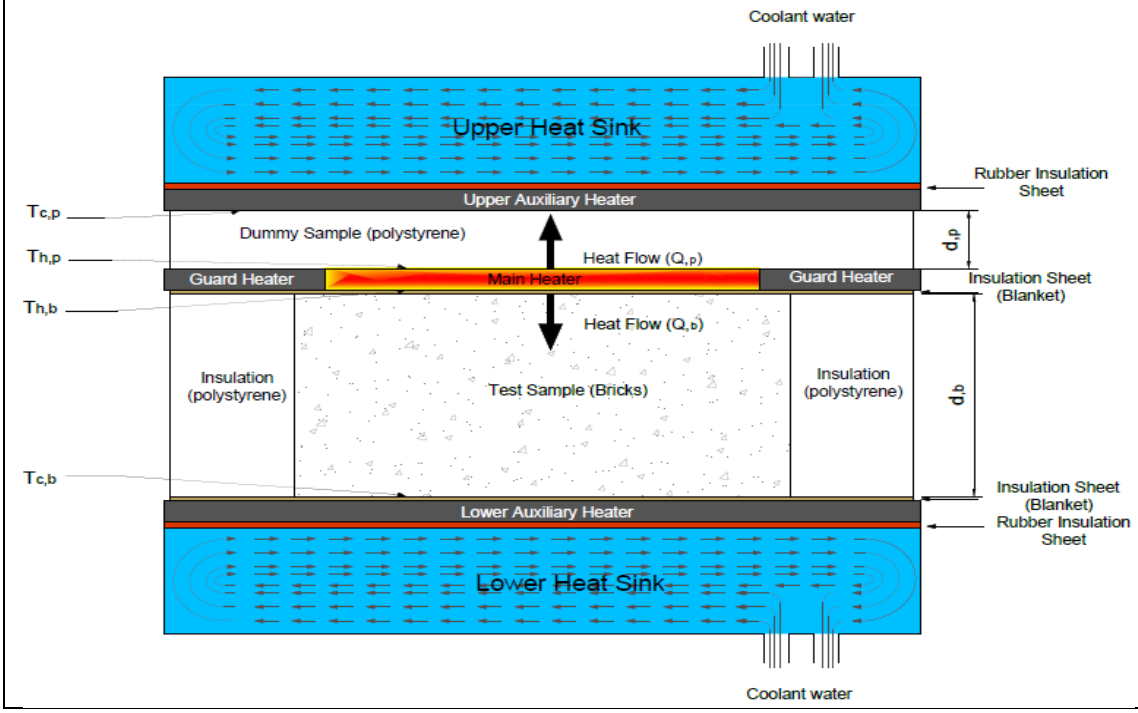

Figure 3.11: Cross-section for guarded hot plate

The equipment measures the thermal conductivity of masonry and insulation building materials such as concrete, clay blocks, polystyrene, and any materials that have a value of thermal conductivity between 0.02 to 2.0 W/m.K. The minimum obtainable temperature is 24°C and the maximum is 230°C and the accuracy of the test is ranging between ±2% to ±4% of the real equivalent thermal conductivity [66]. To a certain degree, the accuracy of results depends on the equipment operator skills and the plate temperatures [66].

The instrument needed two identical or different samples with a maximum thickness of 150 mm. Because the blocks have a thickness more than 150 mm, a calibration dummy polystyrene sample with 5 mm in thickness was utilized on the upper main heater plate to adjust the larger thickness of the blocks under the main heater plate. The samples with size 400 mm x 420 mm were prepared and surrounded by polystyrene board with same thickness of the sample to accommodate the remaining area of the guard heater (610 × 610 mm). In addition, both surfaces of the sample were covered by blankets to minimize the heat loss between the sample surfaces and the plates. Figure 3.12 shows the steps of preparing the sample for the thermal conductivity test using guarded hot plate.

The average temperature during the test was maintained for the samples at around 35.0 ± 2°C and the surface temperature was kept at about 25°C. These temperature values are considered realistic values for exterior and interior of the weather in Saudi Arabia [26]. The two faces of the wall have to be levelled and smooth to reduce the resistance between the sample and plate surfaces. The coarse surfaces result in a considerable temperature change between the two surfaces of the sample and plate. Therefore, five thermocouples were set on each side of the sample within the area of the main heater (350 x 350 mm). The temperatures on both faces were observed using automatic data acquisition system

(Campbell Scientific 21X). The temperature was monitored until a steady-state condition is satisfied.

1-Join Two blocks by normal mortar

2- Surround the blocks by polystyrene board

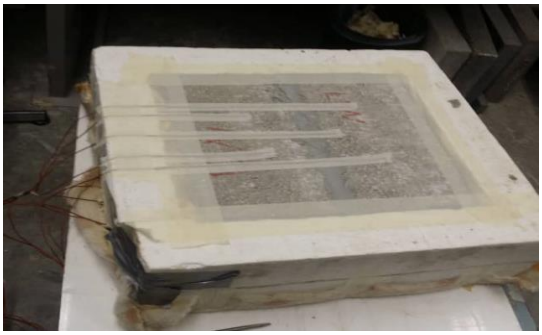

3- Fix the thermocouples on the surface

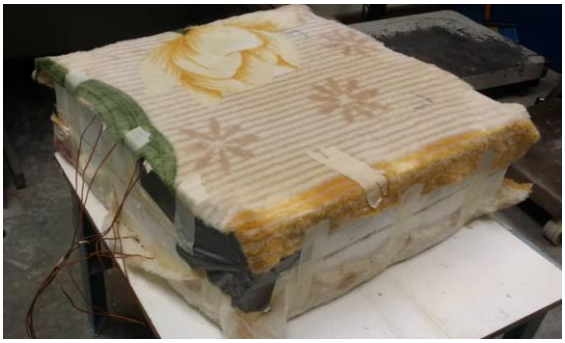

4- Cover the rough surfaces by blankets

Figure 3.12: The steps of preparing sample for thermal conductivity test

The test sample (block) and dummy sample (polystyrene) are shown in Fig. 3.11, when the steady state took place, the equivalent thermal conductivity was calculated according to the following equations [26]:

The heat generated from the main heater was calculated using the following equation:

$$Q = N \times I \times V \tag{3.1}$$

Since, the k_p of dummy sample (polystyrene board) is known, the heat flow (Q_p) through it can calculate by:

$$Q_p = \frac{k_p\, A(T_{h,p} - T_{c,p})}{d_p} \tag{3.2}$$

The equivalent k-value (k_b) of test specimen (the block) was determine by:

$$Q_b = Q - Q_p = NIV - \frac{k_p\, A\, (T_{h,p} - T_{c,p})}{d_p} \quad (3.3)$$

$$k_b = Q - Q_p = \frac{d_p(NIV d_p - k_p\, A\, (T_{h,p} - T_{c,p}))}{d_p\, A(T_{h,b} - T_{c,b})} \quad (3.4)$$

Where:

N: The correction factor of the device = 0.986 [26]

Q: heat generated from main heater,

I: Main heater current, milliampere (mA)

V: The voltage of main heater, in millivolts (mV)

A: Surface area of the main heater (m2)

Q_p: Heat flux of dummy sample (W)

Q_b: Heat flux of test sample (W)

K_p: Thermal conductivity of dummy sample (W/m.K)

K_b: Thermal conductivity of masonry block sample (W/m.K)

$T_{h,d}$: heated surface of dummy sample (°C)

$T_{c,d}$: Cold surface of dummy specimen (°C)

$T_{h,b}$: heated surface of masonry block specimen (°C)

$T_{c,b}$: Cold surface of masonry block specimen (°C)

d_d: Thickness of dummy specimen (m)

d_b: Thickness of test specimen (m)

3.4.2.C Absorption and Density

The density and absorption of the concrete blocks were evaluated accordance to ASTM C140 standard. Three 100 mm cubes were cast for each type of the optimal mix block and put in sweet water for 6 days. Then, the cubes were removed from the curing water and left

to drain on coarse wire mesh for one minute [64], removed all visible water on cube surfaces with a damp cloth, weighed, and recoded the weight as saturated weight (W_s). Subsequently, all cubes were dried in oven at 110 ^oC for 24 h and recorded the dried weight (W_d). The density and absorption were calculated according to the following equations [64]:

$$Density = \frac{w_d}{V_c} \tag{3.5}$$

$$Absorption\ \% = \frac{w_s - w_d}{w_s} \times 100 \tag{3.6}$$

Where,

Ws = Saturated weight of cube, kg

Wd = oven-dry weight of cube, kg

Vc = volume of cube, m^3

3.5 Experimental Program of Mortar

This section presents the mix proportions, casting and curing of the test mortar specimens. Three cubes (50 mm^3) of insulation mortar were cast for each mix. The three insulation materials (VL, PL and RU) were used in the mix as replacement of sand.

3.5.1 Mix Proportions

The dosage of the cement and sand in the control mix followed the conditions of ASTM C270 (i.e., the aggregate sand should be more than 2.5 and less than 3 times of the volume of cement according to ASTM C270) [67]. The sand was replaced by vermiculite, perlite and rubber with percentages of 5, 10 and 15% by weight. Ten mixes were prepared, the control, vermiculite, perlite and rubber mortars, as presented in Table 3.15.

Table 3.15: Mix proportions for one m^3 of control, vermiculite, perlite and rubber mortars

Mix Proportion	Control	VL-5	VL-10	VL-15	PL-5	PL-10	PL-15	RU-5	RU-10	RU-15
Cement (kg)	445	445	445	445	445	445	445	445	445	445
Gross water (kg)	267	377	524	599	315	342	359	265	263	261
Free water (kg)	245	245	245	245	245	245	245	245	245	245
Sand (kg)	1495	1240	918	749	1032	767	597	1334	1192	1065
Vermiculite (kg)	---	65	102	132	---	---	---	---	---	---
Perlite (kg)	---	---	---	---	54	85	105	---	---	---
Rubber (kg)	---	---	---	---	---	---	---	70	132	188

3.5.2 Casting and Curing

For each mortar mix, nine cubes (50 mm) and three discs (50 mm diameter and 25 mm thickness) were cast and compacted using vibration table. The cubes were used to measure the compressive strength, absorption and density while the discs were used to measure the thermal conductivity (See Figure 3.13). Each three cubes were cured for 7, 14 and 28 days in sweet water inside the laboratory.

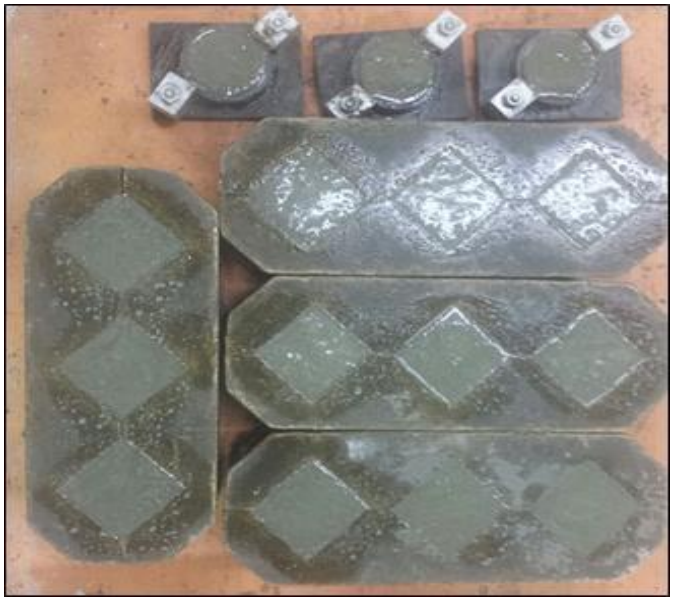

Figure 3.13: 50-mm cubes and thermal discs

3.5.3 Compressive Strength, Absorption and Density

The test procedures for determining the compressive strength, absorption and density were explained in details in Sections 3.4.2.A and 3.4.2.C.

For the compression test of insulation cement mortar, 50 mm cubes were tested for all the ten mixes (vermiculite, perlite and rubber). In addition, three cubes were tested for each mix.

3.5.4 Thermal Performance

For each mix, three discs (50 dia. x 25 mm thickness) were prepared to calculate the k-value. According to ASTM C518-04 and E1530-06, an instrument called FOX50 heat flow was utilized to gauge the thermal conductivity coefficient. As shown in Figure 3.14, the FOX50 works in linking with a cooling unit (air pump and water flow) and desktop computer compatible with a serial RS-232 interface by using Laser Comp's "WinTherm50" software. The tested method is easily operated using "WithTherm50" software whereby the measurer has to only input the file name, and the upper and lower temperatures for plates of the instrument. Normally, the temperature of the upper plate should always be 10 °C (18 F) higher than that of the lower plate [68]. Both plates have a sensitive heat flow transducers and thermocouples [68].

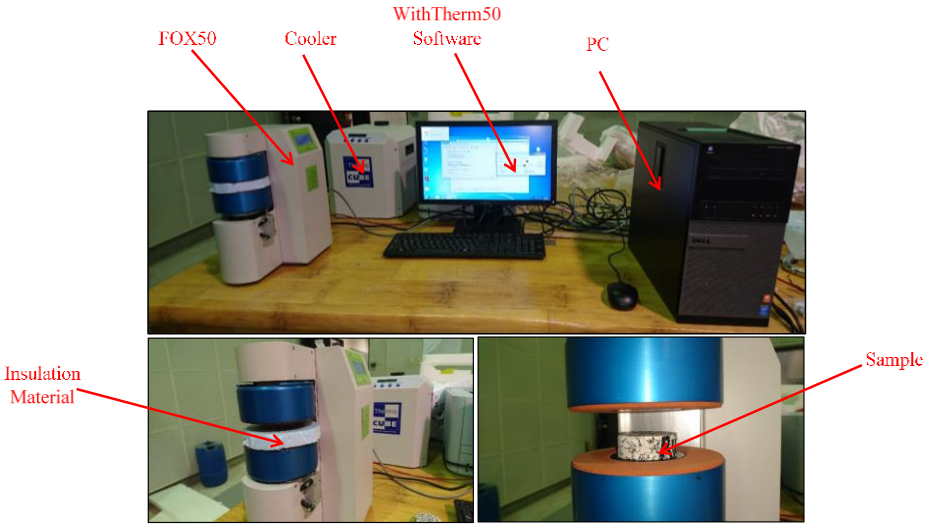

Figure 3.14: FOX50 heat flow meter instrument setup

As shown in Figure 3.15, the specimens must be polished at the top and bottom surfaces because the plates of the thermal machine are very sensitive and smoothening both surfaces of the samples reduce the thermal resistivity due to air gaps [68].

Figure 3.15: Polished specimen from both surfaces

After polishing, all the specimens must be inserted inside the oven under 60°C for 48 hr (Figure 3.16) to ensure that the samples are totally dried because the moisture inside the concrete will affect the readings for thermal conductivity.

Figure 3.16: All samples inside the oven under 60 °C

CHAPTER 4

EXPERIMENTAL RESULTS ANDDISCUSSION

4.1 Introduction

The results and discussion of the experimental work are presented in this chapter. Firstly, the mechanical and thermal properties of masonry blocks were presented, followed by the same properties for insulated cement mortar. For the trial mixes of concrete blocks, cubes (100×100×100 mm) were cast to measure the compressive strength, absorption and density in order to select the optimum mix design proportions. After the optimal mix designs were selected, the insulated concrete blocks were cast and cured to study the compressive strength, density and absorption in order to select the mixes that meet the requirements of ASTM C-129 standard.

For the mortar specimens, compressive strength, absorption and density were studied using cubes (50 mm). Moreover, mortar discs (50 mm diameter and 25 mm thickness) were cast, cured, polished, dried and prepared to measure the k-value of insulated cement mortar using FOX50 heat flow meter instrument.

4.2 Experimental Results for Masonry Blocks

4.2.1 Compressive Strength Test

The trial design of mixes was optimized to get acceptable strength that satisfies the ASTM C129 standard. Tables 3.11 to 3.14 show the results of the 28-day compressive strength

and density for the trial mixes with the optimal mixes for producing the blocks. Three 100-mm cubes and three blocks were cast for each mix.

The optimal mixes were G1-TM5, G3-TM2, G3-TM5 and G1-TM5, as shown in Tables 3.11 to 3.14, respectively, and were presented by volume and weight in Table 4.1. These four mixes were selected because they satisfied the compressive strength requirements of 3.45 MPa (ASTN C129).

Table 4.1: Summary of optimum mix proportions (by weight and Volume)

Materials	Control mix (by weight, kg)	Control mix (by volume %)	EPS mix (by weight, kg)	EPS mix (by volume)	LDPE mix (by weight, kg)	LDPE mix (by volume)	VL mix (by weight, kg)	VL mix (by volume)	VS mix (by weight, kg)	VS mix (by volume)
Gross Water	115	12	115	12	111	11	290	29	173	17
Cement	195	6	195	6	195	6	250	8	195	6
CA 3/16 in	1132	44	1006	39	708	27	856	33	----	----
CA 3/32 in	338	13	----	----	211	8	256	10	----	----
FA (sand)	451	18	576	22	681	27	359	14	792	31
Air	----	10	----	10	----	10	----	10	----	10
EPS	----	----	2.1	13	----	----	----	----	----	----
DLPE	----	----	----	----	102	12	----	----	----	----
VL	----	----	----	----	----	----	58	13	----	----
VS 3/16	----	----	----	----	----	----	----	----	499	33
VS 3/32	----	----	----	----	----	----	----	----	161	10

Table 4.2 presents the compressive strength and other properties of these five optimal mixes. Five types of hollow blocks (control, polystyrene, low-density polyethylene, vermiculite and scoria blocks) were cast to conduct the compressive strength test. The results showed that all blocks had compressive strength higher than 3.45 MPa, which is

considered as the minimum value for non-load bearing concrete block as per ASTM C129 [69].

Table 4.2: Mechanical properties of blocks

Block type	Block strength (MPa)	Weight (kg)	Density (kg/m^3)	Absorption (kg/m^3)	Absorption (%)
Control	7.26	19.91	1882	103	5.5
EPS	4.59	16.72	1775	149	7.75
LDPE	4.45	18.16	1875	130	6.88
VL	3.87	18.62	1855	254	13.42
VS	3.53	16.25	1751	134	7.66

As expected, the control blocks achieved the highest compressive strength value with 7.26 MPa without adding any insulation materials in the mix, while the VS blocks got the lowest value of 3.53 MPa. The reduction in strength was 51, 47, 39, and 37% for the VS, VL, LDPE, and EPS blocks, respectively, as compared to the control block, as shown in Fig. 4.1.

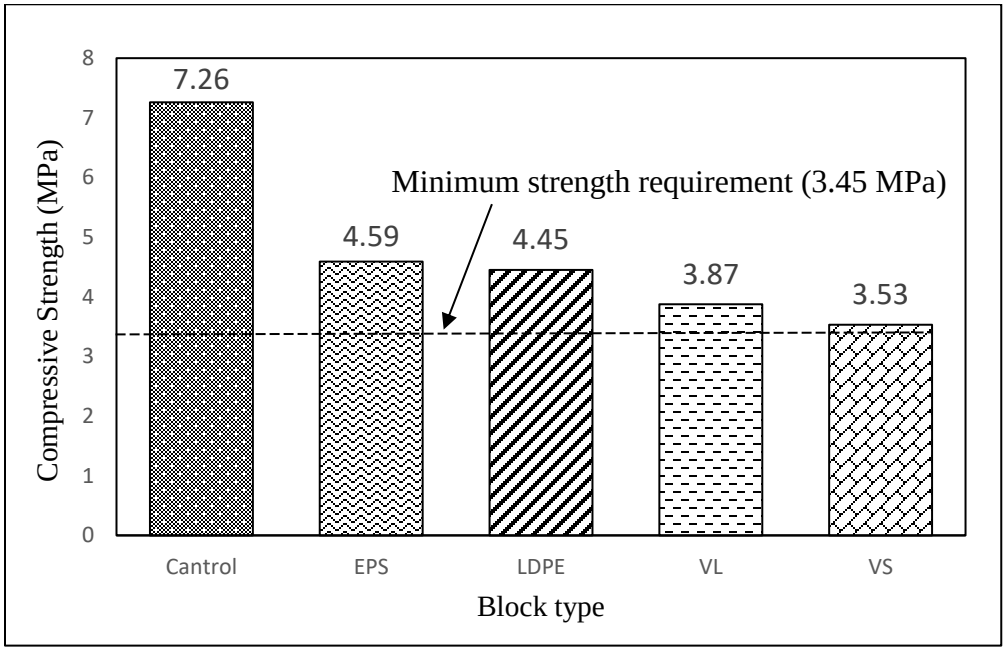

Figure 4.1: Compressive strengths for hollow insulation blocks

During the compressive test, cracking was not observed during the early loading. With the increase in the load, the cracks took place emanating from the corners on the short side and then they were developed continually downward and upward to form hourglass shape due to stress concentration, as shown in Figure 4.2. In addition, the corner cracks went to the middle of the long side of the block because the outer narrow widths of the block had no concrete stiffener in the middle to prevent the plane deformation.

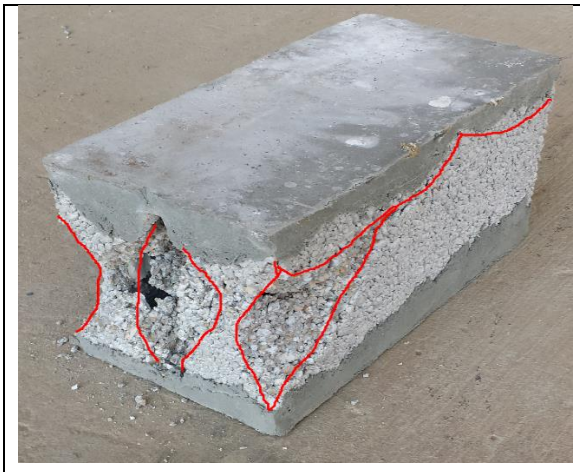

Crack of control block

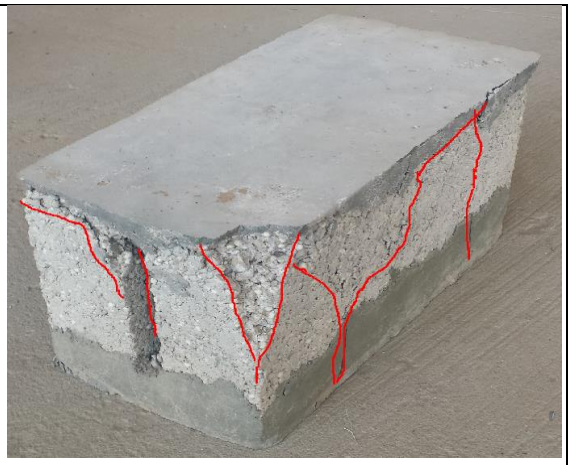

Crack of EPS block

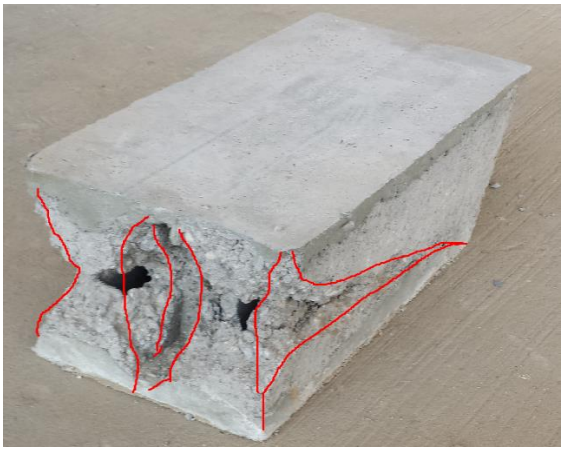

Crack of LDPE block

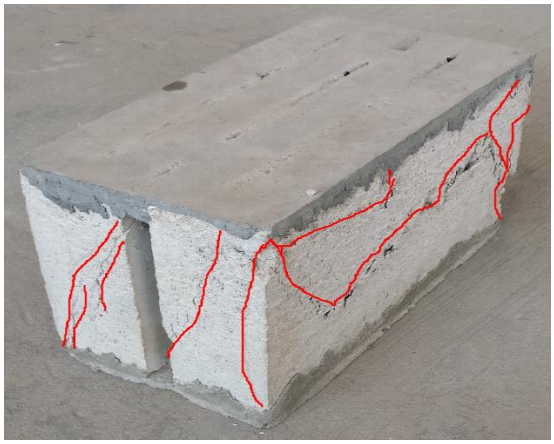

Crack of VL block

Figure 4.2: Crack development during compression of hollow blocks

4.2.2 Equivalent Thermal Conductivity

The equivalent thermal conductivity of the developed blocks was determined experimentally using the guarded hot plate (ASTM C177). Table 4.3 presents the k-values for each block and their % reduction, as compared with that of the control block. The equivalent thermal conductivity of the VS block was the lowest value (0.340 W/m.K) followed by the EPS block (0.371 W/m.K) and then by both LDPE and VL.

Table 4.3: Equivalent thermal conductivity of blocks

Block Type	k-value (W/m.K)	Improvement (%)
Control	0.460	---
EPS	0.371	19.3
LDPE	0.382	17.0
VL	0.383	16.7
VS	0.340	26.1

Since the order of blocks from the point of low density (from lowest to highest) was VS, EPS, VL, LDPE and control block, as shown in Table 4.2. It is logically that the order of blocks in terms of the thermal conductivity coefficient should the same becuase there is a direct correlation between the density and the thermal conductivity [29]. However, the LDPE block had slightly lower equivalent thermal conductivity than VL block. The reason for this difference could be ascribed to the fact that the VL block retained some water inside the flakes of vermiculite, which is difficult to remove by field exposure, and if the block is placed in the oven at relatively high temperature, hair cracks may develop and the heated flow through the block will increase. In addition, the test will not represent the real case of the masonry block in the field and the value of the thermal conductivity in reality will be

higher than that was experimentally determined because the thermal conductivity increased with increasing the water content in the block [70].

The control hollow block had higher equivalent thermal conductivity than all the other insulated hollow blocks by 26.1, 19.3, 17.0, and 16.7% for VS, EPS, DLPE, and VL blocks, respectively. Since the geometry layout of the cavities was the same for all the hollow blocks, the reduction was totally ascribed to the thermal conductivity of the replacement materials.

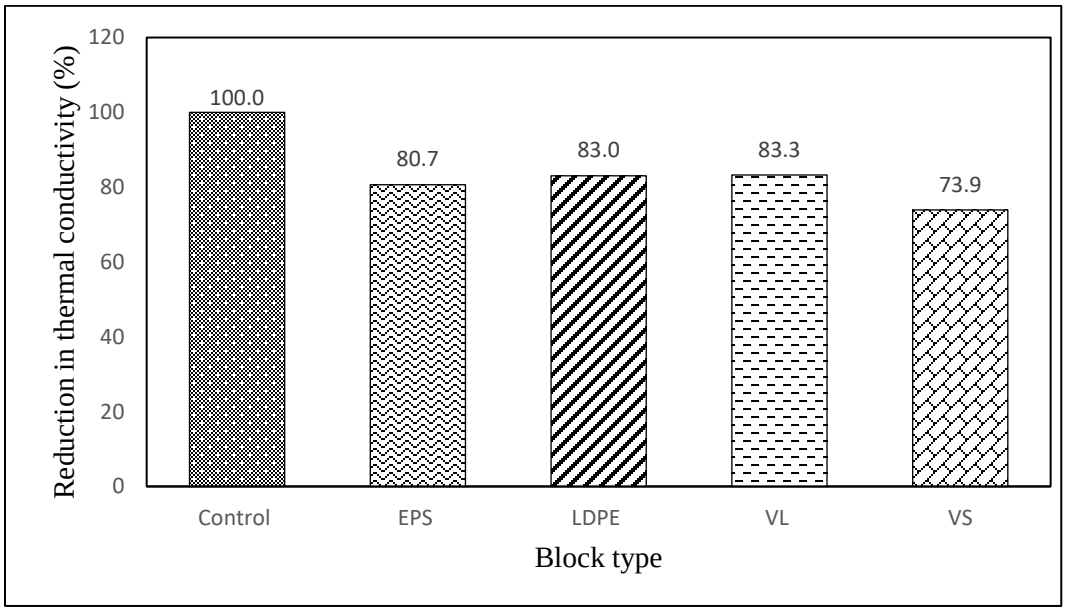

Figure 4.3: Reduction in equivalent thermal conductivity, as compare with control hollow blocks

4.2.3 Density and Absorption

According to the weight of masonry blocks, ASTM C 90 classifies the block into three categories: lightweight, medium weight and normal weight [71], as presented in Table 4.4. All the blocks in this research were considered as medium-weight masonry blocks because their dry densities were between 1680 and 2000 kg/m^3, as shown in Figure 4.4.

Table 4.4: ASTM C-90 absorption requirements

Water Absorption, max (kg/m^3)		
Lightweight, less than (1680)	Medium weight (1680-2000)	Normal Weight, (2000) or more
288	240	208

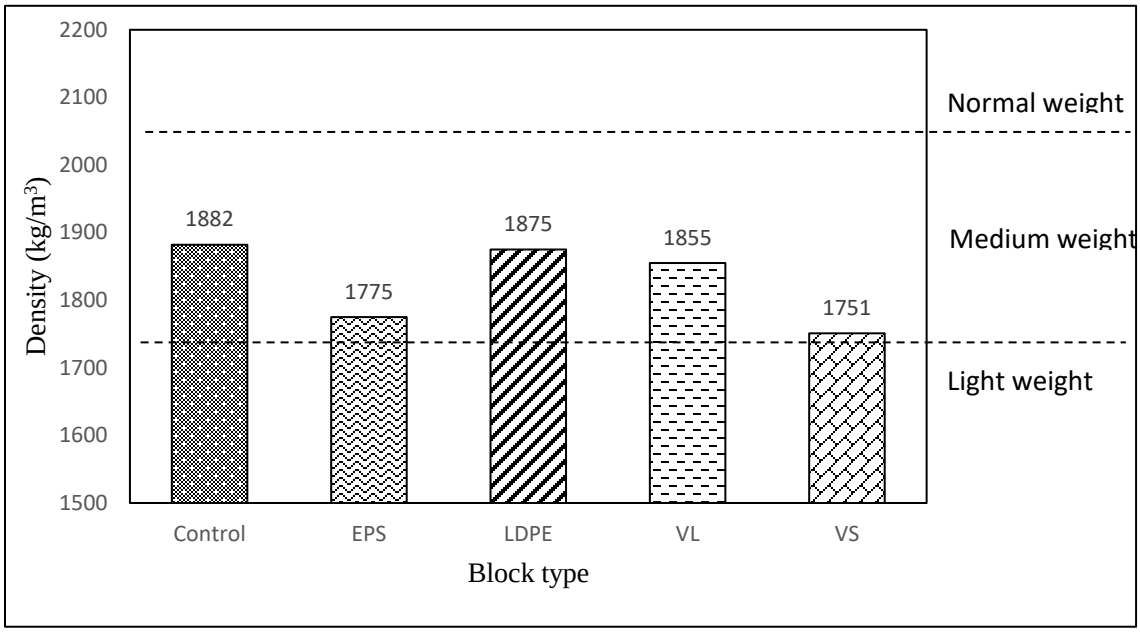

Figure 4.4: Density of control and developed hollow blocks.

Although the EPS aggregate is the lightest material, the VS block had the lowest density in this work because the dosage of the VS aggregate was 43% per meter cube, whereas the dosage of the EPS aggregate was 13% per meter cube because the EPS is a very weak material (i.e., very low density) and if the dosage of the EPS increases, the strength will dramatically decrease. The control block had the highest density which is slightly higher than LDPE and VL block by 0.37% and 1.43%, respectively. It is to be noted that the sand was increased in the mixes of LDPE and VL in order to increase the cement paste. For this reason, the voids were reduced and the sample became denser. Further, the control mix had higher density than EPS and VS blocks by 5.69 and 6.96%, respectively, as shown in Figure 4.4.

It can be noted that EPS block had a higher water absorption than LDPE block, as illustrated in the Table 4.2. Since both EPS and LDPE have low absorptive capacity, the difference was ascribed to the air gaps inside the EPS block due to the high CA/TA ratio in the mix, which leads to store more water, thus increasing the absorption in the block. In contrast, the ratio of CA/TA in the mix of LDPE block was higher as compared to VS block, but the absorption of VS block was higher than LDPE. The reason for that is ascribed to the fact that the VS aggregate has higher absorptive capacity and its dosage was high in the mix (43%). The absorption of VS, LDPE and EPS aggregates was 11, 0, 1.5%, respectively. The control block had the lowest water absorption, which was lower by 26, 30, 45 and 147%, as compared with the LDPE, VS, EPS, and VL blocks, respectively. All blocks met the ASTM C90 requirement for the absorption of medium weight blocks (240 kg/m^3), except for the VL block which had a little higher absorption than the maximum value for ASTM C90 requirement, as illustrated in Figure 4.5. From the literature [36] and the work in this research, the water absorption of the VL aggregate is estimated to be around 450% [49]. That is why the VL block had the highest water absorption.

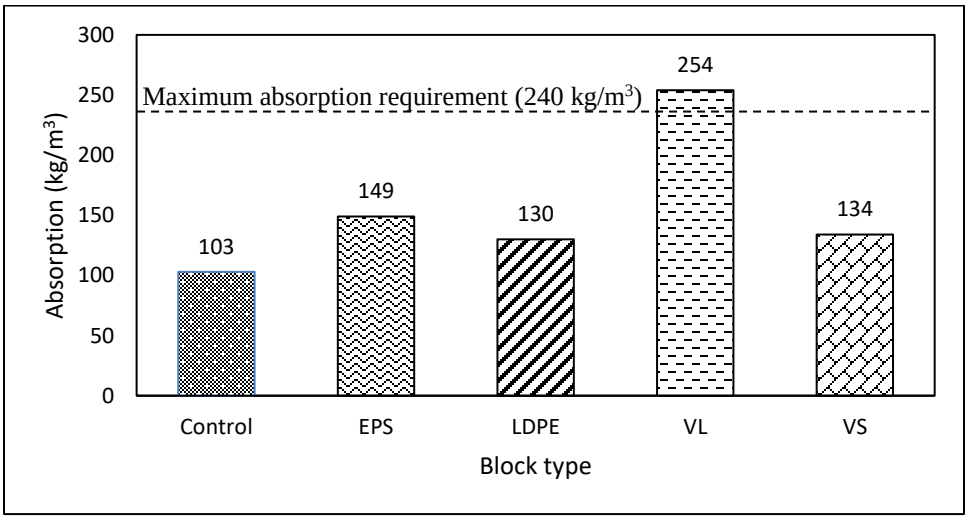

Figure 4.5: Absorption of control and developed hollow blocks

The weight of the volcanic scoria block was 16.25 kg, which was the lightest, as compared to the other hollow blocks in this research. The expanded polystyrene was the second lightest block by 16.72 kg, while the control block was the heaviest block by 19.91 kg with the differences of 1.29 kg (7%), 1.75 kg (9%), 3.19 (16%) and 3.66 kg (18%), as compared to the VL, LDPE, EPS and VS blocks, respectively, as shown in Figure 4.6. This reduction in weight for insulation blocks would minimize the dead load on the structural members, which is considered the largest load on structures [72].

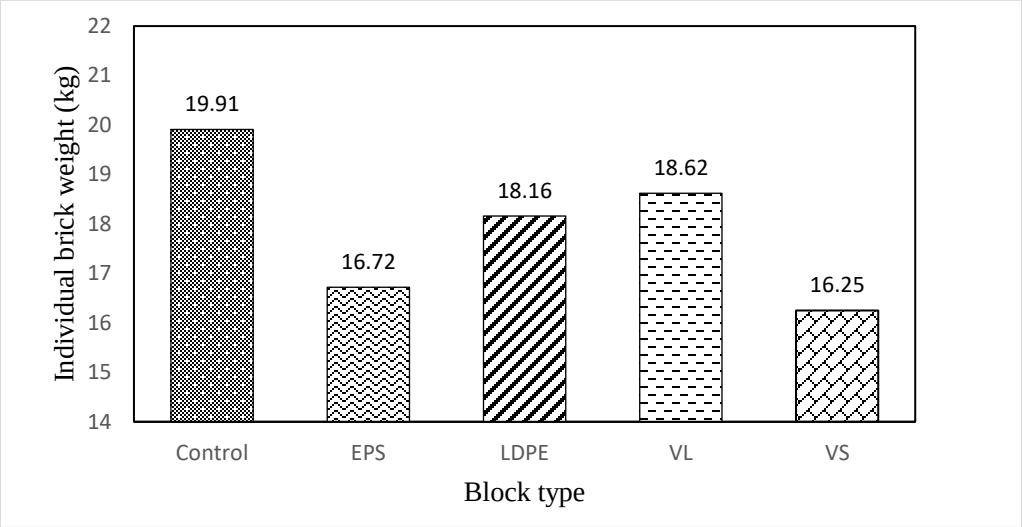

Figure 4.6: Weight of control and developed hollow blocks

4.3 Experimental Results for Insulation Mortar

4.3.1 Compressive Strength Test

The compressive strength of the control, perlite, vermiculite and rubber mortar mixes was summarized in Table 4.5 after a curing period of 7, 14 and 28 days. All the strengths satisfied the ASTM C 270 for mortar specifications (5.4 MPa) [10] even after 7 days of curing. For the control mortar, 80% of the strength was gained in the first 7 days with 22.42 MPa and increased slightly to 27.52 and 32.16 MPa, for 14 and 28 days, respectively.

Table 4.5: Compressive strength of control, perlite, rubber and vermiculite

Time (Days)	Control (MPa)	Perlite (MPa)			Rubber (MPa)			Vermiculite (MPa)		
		5%	10%	15%	5%	10%	15%	5%	10%	15%
7	22.42	13.39	12.05	11.49	20.00	14.08	7.75	10.84	7.73	5.61
14	27.52	22.32	17.92	16.96	22.68	17.27	10.67	12.36	8.60	6.96
28	32.16	26.84	19.48	18.68	25.95	19.21	12.31	15.84	11.41	7.08

As shown in Fig. 4.7, the strength of perlite mixes was lower than the control by 48, 55 and 62% for 5, 10 and 15% perlite mortar, respectively, for 7 day curing. The strength was reduced sharply because the pozzolanic reaction might have not been fully activated. Thereafter, the strength gain increased gradually till 28 days with an increment of about 50%.

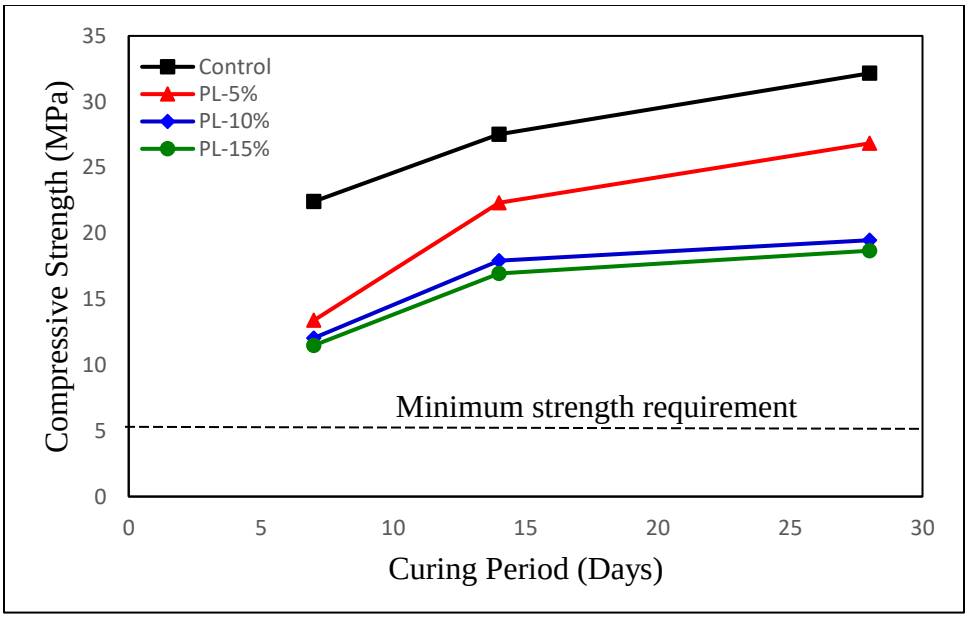

Figure 4.7: Compressive strength for perlite mortar

The strength of vermiculite and rubber mortars was decreased with increasing the dosage of insulation material, as shown in both Figures 4.8 and 4.9. For the rubber mortar, the strength was decreased by 21, 41 and 63% for 5, 10 and 15% of rubber contents,

respectively. For the vermiculite mortar, the reduction of strength was 52, 65 and 79% for 5, 10 and 15% of the vermiculite contents, compared to the control mortar after 28 days.

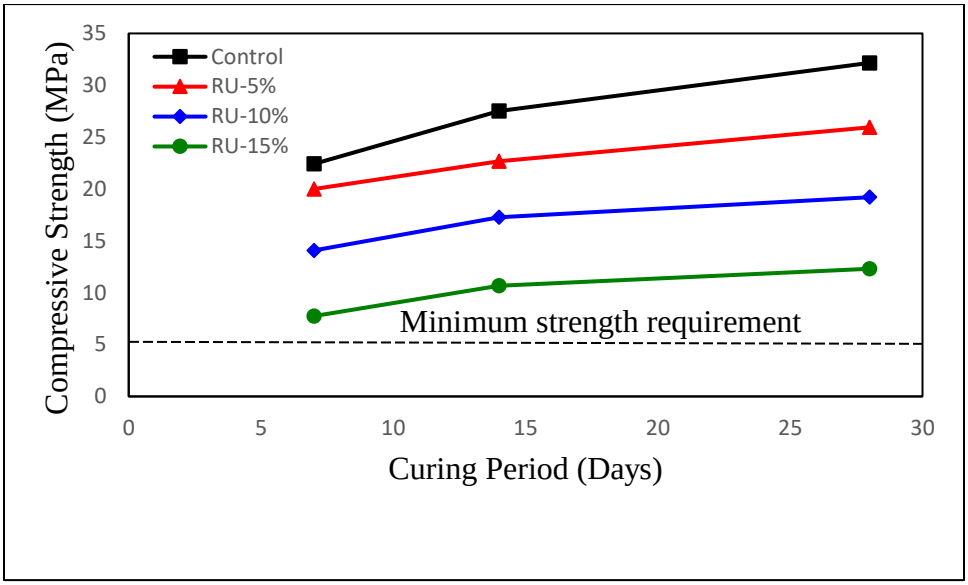

Figure 4.8 Compressive strength for rubber mortar

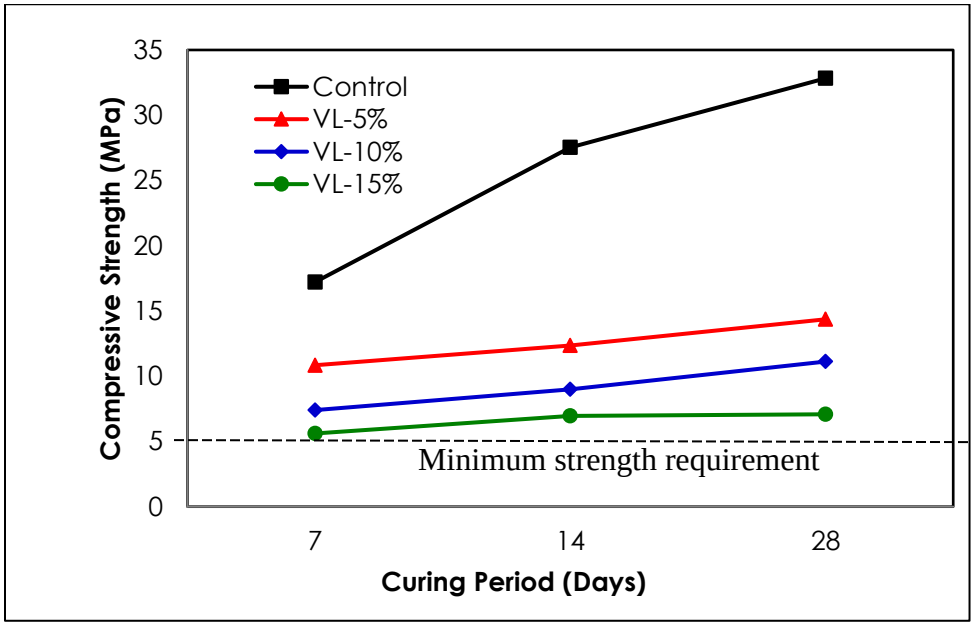

Figure 4.9 Compressive strength for vermiculite mortar

Figures 4.10 and 4.11 compare the compressive strength of perlite, rubber and vermiculite mortars with the contents of 5, 10 and 15%. The trend of compressive strength for rubber

and vermiculite mortars are nearly the same whereby the strength increased linearly with time for all dosages in Figs. 4.10. As shown in Figures 4.10 and 4.12, the strength of rubber mortar was higher than perlite by 20 and 30% for the content of 5 and 10%, respectively, after 7 days. On the other hand, the difference was minimal after 14 and 28 days for both perlite and rubber, which could be ascribed to the perlite powder that can be used as supplementary "pozzolanic" material because it has high content of silica, as shown in Table 3.10.

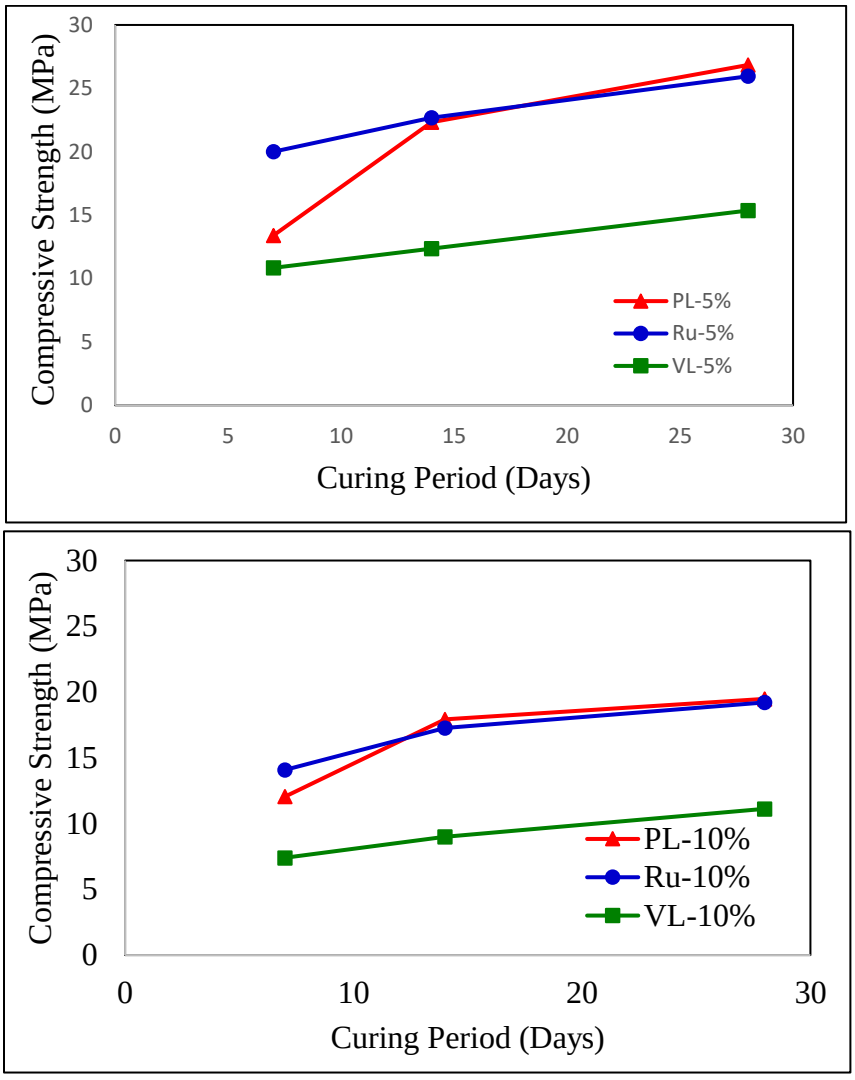

Figure 4.10: Comparison between compressive strength for perlite, rubber and vermiculite mortar (5 and 10%)

For the content of 15%, the strength of perlite mortar was higher than that of rubber and vermiculite mortars. The reason behind the reduction in the strength of rubber mortar with 15% could be ascribed to the formation of air pockets in the matrix of the mortar, as shown in Figure 4.11.

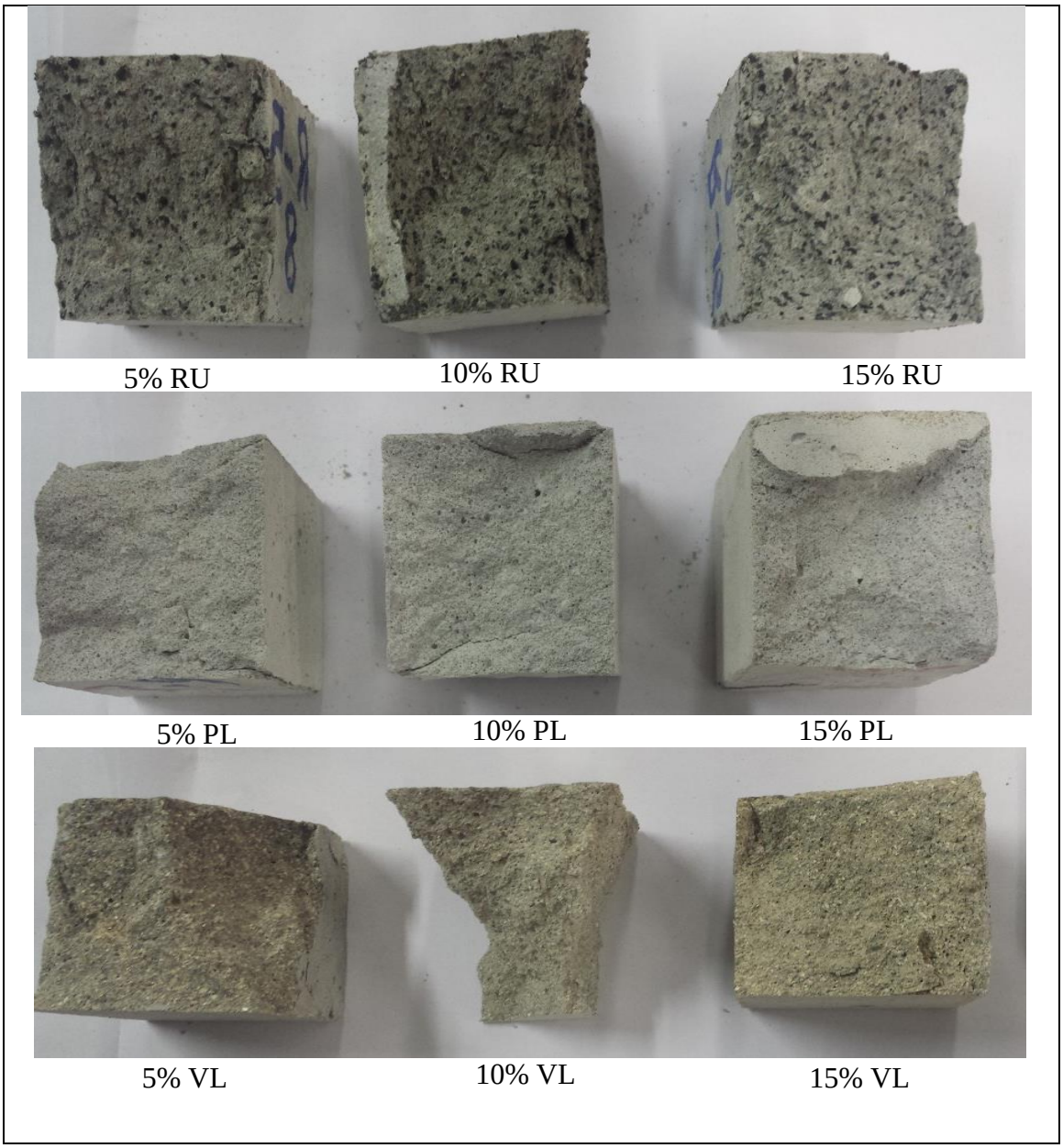

Figure 4.11: Distribution of insulation ingredients in the mortar

On the other hand, the strength of perlite mortar was increased with time, which is attributed to the increase in cement hydration in the presence of perlite due to the high content of silica (i.e., 33.8%). Due to this quantity of silica, the perlite may be used as a supplementary cementing material [73], as illustrated in the following pozzolanic reactions [74]:

During the hydration of cement, the calcium silicate hydrate and portlandite are produced

$$\underset{(C_3S \text{ or } C_2S)}{CS} + \underset{H_2O}{H} \dashrightarrow \underset{\text{(Calcium silicate hydrate)}}{C\text{-}S\text{-}H} + \underset{[Ca(OH)_2 \text{ or portlandite}]}{CH} \qquad (4.1)$$

This calcium hydroxide (or portlandite) reacts chemically with the silica in the presence of moisture at ordinary temperature to form compounds possessing cementitious properties, as illustrated in Equation 4.2.

$$\underset{\textit{(amorphous silica from perlite)}}{SiO_2} + \underset{\text{portlandite from cement}}{Ca(OH)_2} \xrightarrow[\textit{Normal temperature}]{H_2O} \underset{\textit{(secondary)}}{C\text{-}S\text{-}H} \qquad (4.2)$$

The calcium silicate hydrate (C-S-H) formed is known as “secondary” to differentiate it from the primary C-S-H, the latter being formed by the reactions of C_3S and C_2S phases during cement hydration. Therefore, the perlite can use as a filler material (physical reaction) and/or pozzolanic material (chemical reactions).

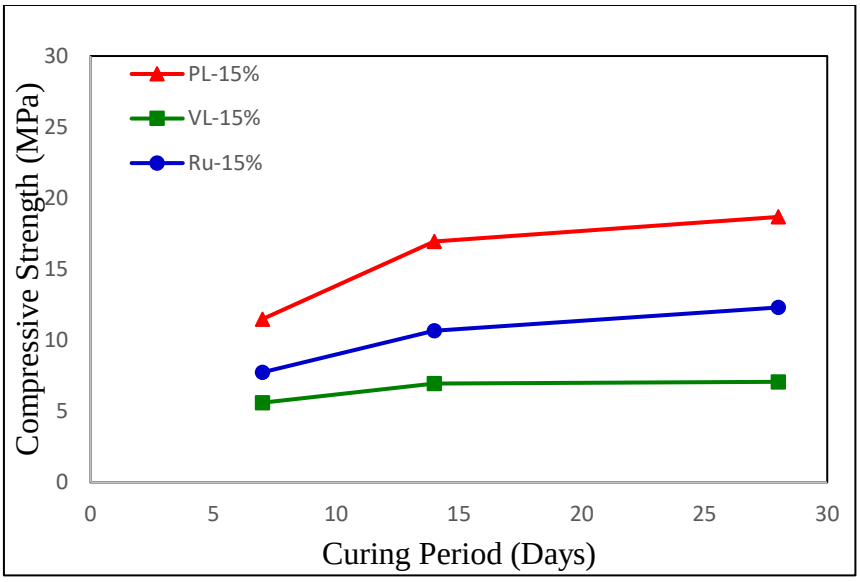

Figure 4.12: Comparisons between compressive strength for perlite, rubber and vermiculite mortar (15%)

4.3.2 Thermal Conductivity

The results of thermal conductivity (k-value) of the mortar using vermiculite, perlite and rubber are summarized in Table 4.6 for the contents of 5, 10 and 15%. The data in this table indicate that the k-values decreased with increasing the content of rubber, perlite and vermiculite. Further, the mortar specimens with vermiculite achieved the lowest thermal conductivity, as shown in Fig. 4.13. The maximum reductions were 57, 47 and 36% for vermiculite, perlite and rubber, respectively, for the replacement content of 15%. The thermal conductivity tends to decrease with increasing the content from 5 to 10% by about 20% for vermiculite and perlite mortars and 17% for rubber mortar, while this reduction slightly decreased with increasing the content from 10 to 15% by about 16, 15 and 17% for vermiculite, perlite and rubber, respectively.

Table 4.6: Thermal conductivity of perlite and rubber mortars

Content	Thermal Conductivity (W/m.k)		
	Vermiculite	Perlite	Rubber
0	1.23	1.23	1.23
5	0.80	0.95	1.14
10	0.63	0.76	0.95
15	0.53	0.65	0.79

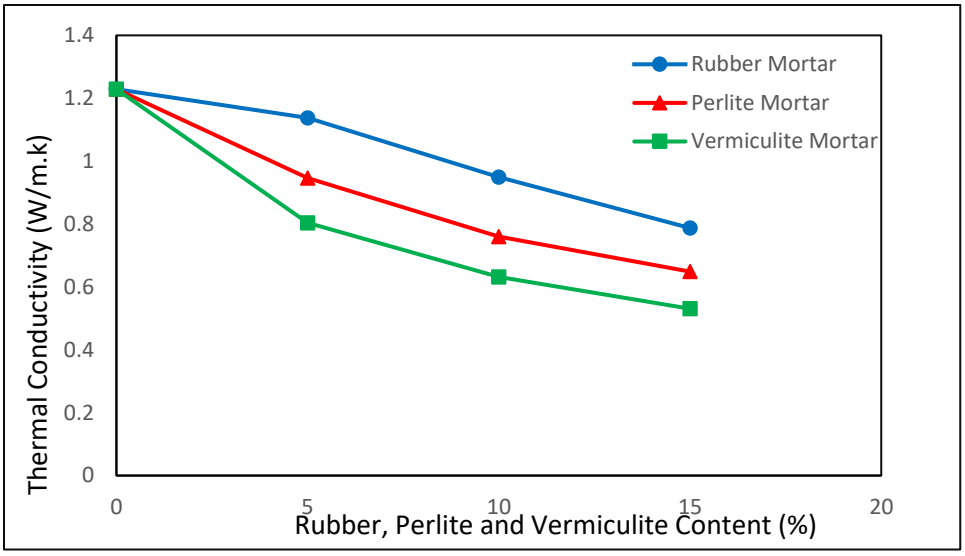

Figure 4.13: Thermal conductivity for vermiculite, perlite and rubber mortars

4.3.3 Density and Absorption

The results of density and absorption are summarized in Table 4.7 for rubber, perlite and vermiculite mortars. The density was in the range of 1420 to 2150 km/m^3.

Table 4.7 Absorption, wet and dry densities of perlite and rubber mortars

Mortar	Control	Rubber			Perlite			Vermiculite		
Content	0	5%	10%	15%	5%	10%	15%	5%	10%	15%
Density (kg/m^3)	2150	2080	2030	1830	1830	1630	1560	1780	1580	1420
Absorption (%)	7.1	6.5	7.4	9.3	12.2	15.8	17.4	14.2	18.8	23.8

The density of the vermiculite and the perlite mortars was much lower than the density of the rubber mortars because the specific gravity of vermiculite and perlite is much lower

(0.12 for vermiculite and 0.15 for perlite) than the specific gravity rubber (1.12). The density of the vermiculite mortar is the lowest in this research and it is lower than the control mortar by about 17, 27 and 34% for 5, 10 and 15% of vermiculite contents, respectively. The perlite mortar density was reduced by about 15, 24, and 27% with increasing the perlite content to 5, 10 and 15%, respectively, as compared to the control mortar (Fig. 4.14).

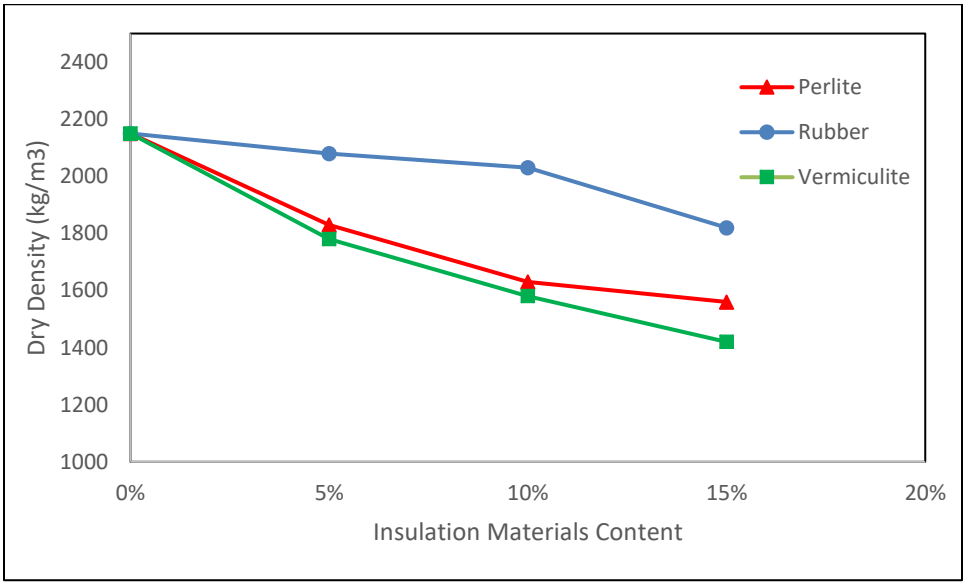

Figure 4.14: Density of vermiculite, perlite and rubber mortars

The absorption of the control mortar was 7.1%, which was increased sharply for perlite mortar by 72, 123 and 145%, for 5, 10 and 15% perlite content, respectively, as illustrated in Table 4.7. For the rubber mortar, since the absorption of sand was higher than that of rubber (rubber has almost no absorption), the absorption of 5% rubber mortar was reduced by 8%, as compared to the control mortar. Although the amount of sand was higher in the control mortar, the absorption was slightly lower (4%) than 10% rubber mortar, which could be ascribed to the formation of air pockets, as shown in Figure 4.11. Similarly, the 15% rubber mortar has much higher absorption than the control mortar by about 31%. All

the absorption of mortar specimens satisfies the ASTM C 270 requirements for mortar specification (i.e., 18%) except for VL-10% and VL-15% (higher 18%), as displayed in Figure 4.15. Since vermiculite absorption is estimated by 530% [49], the vermiculite mortar had the highest water absorption by 100, 165 and 235% for 5, 10 and 15% vermiculite contents, compared to the control mortar. Due to this high absorption, the 10 and 15% dosages of vermiculite exceeded the ASTM C270 limit for the maximum water absorption, as shown in Figure 4.15.

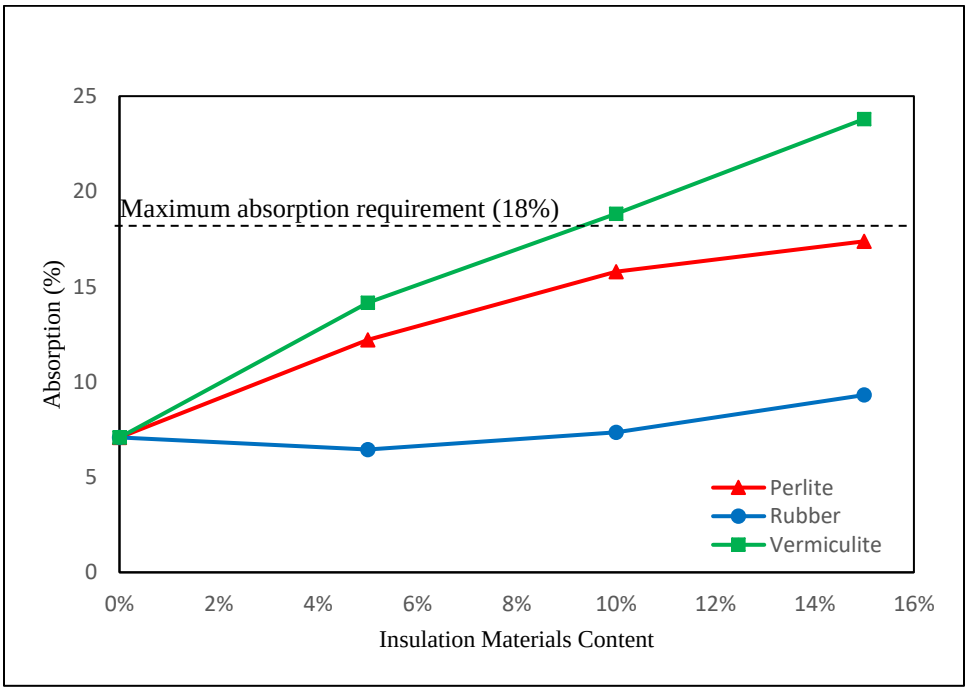

Figure 4.15: Absorption of vermiculite, perlite and rubber mortars

CHAPTER 5

FINITE ELEMENT MODELING

5.1 Introduction

Heat transfer phenomenon is a physical act of the thermal energy which is produced by dissipating heat between two systems. The heat flow and different temperature surfaces are the components of heat transfer. The heat flow from a surface to another is activated by thermal energy and can be drived by the different temperature between the surfaces.

In this research, ANSYS Fluent 19.2 software was used to validate the results obtained from the model developed in ANSYS and the results of guarded hot plate test results which were addressed in Chapter 4. Two hollow blocks were used to simulate the blocks which were tested in the guarded hot plate. Thereafter, the validated model was utilized to conduct a parametric study to investigate the effect of block type and plastering on the heat transfer through the wall. The parametric study of the thermal analysis of wall included using four types of block (PS, LDPE, VL and VS block) and three types of mortar and plaster (VL, PL and RU).

According to the Energy Conservation law, kinetic energy produces thermal energy and vice versa [75]. When the temperature rises, the molecules move in linear motion and vibration. The molecules in high kinetic energy region try to transfer the energy to the lower kinetic energy region. In general, the following three phenomena can occur during

heat transfer through hollow blocks wall: Conduction, convection, and radiation, as shown in Figure 5.1 [76].

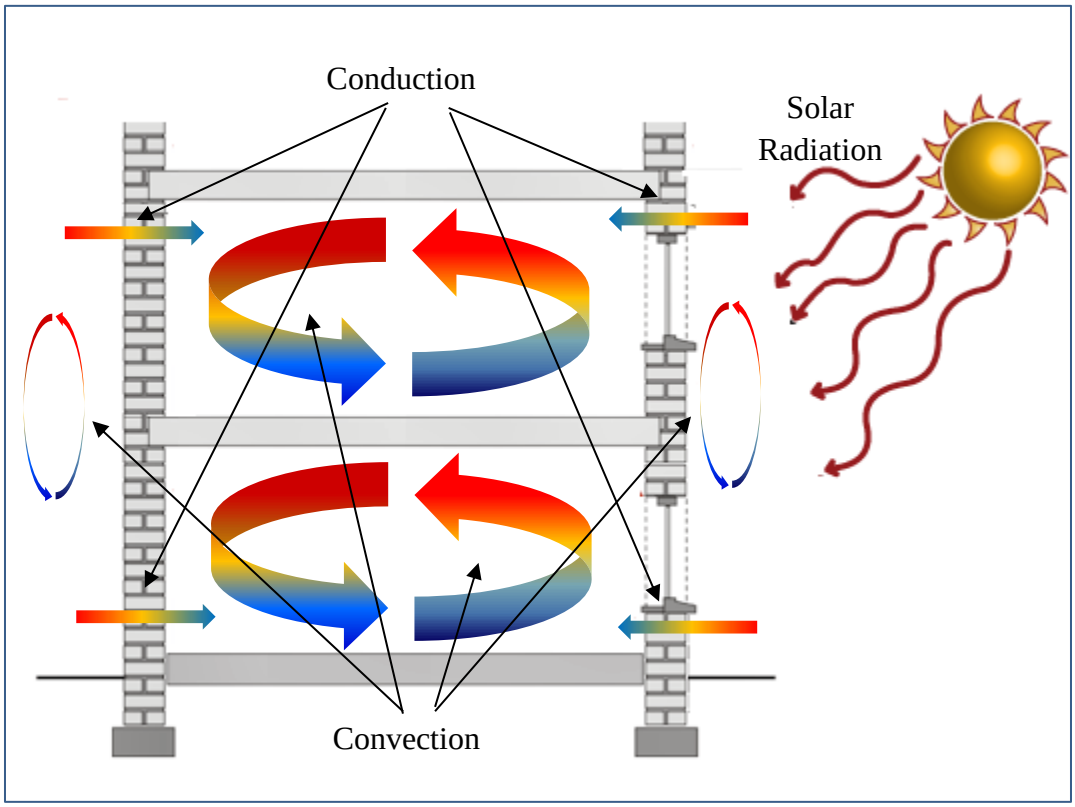

Figure 5.1: Heat transfer phenomena: Conduction, convection and radiation.

5.1.1 Conduction

Conduction is caused by direct molecular impact. A region with higher kinetic energy transfers the thermal energy to a region with lower kinetic energy [77]. Particles with high speed collide with particles with slow speed. As a result of this collision, the kinetic energy for slow speed particles increases and causes the particles to have high speed and, therefore, the heat transfer becomes continuous.

The heat conduction process depends on the following factors: Different temperature between the exterior and interior block surfaces, cross-section of the hollow block, travel

path length (rib concrete hollow block), and the thermal conductivity of block walls. As shown in Fig. 5.2, both the travel path and thermal conductivity of block play a significant role in conduction. The greater is the path length, the higher is thermal resistance and more energy is needed to heat the inner surface. The lower thermal conductivity is, the lower will be the heat flow transfer [78].

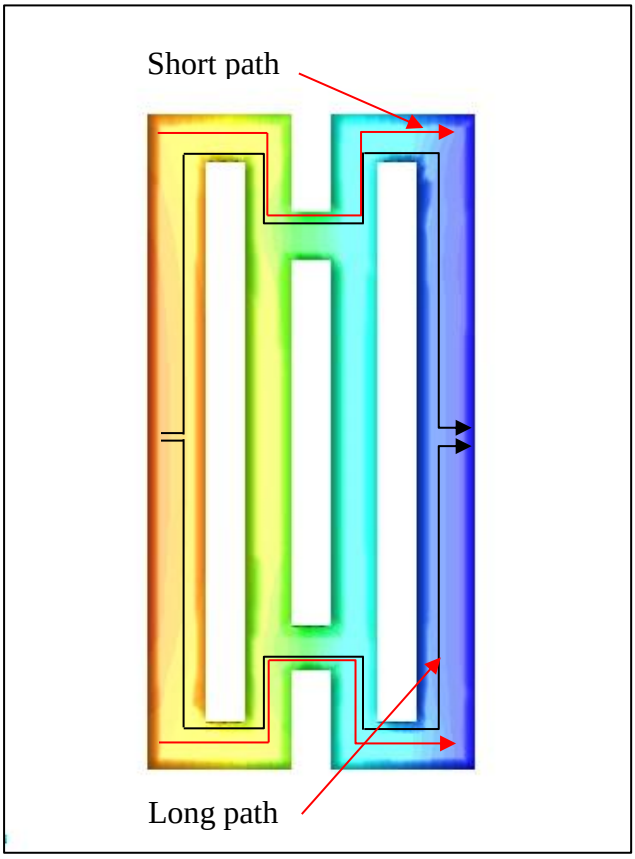

Figure 5.2: Long and short paths of heat transfer

The following equation calculates the rate of conduction [77]:

$$Q_{cond} = \frac{K\ A\ (T_{hot} - T_{cold})}{d} \tag{5.1}$$

Where

Q_{cond} = heat transferred due to conduction (W).

K = thermal conductivity of the block mix design (W/m.K).

A = heat-transfer area (m^2).

d = block thickness (m).

T_{hot} = temperature of hot region (K).

T_{cold} = temperature of cold region (K).

5.1.2 Convection

The convection phenomenon is the heat transfer due to the macroscopic motion of fluid (i.e., the gas or liquid moves from one region into another). It occurs between the layers of fluid as well as between the solid and fluid surfaces when they are in contact. When the fluid is heated, the hotter fluid becomes less dense and tends to rise, while the colder fluid becomes denser and tends to sink under the gravity influence. Thereby, the heat is transmitted due to this motion. There are two types of convection: Natural convection and forced convection. The natural convection occurs due to the variation of density within the fluid (liquid or gas) due to heating or cooling [77]. The forced convection occurs due to the pressure differences within the fluid [77]. Through the hollow blocks, the natural convection takes place and occurs on the exterior and interior surfaces of the wall and inside the cavities of the block, as shown in Figure 5.3 [79].

The heat convection process depends on the following factors: Aspect ratio, cavity width, cavity shape and number of cavities. However, the aspect ratio plays the most important part in convection process through hollow block [39, 81–84]. It is defined as the ratio between the cavity width (parallel to heat flux) to the cavity height. Increasing the aspect

ratio will decrease the heat transfer through the cavities [39, 81–84]. The equation for the heat transfer rate due to the convection is calculated as follows [77]:

$$Q_{conc} = h \times A \times (T_{hot} - T_{cold}) \quad (5.2)$$

where

Q_{cond} = heat transfer rate due to conduction (W).

h = heat transfer coefficient ($W/m^2.K$).

A = heat-transfer area [fluid area (m^2)].

T_{hot} = temperature of hot region (K).

T_{cold} = temperature of cold region (K).

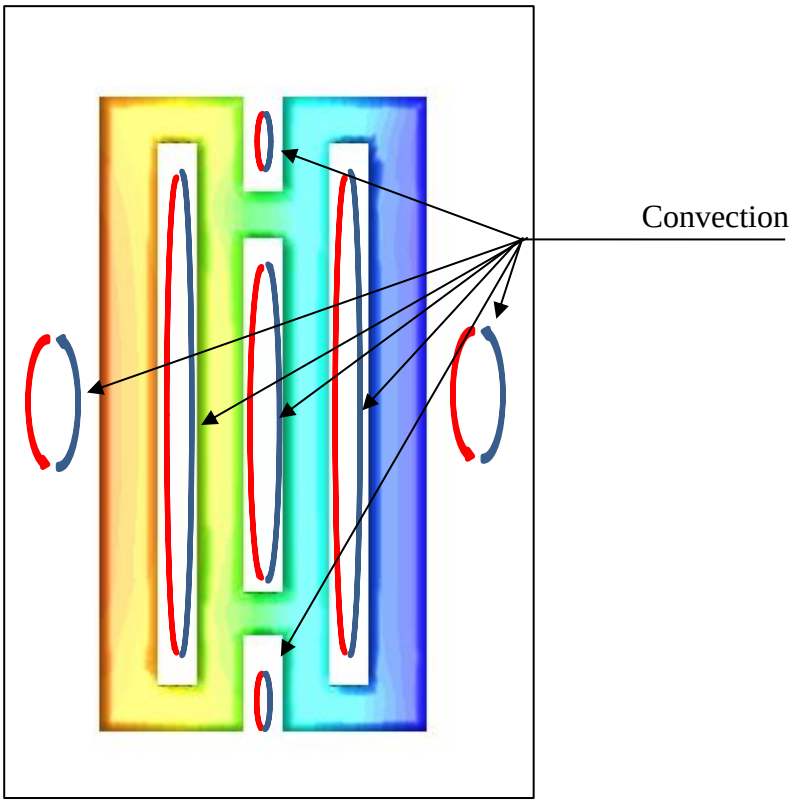

Figure 5.3: Convection around exterior and interior surfaces and inside the cavities.

5.1.3 Radiation

Thermal radiation is produced from the electromagnetic emitted waves. This means the two objects are not supposed to contact each other to transfer the heat or need fluid flow between the objects to transfer the heat [77]. The waves transmit the thermal energy away from the emitting body. Radiation is transferred through vacuum, air or any transparent medium (fluid or solid). Thermal radiation is generated from random movement of molecules and atoms in materials [77].

The materials radiate thermal energy according to their temperature. All objects that have temperature higher than 0 °K emit thermal radiation. The hotter is a body, the more radiation will develop. Further, they could absorb the thermal radiation emitted by the surrounding bodies. The difference between the total amount of emitted and absorbed radiation for any object leads to heat transfer which will make a change in the temperature of that object. Thermal radiation is calculated using the Stefan-Boltzmann law [84]:

$$q_{rad} = \varepsilon\sigma\ (T_r{}^4 - T_c{}^4) \tag{5.3}$$

Where:

q_{rad} = heat transferred due to radiation (W/m^2)

ε = emissivity coefficient of concrete block

σ = Stefan's constant, which equals 5.67 x 10-8 ($W/m^2.K^4$)

T_r = temperature of radiated surface (K).

T_c = temperature of surrounding air (K).

5.2 Geometry of Masonry Blocks

In this study, the hollow blocks with the same geometry of the specimen used in the guarded hot plate test was modeled using Fluent software. In this model, two block specimens were joined together with mortar. Thereafter, the two blocks were insulated by polystyrene board with the same dimension that was used in the guarded hot plate test as can be seen in Figure 5.4. Finally, the model was validated by comparing the results obtained from the model with the experimental one.

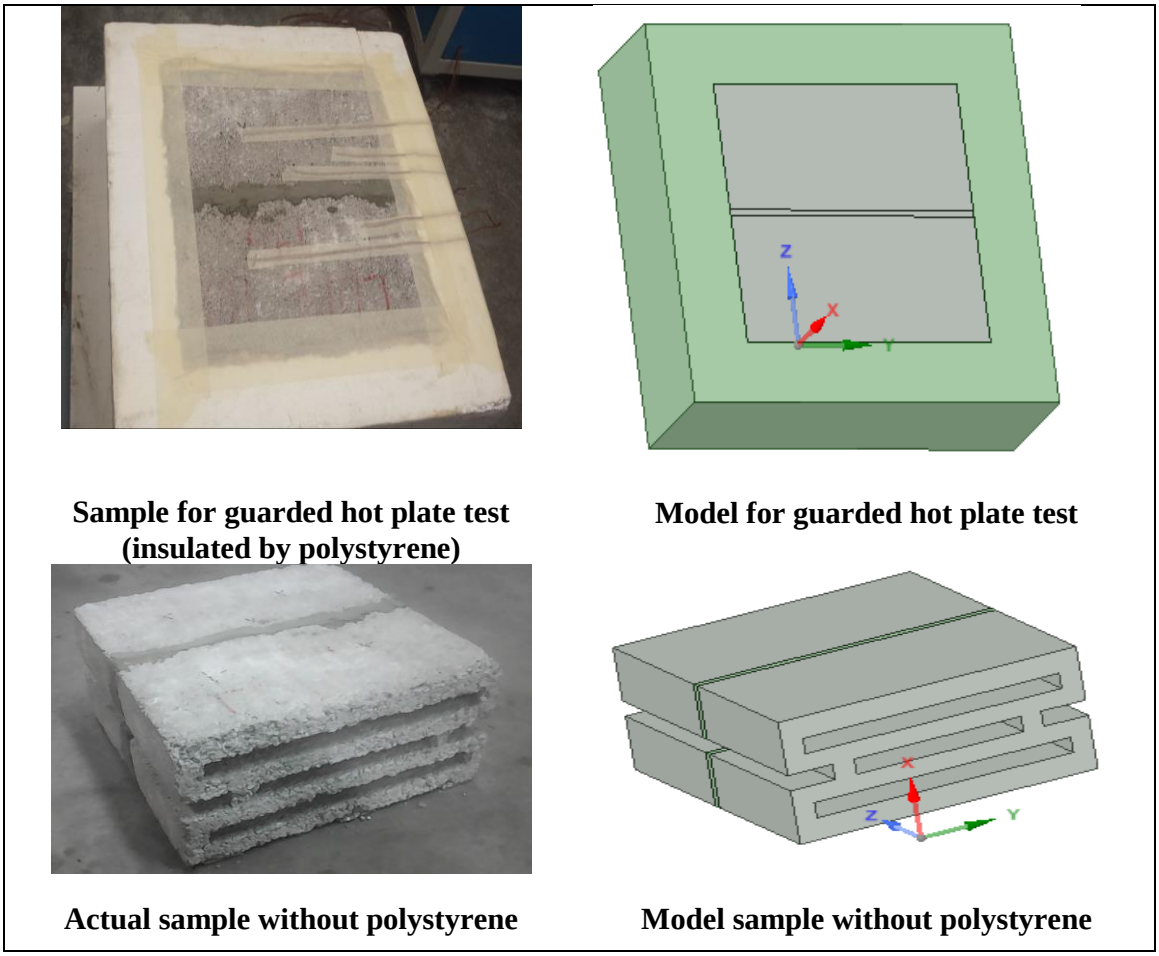

Figure 5.4: Geometry of actual and model guarded hot plate

The geometry in Figure 5.4 was only used to verify the result of the guarded hot plate to ensure that the simulation model is working correctly. Then, three parametric studies were investigated using the geometry in Figure 5.5. In the first study, the effect of the block type was studied using five insulated blocks (control, EPS, LDPE, VL and VS) with the same normal mortar (control mortar) for all these cases. In the second study, the effect of the mortar type was investigated using ten types of insulated mortars [control, (5%, 10% and 15% of VL), (5%, 10% and 15% of PL) and (5%, 10% and 15% of RU)] and used the control block for all these cases. In the third study, the effect of the plaster type was examined using ten types of insulated plasters [control, (5%, 10% and 15% of VL), (5%, 10% and 15% of PL) and (5%, 10% and 15% of RU)] and used the control block for all these cases.

Since the wall was symmetrical, a part of the wall was simulated only to facilitate the solution process and reduce the solution time, as shown in Fig. (5.5).

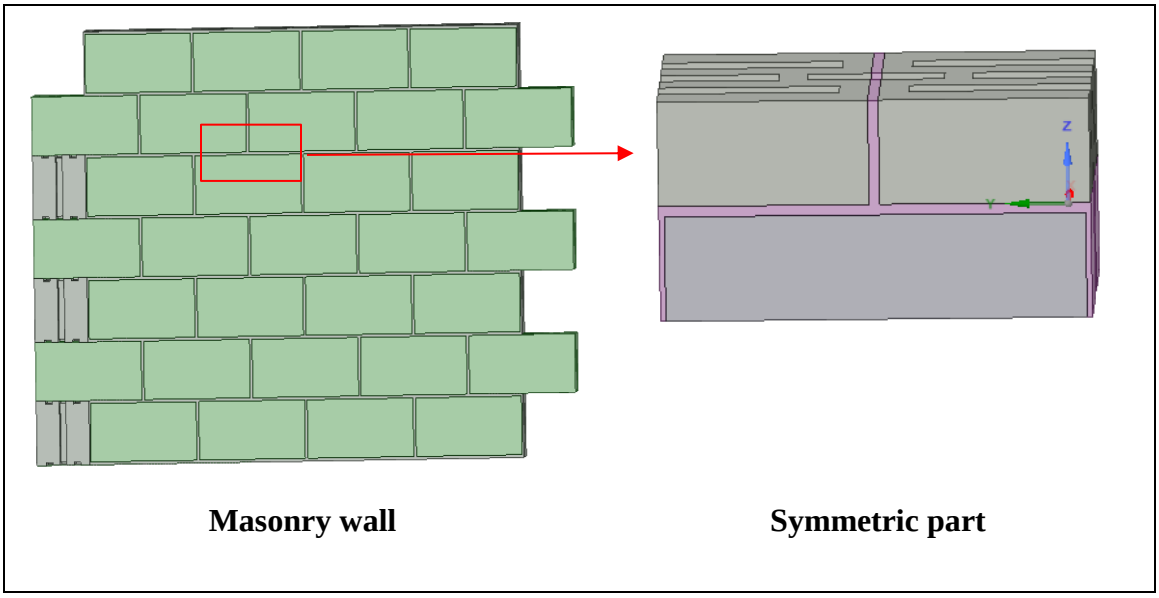

Figure 5.5: Model of masonry wall and symmetric part

5.3 Mathematical Formulation

For steady-state heat conduction with no heat generation, the partial derivative of the temperature with time equals to zero. Each cavity was filled with air and was modeled as a Newtonian fluid with constant physical properties except for the density because the natural convection depends on the gravity. Air density was assumed to be temperature dependent according to Boussinesq approximation [25]. The governing conduction, mass, momentum and energy equations in primitive variables are as follows [25]:

The solid wall

Conduction equation:

$$\frac{\partial T}{\partial t} = \alpha \left[\frac{\partial^2 T}{\partial x^2} + \frac{\partial^2 T}{\partial y^2} + \frac{\partial^2 T}{\partial z^2} \right] \tag{5.4}$$

Inside the air-filled cavities

Continuity equation:

$$\frac{\partial u}{\partial x} + \frac{\partial v}{\partial y} + \frac{\partial \mathrm{w}}{\partial z} = 0 \tag{5.5}$$

x-Direction momentum

$$\frac{\partial u}{\partial t} + u\frac{\partial u}{\partial x} + v\frac{\partial u}{\partial y} + w\frac{\partial u}{\partial z} = -\frac{1}{\rho}\frac{\partial p}{\partial x} + v\nabla^2 u \tag{5.6}$$

y-Direction momentum

$$\frac{\partial v}{\partial t} + u\frac{\partial v}{\partial x} + v\frac{\partial v}{\partial y} + w\frac{\partial v}{\partial z} = -\frac{1}{\rho}\frac{\partial p}{\partial y} + v\nabla^2 v + g\beta(T - T_c) \tag{5.7}$$

z-Direction momentum

$$\frac{\partial w}{\partial t} + u\frac{\partial w}{\partial x} + v\frac{\partial w}{\partial y} + w\frac{\partial w}{\partial z} = -\frac{1}{\rho}\frac{\partial p}{\partial z} + v\nabla^2 w \tag{5.8}$$

Energy equation:

$$\frac{\partial w}{\partial t} + u\frac{\partial T}{\partial x} + v\frac{\partial T}{\partial y} + w\frac{\partial T}{\partial z} = \alpha\nabla^2 T \tag{5.9}$$

5.4 Boundary Conditions

The boundary conditions (BCs) of the model to simulate guarded hot plate test are shown in Figure 5.6. From the test (Table 5.1), the heat flux applied on the hot surface was 46.37 W/m^2 and the temperature at the cold surface was taken as 25.23ºC. The flux was assumed to be zero for the outer surfaces of polystyrene board because they were insulated.

For the parametric study, the BCs are shown in Figure 5.7. The temperature at the exterior surface of the wall was assumed to be $T_h = 50^oC$ and the temperature at the opposite surface (interior surface) was assumed to be $T_c = 20^oC$ [25]. All the other surfaces were defined as symmetric surfaces (flux is zero).

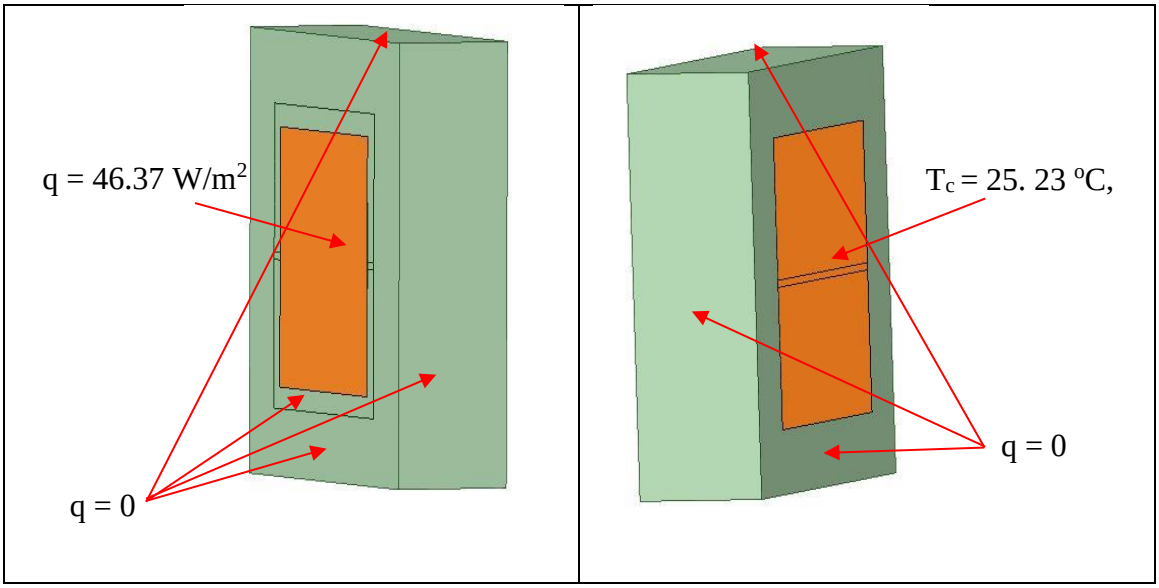

Figure 5.6: Boundary condition of guarded hot plate

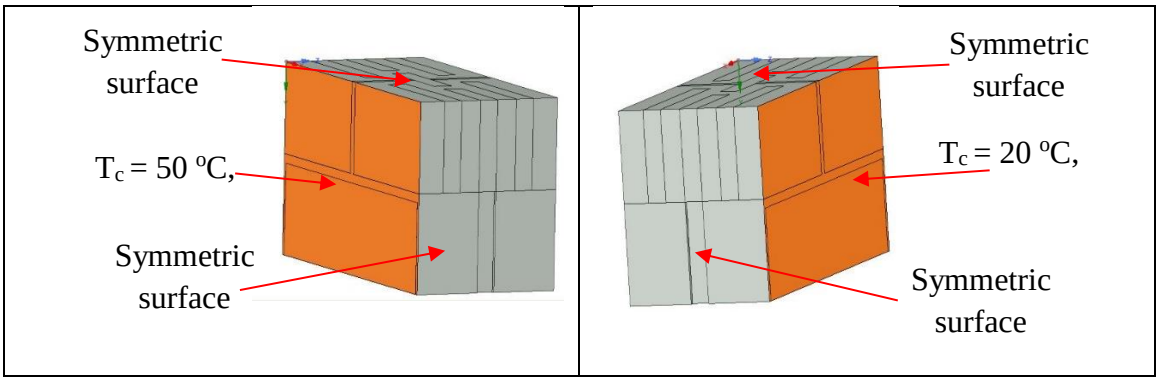

Figure 5.7: Boundary condition of the parametric studies

5.5 Mesh Independence

In the preliminary simulation, mesh independence was conducted for the geometry in Figure 5.6 because the results of FEM were changed with the variation of the mesh size of the model. Because the geometry is of a symmetrical shape, only a quarter of this geometry was selected to study the mesh independence for saving time and effort. The current model presents a solid concrete block surrounded by an air-filled rectangular cavity. The variation of temperature along the solid–air interfaces are considered as the main part (because the motion of the cold and hot air takes place in this region) when the mesh was studied. Five independent meshes were conducted to carry out the best grid's independence. In the air-filled cavities, more than one equation was taken place to simulate the convection and radiation inside the cavities. However, in the solid part, only one equation was conducted to present the conduction heat flux. Therefore, the mesh was discretized in cavities and it was made gradually finer near the solid-air interface to calculate the heat change in this zone, as shown in Figure 5.8.

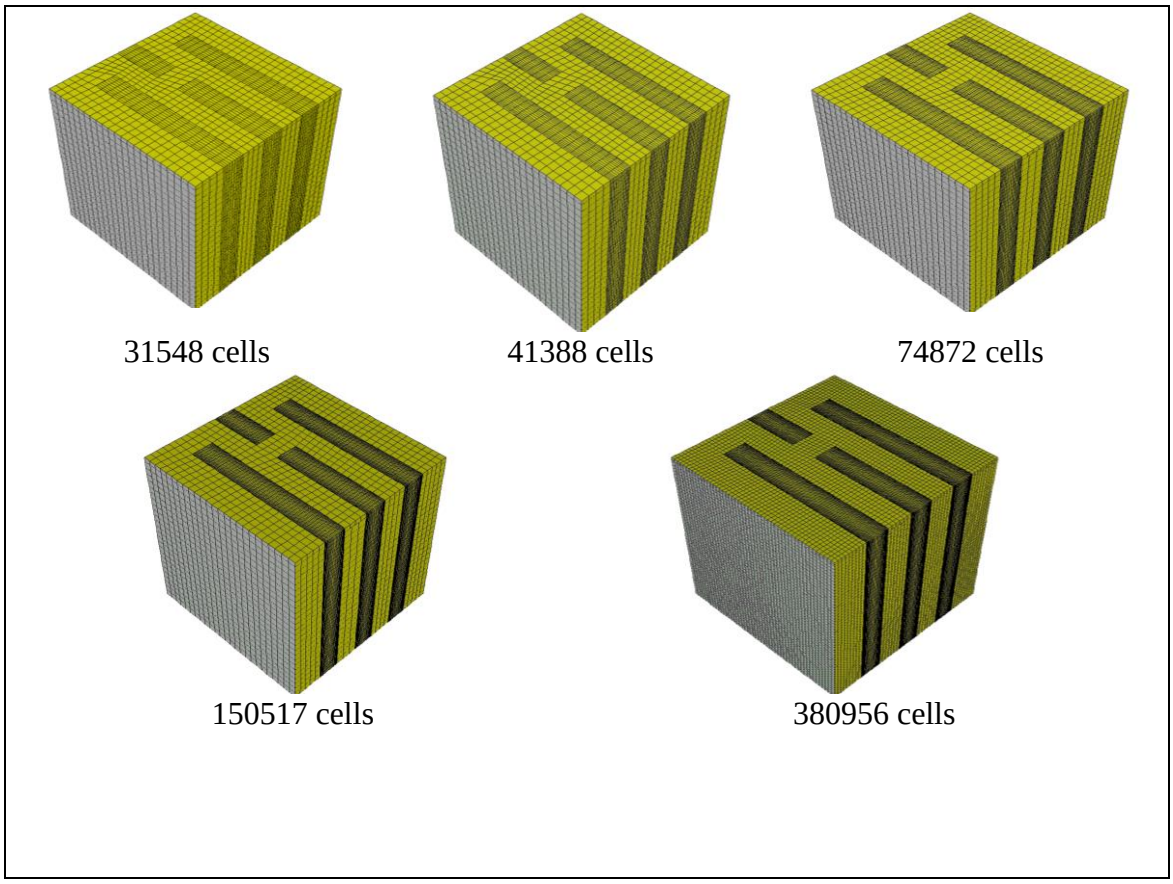

Figure 5.8: Geometries of mesh independence

The results of mesh optimization have been examined in terms of temperature differences at the inner and outer surfaces of the masonry walls. From Figure 5.9, it is obvious that the mesh independence can be selected for 74872 cells with different sizes, as shown in Figure 5.8. However, to make sure that the mesh was independence, the mesh with 150517 cells was taken to test all running cases.

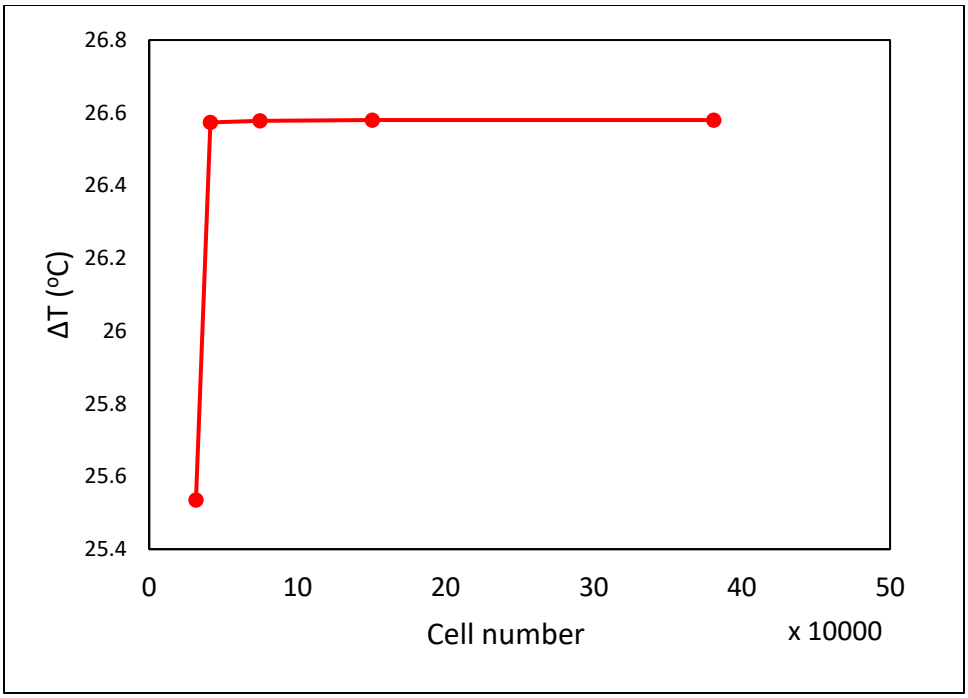

Figure 5.9: Mesh optimization

5.6 Modelling Results

5.6.1 Validation of the Experimental Results

Figure 5.9 shows the test experimental sample and its model. Four points were selected to measure the temperature on the surface using Copper-Constantan thermocouple (T-type) during the guarded hot plate test. The coordinates of these points were measured and selected on the same locations in the model to get good relative evaluation, as shown in Fig. 5.10.

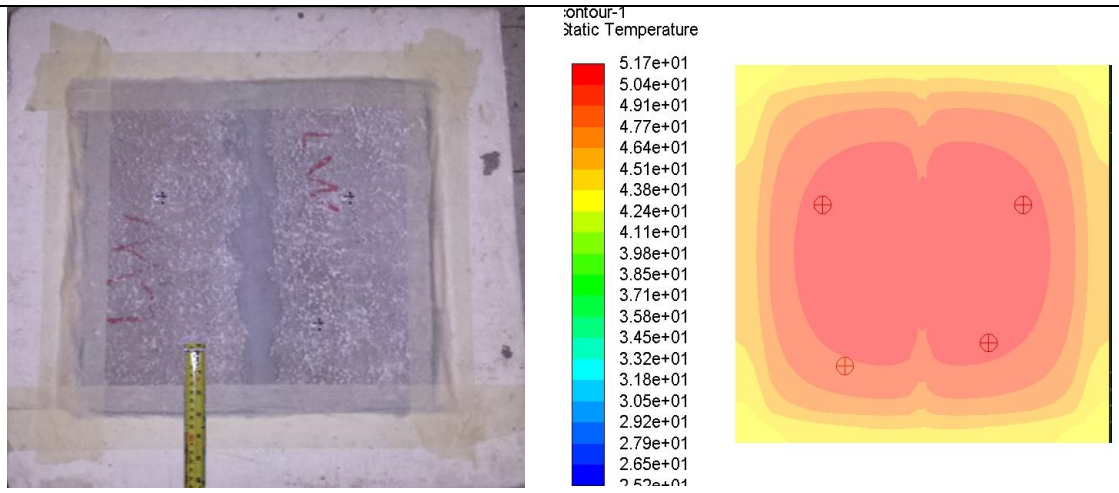

Sample for guarded hot plate test **Validation for guarded hot plate test**

Figure 5.10: Actual and simulated samples of guarded hot plate.

The input data used in the modeling was obtained from the experimental tests in Chapters 3 and 4 except for the emissivity and specific heat coefficients which were obtained from the literature [48], as listed in Table 5.1.

Table 5.1: Thermal properties of masonry wall.

Property	Value (Units)
Control blocks thermal conductivity (K)	0.46 (W/m.K)
Control mortar thermal conductivity (K)	1.23 (W/m.K)
Control blocks density (ρ)	1882 (kg/m^3)
Control mortar density (ρ)	2150 (kg/m^3)
Heat flux of heated generator (q)	46.37 (W/m^2)
Cold surface of test sample (T_c)	25.225 (^{o}C)
Emissivity coefficient ($\mathcal{E}$)	0.88
Specific heat of block (C_p)	840 (j/kg.K)
Specific heat of mortar (C_p)	880 (j/kg.K)

The comparison between the temperature results of heated surface of the sample test from the experimental measurement and simulated modeling is summarized in Table 5.2.

Table 5.2: Comparison of the surface temperature results of the heated surface.

Location reading	Exp. T (°C)	Modeling T(°C)	Different. T (°C)	Error %
Point 1	50.96	50.36	0.60	1.20%
Point 2	51.04	50.73	0.31	0.62%
Point 3	52.18	50.74	1.44	2.84%
Point 4	50.80	50.07	0.73	1.45%
Avg. Point (T)	51.25	50.47	0.77	1.53%

The data in Table 5.2 illustrate the good agreement between the heated surface temperature values from the experimental measurement and simulated modeling with an average error 1.53%. In addition, all the values of the temperature difference between experimental and modeling were less than 0.903°C (error accuracy) except for Point 3. However, the average different temperature value was 0.77°C, which was in the range of the error accuracy measurement of guarded hot plate and its connected instruments (thermocouples and datalogger), as calculated using Equation 5.10.

$$Error\ accuracy\ (\ ^{o}\mathrm{C}) = \pm\sqrt{{T_h}^2 + {D_l}^2 + {G_p}^2 + N^2} \tag{5.10}$$

$$Error\ accuracy = \pm\ 0.903\ \ ^{o}\mathrm{C}$$

Where:

All data of Equation 5.10 were taken from the Table 5.3.

Table 5.3: List of parameters measured of guarded hot plate [26,86]

Symbol	Parameter/Datalogger	Instrument	Range	Accuracy (°C)
T_h	Heated sample surface temperature	Copper-Constantan thermocouple (T-type)	0–350°C	±0.5
D_l	Datalogger	Campbell Scientific 21X	−35–50 °C	±0.3
G_p	Guarded hot plate	Dynatech, model TCFG-R4-6	0.02 - 2 W/m.K.	±0.424*
N	Correction factor of the instrument, N (0.987)		0.986	±0.544*

*The accuracy of the guarded hot plate (G_p) is 4%. Therefore, the value of thermal conductivity of the materials (block and mortar) was increased by 4%, then the temperature difference (before and after 4%) was calculated to find out the accuracy in terms of temperature. For the accuracy of the correction factor, the flux of guarded hot plate was calculated without the correction factor to obtain how much the temperature difference will increase.

5.6.2 Parametric Studies

There are three parametric studies in the model part of this research. In the first study, five walls were modeled using the five types of blocks and the control mortar that were produced and tested in the experimental part. In the second study, ten types of mortars were simulated to examine the effect of mortar on the thermal performance of the wall. In the third study, ten types of plaster (i.e. used the same density and thermal conductivity of mortar) were applied on the inner and outer surfaces of the wall to reduce the heat flow and carry out the optimal wall that have the highest thermal resistance (lowest thermal conductivity). For all cases, the temperature on the outer and inner surfaces were fixed at $T_o = 50^oC$, and $T_i = 20^oC$, respectively. The thermal performance was evaluated using the data in Table 5.1.

5.6.2.A Thermal Resistance and Heat Flux of Blocks

For the first study, the heat rate (heat flux) through the wall of the control block was 50.19 W/m^2. The heat flux decreased to 46.21, 46.12, 45.66 and 43.73 W/m^2 for VL, LDPE, EPS, and VS, respectively. These materials improved the thermal resistance by 8.6, 8.8, 9.9 and 14.8% for VL, LDPE, EPS and the VS, respectively, as compared to the control concrete block wall, as shown in Table 5.4. Since all the masonry blocks have the same geometry, the improvement in thermal resistance was totally ascribed to the thermal conductivity of the replacement materials.

Table 5.4: Heat flux and thermal resistance for different blocks

Type masonry block	ΔT (^oC)	Heat flux through the wall (W/m^2)	Thermal resistance ($m^2\ ^oC/W$)	Reduction in heat flux (%)	Improvement in resistance (%)
Control	30	50.19	0.598	---	---
EPS	30	45.66	0.657	9.0	9.9
LDPE	30	46.12	0.651	8.1	8.8
VL	30	46.21	0.649	7.9	8.6
VS	30	43.73	0.686	12.9	14.8

Moreover, all the developed blocks had much higher thermal resistance than the conventional "market" concrete block (Fig. 5.11). The thermal conductivity and thermal resistance of the conventional block was 0.976 W/m K and 0.205 $m^2\ ^oC/W$, respectively [26]. Therefore, the improvement in the thermal resistance was more than 190% for all developed blocks, as compared to the conventional concrete block, as shown in Table 5.5.

Table 5.5: Comparison of the thermal resistance for the market block and developed blocks.

Type masonry block	Thermal resistance (m^2 $^oC/W$)	Improvement in resistance (%)
Conventional block	0.205	----
Control	0.598	192
EPS	0.657	220
LDPE	0.651	218
VL	0.649	217
VS	0.686	235

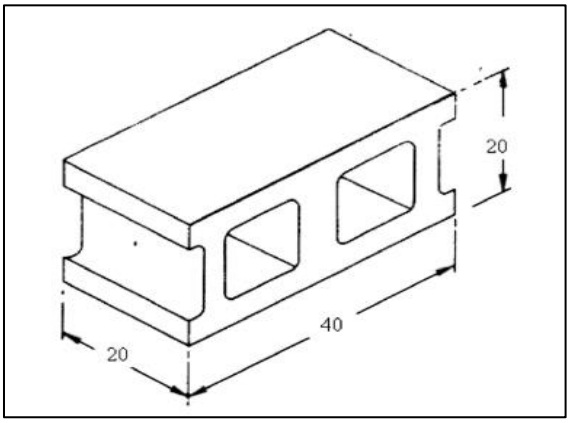

Figure 5.11: Conventional "market" concrete block

5.6.2.B Thermal Resistance and Heat Flux of Mortar

Usually, the intensity of heat flux increases in the high thermal conductivity medium [42]. Since the mortar has higher thermal conductivity than the block, the heat flow passing through the mortar is much intense than through the block. The data in Table 5.6 compare the heat flux passing through the blocks and mortar individual, then passing through the entire wall for both the control and VS walls. The control wall was made by control blocks and control mortar, while the VS wall was made by VS blocks and control mortar. It was clarified that the heat flow increased through the mortar medium (from 120.83 to 128.28

W/m^2) when the block resistance was increased (from 0.67 to 0.81 $m^2\,^oC/W$). However, the high heat rate through mortar did not have much effect when calculating the total flow of heat through the entire wall (0.6 and 0.69 $m^2\,^oC/W$) because the mortar area (perpendicular to the heat direction) is much smaller than block area.

Table 5.6: Heat flux and thermal resistance for the block, mortar and entire wall

Wall type	Medium type	ΔT (^oC)	Heat flux through the wall (W/m^2)	Thermal resistance ($m^2\,^oC/W$)
Control wall	Block only	30	44.80	0.67
	Mortar only	30	120.83	0.25
	Entire wall	30	50.19	0.60
VS wall	Block only	30	37.29	0.81
	Mortar only	30	128.28	0.23
	Entire wall	30	43.73	0.69

All types of mortars (1-cm thickness) were evaluated by modeling the walls with the control blocks and using different types of mortars to join them. From Table 5.7, it is clear that the wall with 15% VL mortar had the highest thermal resistance 0.635 $m^2\,^oC/W$. The improvement in the thermal resistance due to the mortar with 15% VL was 6.2%, as shown in Table 5.7. The second highest thermal resistance was in the wall with mortar of 10% VL. The wall with 15% PL mortar has a thermal resistance closer to the wall with 10% VL and their thermal resistance was 0.628 and 0.629 $m^2\,^oC/W$, respectively, as shown in Table 5.7. The walls with rubber mortar had lower thermal resistance as compared to the vermiculite and perlite mortars because the thermal conductivity of rubber (0.243 W/m.K) was higher than that of vermiculite (0.06 W/m.K) and perlite (0.07 W/m.K).

Table 5.7: Thermal performance of the wall with different types of mortar.

Type of block and	ΔT (°C)	Net heat flux through the wall (W/m^2)	Thermal resistance (m^2 °C/W)	Improvement in heat flux %	Improvement in resistance %
C	50.19	30	0.598	0.0	0.0
C+CU 5%	49.84	30	0.602	0.7	0.7
C+RU 10%	49.09	30	0.611	2.2	2.2
C+RU 15%	48.41	30	0.620	3.5	3.7
C+PL 5%	49.07	30	0.611	2.2	2.3
C+PL 10%	48.29	30	0.621	3.8	3.9
C+PL 15%	47.80	30	0.628	4.8	5.0
C+VL 5%	48.47	30	0.619	3.4	3.6
C+VL 10%	47.72	30	0.629	4.9	5.2
C+VL 15%	47.26	30	0.635	5.8	6.2

5.6.2.C Thermal Resistance and Heat Flux of Plaster

The same previous mortars were modeled as plasters that were applied on both surfaces of the walls (exterior and interior) to study the heat reduction rate when they had used them as plasters. The thickness of both surfaces was 15 mm which was closer to the nominal plaster thickness of ASTM C926 standard was 16 mm [86]. The control block and other thermal properties in Table 5.1 were used to carry out all the simulations in the parametric study. The data in Table 5.8 indicate that the wall made of control block, mortar and plaster without any insulated materials (C+C) improves the thermal resistance of wall by 4.2%, as compared with the control wall [(wall without any plaster (C)]. Since there were no insulation materials in the wall C and C+C, the improvement of the resistance in wall C+C was totally ascribed to increasing the wall thickness by about 30 mm.

The walls with 5, 10 and 15% of VL plaster gave better results with higher thermal resistance than the control wall by 9.9, 13.3 and 16.0%, respectively, as shown in Table 5.8. However, the 10 and 15% VL did not meet the ASTM C270 standard for the water

absorption (as was reported earlier in the Section 4.3.3). The walls with PL plaster had higher thermal resistance than the walls with RU plaster, as shown in Table 5.8. The optimal wall from the point of view of the thermal performance for all cases was the wall with VS blocks and 15% VL. The thermal resistance was 0.795 (m^2 $^oC/W$), which is higher than the control wall by about 33%, as shown in Figure 5.12.

Table 5.8: Thermal performance of the wall with different types of plaster.

Type of block, mortar and plaster	ΔT (^oC)	flux through the wall (W/m^2)	Thermal resistance (m^2 $^oC/W$)	Reduction in heat flux (%)	Improvement in resistance (%)
C	30	50.19	0.598	0.0	0.0
C+C	30	48.17	0.623	4.0	4.2
C+RU 5%	30	47.68	0.629	5.0	5.2
C+RU 10%	30	46.63	0.643	7.1	7.6
C+RU 15%	30	45.57	0.658	9.2	10.1
C+PL 5%	30	46.60	0.644	7.1	7.7
C+PL 10%	30	45.34	0.662	9.7	10.7
C+PL 15%	30	44.45	0.675	11.4	12.9
C+VL 5%	30	45.67	0.657	9.0	9.9
C+VL 10%	30	44.28	0.677	11.8	13.3
C+VL 15%	30	43.27	0.693	13.8	16.0
VS+PL 15	30	38.76	0.774	22.8	29.5
VS+VL 15	30	37.72	0.795	24.8	33.0

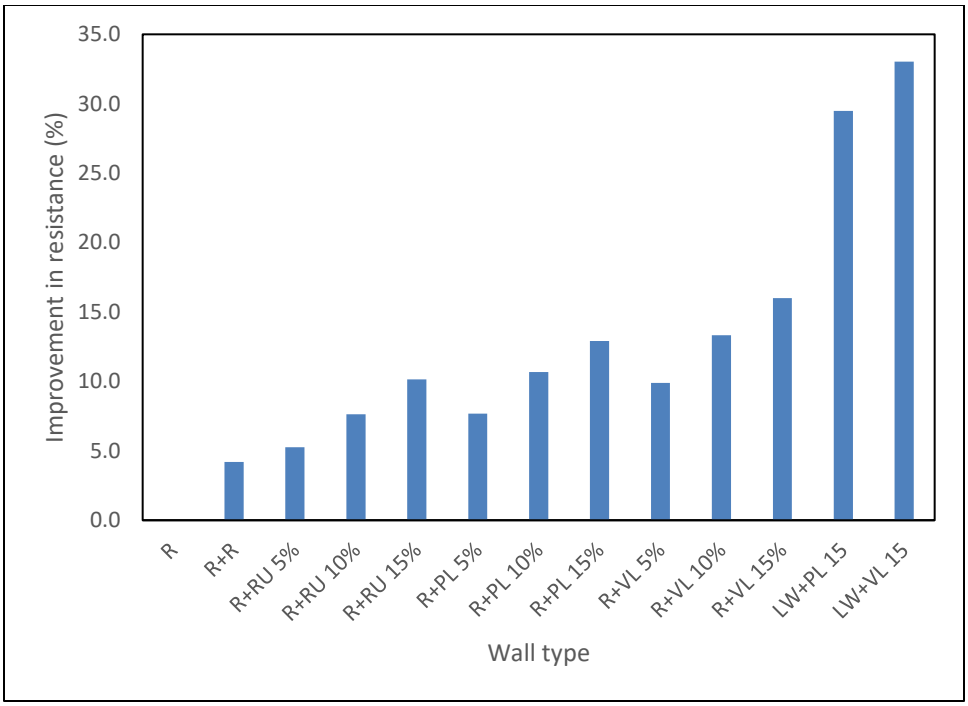

Figure 5.12: Thermal resistance of the walls with plaster

5.7 Cost Analysis

In order to know the total cost of each the wall per meter square. the price of each component in the mix design, the operating cost and profit rate were calculated according to the market price for masonry block (Advanced Concrete Products, Ltd., Company). Table 5.9 summarizes the prices of all materials that were used to produce the masonry hollow block walls. The current price of conventional “market” concrete block is 1.45 SR/block and the price of the control block, which was calculated in Table 5.9, is 1.42 SR/block. Since the difference between the calculated value (1.42 SR/block) and the market price value is 0.03 SR/Block, this proves that all prices and calculations in Table 5.8 are correct. The lowest price of the newly developed block is the EPS block by about 1.52 SR/block. It is lower than that of LDPE and VL block price by about 50% while it is slightly lower than VS by about 11%, as shown in Tables 5.9.

Table 5.9: Cost analysis for a meter square of the masonry wall

Materials	Mix proportions by weight (kg/m)^3										
	Materials	Control		EPS		LDPE		VL		VS	
	kg/SR	kg	SR	kg	SR	kg	SR	kg	SR	kg	SR
Cement content	0.225	195	44	195	44	195	44	250	56	195	44
Water content	0.007	115	1	115	1	111	1	290	2	173	1
Coarse aggregate (3/8 in)	0.024	1131	27	1006	24	708	17	856	20	---	---
Coarse aggregate (3/16 in)	0.023	338	8	---	---	211	5	256	6	---	---
Replacement (3/8 in)	---	---	---	2	32	102	255	58	232	159	13
Replacement (3/16 in)	---	---	---							48	4
Fine aggregate (Sand)	0.006	452	3	576	4	681	4	359	2	359	2
Σ		2683	85	2470	107	2689	330	2428	321	1293	66
Weight/ Block (kg)		19		17		18		17		17	
No. of blocks		138		150		147		139		74	
Materials cost/block (SR)		0.62		0.72		2.24		2.31		0.89	
Operating cost/block (SR)		0.30		0.30		0.30		0.30		0.30	
Profit (SR)		0.50		0.50		0.50		0.50		0.50	
Total cost/block (SR)		1.42		1.52		3.04		3.11		1.69	
mortar cost (SR/m^2)		0.17		0.17		0.17		0.17		0.17	
wall cost (SR/m^2)		17.86		19.12		38.16		39.01		21.29	
wall cost ($/m^2)		4.76		5.10		10.18		10.40		5.68	

Note: the price of EPL, LDPE, VL and VS is 15, 2.5, 4, and 0.079 SR/kg.

The price of the developed blocks and some blocks in the market was listed in Table 5.10.

It is clarified that all developed blocks have lower price than the insulation blocks available

in the market. Further, the price of the commercial volcanic block in the Eastern Province in Saudi Arabia is 3.0 SR/block (according to Fahd Al Shaibani Company) while the price of the developed block (VS) is 1.69 SR/block, as shown in Table 5.10. The variation of the price could be ascribed to the low dosage of cement content of the developed block.

Table 5.10: Comparison of the price for the developed blocks and the blocks in the market

Block Type	Type	Cost/block (SR)	Cost increased/block
Normal Block Available	Available in markets	1.45	0
Control Block	New designed block	1.42	-0.03
Expanded Polystyrene	New designed block	1.52	0.07
Volcanic Scoria	New designed block	1.69	0.24
Polyethylene	New designed block	3.04	1.59
Vermiculite	New designed block	3.11	1.66
Scoria Block	Available in markets	3.00	1.55
Expanded Polystyrene	Available in markets	3.50	2.05
Extruded Polystyrene	Available in markets	5.50	4.05
Siporex	Available in markets	4.25	2.8

A cost analysis has been evaluated for all types of blocks used in this research. In order to figure out the payback period for the developed insulated walls in comparison to the normal concrete wall (control blocks and mortar without insulated materials), the cost of electrical energy must be determined for all types of the masonry walls. The energy consumed by the air-condition is calculated using the following equation [26]:

$$E = \frac{0.024 \times D}{R \times C} \ kWh/m^2 \quad (5.11)$$

Where:

R: Thermal resistance of the wall ($m^2\ ^oC/W$).

D: Degree-days of the location (D = 2185) [26].

C: Thermal performance coefficient of the air-condition (C = 2.16) [26].

The total cost of the discounted of energy and block [net present value (NPV)] per square meter of wall is calculated using the following equation [26]:

$$\mathrm{NPV} = \mathrm{E} \times \mathrm{EC} \times \mathrm{PWF} + \mathrm{BC} \tag{5.12}$$

Where:

E: Consumption of annual energy (kWh/m^2).

EC: Energy tariff (6.67 cents/kWh).

PWF: Present worth factor.

BC: Cost wall per meter square ($/m^2).

The PWF is calculated using the following equation [26].

$$\mathrm{PWF} = \frac{1}{\mathrm{i} - \mathrm{e}}\left(1 - \left(\frac{1+\mathrm{e}}{1+\mathrm{i}}\right)^{\mathrm{n}}\right) \text{ for } \mathrm{e} \neq \mathrm{i} \tag{5.13}$$

$$\mathrm{PWF} = \mathrm{n} \cdot (\mathrm{i} + \mathrm{e}) \text{ for } \mathrm{e} = \mathrm{i} \tag{5.14}$$

Where:

e: Energy inflation rate of Saudi Arabia (2%) [87].

i: Discount rate of Saudi Arabia (2.5%) [87].

n: Lifetime of the block (assumed 30 years) [88].

The cost analysis of the NPV for different types of masonry walls is presented in Table 5.11. The cost of the annual ranged from 2.13 (VS block) to 7.90 $/m^2 [conventional concrete block (CCB)], as shown in the second column in Table 5.11. The payback period analysis is conducted to obtain the payback per year for different types of walls, as compared to the CCB. It is obtained by dividing the (annual energy saving) to the (increasing the block cost) related to the conventional block, as shown in Table 5.11. The analysis indicates that the wall with VS block has the lowest NPV among all the types of

walls examined (without plaster). It was lower than the conventional block by 71%. Further, it is worthwhile to observe that the NPV of the conventional concrete block (Fig. 5.11) is 220.2 $/m^2. By changing the geometry of concrete block (Fig. 3.9), the NPV value was reduced to 83.5 $/m^2 (i.e., reduction in the NPV was about 62.1%). Moreover, the optimal wall (VS block plus 15% VL mortar and plaster) improves the thermal resistance by about 290% when compared to conventional concrete blocks. This improvement could reduce the energy consumption from 118.43 to 30.35 KWh/m^2 (about 3.9 times of reduction) annually. This optimal wall is proposed to be used in the domestic and industrial buildings instead of the traditional walls.

Table 5.11: Energy and cost analysis for different masonry wall

Sample type	Annual energy (kWh/m^2)	Annual energy cost ($/m^2)	Annual energy saving ($/m^2)	Block cost ($/m^2)	Increase in block cost ($/m^2)	Simple payback period (yr)	NPV ($/m2) (n=30yrs)
CCB	118.43	7.90	0.00	4.76	0.00	0.00	220.2
Control	43.26	2.88	5.01	4.76	0.00	0.00	83.5
ESP	35.05	2.34	5.56	5.10	0.34	0.06	68.9
VS	31.92	2.13	5.77	5.68	0.91	0.16	63.8
LDPE	35.83	2.39	5.51	10.18	5.41	0.98	75.4
VL	35.97	2.40	5.50	10.40	5.64	1.03	75.8
VS+ VL15	30.35	2.02	5.87	6.68	1.91	0.33	60.0

- (CCB) means conventional concrete blocks with two cavities
- Energy saving and increase in block cost are obtained with reference to normal concrete block (CCB) values. Energy cost is taken as 6.67 cents/kWh. Also, the energy and cost values are normalized to block wall surface area.
- NPV = Net present value or the total discounted cost (discount rate, i = 2.5%, energy inflation rate, e = 2%) over the lifetime of the block (n = 30 years).

CHAPTER 6

CONCLUSIONS AND RECOMMENDATIONS

In this Chapter, the results of the simulation and experimental programs were summarized in the Conclusions Section. Further, some relevant ideas and subjects, which could be executed in future studies, are presented in the Recommendations Section.

6.1 Conclusions

This work reports the thermal and mechanical properties of masonry block walls. The additive insulation materials (expanded polystyrene, low density polyethylene, vermiculite and scoria for the concrete blocks and perlite, vermiculite, and rubber particles for the cement mortar) have a significant effect on increasing the thermal efficiency of blocks and mortar. Based on the results reported in this investigation, the following conclusions could be drawn:

1. Polystyrene, low density polyethylene, vermiculite and volcanic scoria were used to produce insulation concrete hollow blocks with both lightweight characteristics and low thermal conductivity to be used in non-load bearing walls. Firstly, the dosages of these materials were optimized to satisfy the ASTM C129 criteria for strength requirement. Therefore, the compressive strength, thermal conductivity, density and

absorption were initially measured. Based on the results of this part of the study, the following conclusions could be drawn:

- The maximum reductions of thermal conductivity were 26.1, 19.3, 17 and 16.7% for VS, EPS, LDPE and VL, respectively, as compared to the control block.
- The dry density was marginally reduced by 0.37, 1.43 and 5.69% for LDPE, VL and EPS blocks relative to the control concrete block, respectively.
- The absorption of the control block was 5.47%, which was increased sharply for VL block to 60% and was lowered by 21 and 35%, for the LDPE and EPS block, respectively.
- The strength of EPS, LDPE, VL and VS blocks was reduced by 37, 39, 47 and 51 %, respectively, after 28 days, as compared to the control block.
- All the blocks in this research were considered as medium-weight masonry blocks because their dry density was between 1680 and 2000 kg/m^3 (ASTM C-90).
- The weight of the volcanic scoria block was 16.25 kg, which was the lightest, as compared to all the other hollow blocks. The expanded polystyrene was the second lightest block by 16.72 kg. However, the control block was the heaviest block by 19.91 kg with the differences of 1.29 kg (7%), 1.75 kg (9%), 3.19 (16%) and 3.66 kg (18%), as compared to the VL, LDPE, EPS and VS blocks, respectively.
- The control block had the lowest water absorption, which was lower by 26, 30, 45 and 147%, for the LDPE, VS, EPS, and VL block, respectively.

- All the blocks met the ASTM C90-03 requirement for the absorption of medium weight block (240 kg/m^3), except the VL block which had higher absorption.

2. For the insulation mortar, its compressive strengths decreased significantly due to the insulated materials, as compared to that of the control mix. On the other hand, the thermal conductivity was improved with increasing the content of vermiculite, perlite and rubber.
3. The details of the compressive strengths and the thermal conductivity of the vermiculite, perlite and rubber mortars could be clarified as follows:
    - The 28-day compressive strength of mortar decreased by 78, 63 and 36% for vermiculite, rubber and perlite, respectively, as compared to the control mortar for the content of 15% after 28 days.
    - The maximum reductions of thermal conductivity were 57, 47 and 36% for vermiculite, perlite and rubber, respectively, as compared to the control mortar for the content of 15%.
    - The dry density of vermiculite and perlite mortar was much lower than that of the rubber mortar and the maximum reduction was 15, 27 and 34% for the 15% of rubber, perlite and vermiculite content, respectively, as compared to the control mortar.
    - The vermiculite mortar displayed the highest water absorption by 100, 165 and 235% for 5, 10 and 15% vermiculite content. Due to this high absorption, 10 and 15% dosages of vermiculite exceeded the ASTM C270 limits for the maximum water absorption.

4. The data of Guarded Hot Plate were analyzed and validated using FEM (Fluent package in ANSYS workbench). The agreement between the experimental data and the modeling results was excellent with maximum variation of 1.53%.
5. The optimal wall from the point of view of the thermal performance for all cases was the wall with VS blocks and 15% VL. Its thermal resistance was 0.795 ($m^2 {}^oC/W$) and it was higher than that of the control wall by about 33%.
6. The optimal wall (VS block plus 15% VL mortar and plaster) improves the thermal resistance by about 290% when compared to conventional concrete blocks. This improvement could reduce the energy consumption from 118.43 to 30.35 KWh/m^2 (about 3.9 times) annually. This optimal wall is recommended to be used in the domestic and industrial buildings instead of the traditional walls.
7. The net present value of a normal concrete block can be reduced significantly (about 62.1%) by fabricating the cavities of the hollow concrete block and the optimal wall (VS block plus 15% VL mortar and plaster) can be reduced by 73%, as compered to the conventional concrete block.

6.2 Recommendations

From the analytical and experimental programs conducted in this research, the following recommendations could be stated for future studies:

1. Conduct a survey on the available blocks in the Saudi market to form a data bank to be used to assess their thermal efficiency using FEM without the need to conduct experimental program.
2. For the experimental program, the cavities of the hollow blocks could be filled with other insulation materials, such as crumb rubber, plastic, graded perlite and polystyrene beads, which would increase the thermal resistance inside the cavities.
3. Use air-entrained agents in the concrete mix of the masonry blocks to increase the thermal resistance.
4. Use supplementary cementitious materials such as lime and powder perlite to increase the strength and reduce the cost of the masonry blocks.

References

[1] Naji El Haddad, R. Singh, and R. Sahi, “Energy Efficiency in Buildings,” *ENERGY Effic. EXPO*, no. January, 2018.

[2] M. Krarti, K. Dubey, and N. Howarth, “Evaluation of Building Energy Efficiency Investment Options for The Kingdom of Saudi Arabia,” *Energy*, vol. 134, pp. 595–610, 2017.

[3] A. H. Almasoud and H. M. Gandayh, “Future of Solar Energy in Saudi Arabia,” *J. King Saud Univ. - Eng. Sci.*, vol. 27, no. 2, pp. 153–157, 2015.

[4] S. A. Al-Ajlan, A. M. Al-Ibrahim, M. Abdulkhaleq, and F. Alghamdi, “Developing Sustainable Energy Policies for Electrical Energy Conservation in Saudi Arabia,” *Energy Policy*, vol. 34, no. 13, pp. 1556–1565, 2006.

[5] Y. Alyousef and M. Abu-ebid, “Energy Efficiency Initiatives for Saudi Arabia on Supply and Demand Sides,” *Energy Effic. Bridg. to Low Carbon Econ.*, no. InTech., pp. 280–308, 2012.

[6] S. A. Al-Ghamdi, A. Al-Gargossh, and K. A. Al-Shaibani, “Energy Conservation by Retrofitting : an Overview of Office Buildings in Saudi Arabia,” in *International Conference on IT, Architecture and Mechanical Engineering-Dubai- UAE*, 2015, pp. 8–13.

[7] A. Zhou, K. W. Wong, and D. Lau, “Thermal Insulating Concrete Wall Panel Design for Sustainable Built Environment,” *Sci. world J.*, vol. 11, pp. 1–12, 2014.

[8] I. M. Al-Naimi, “The Potential for Energy Conservation in Residential Buildings in Dammam Region, Saudi Arabia,” *PhD Thesis, Sch. Archit. Plan. Landscape, Univ. Newcastle upon Tyne, United Kingdom.*, no. October, 1989.

[9] A. Almujahid and Z. Kaneesamkandi, “Construction of a Test Room for Evaluating Thermal Performance of Building Wall Systems Under Real,” *Int. J. Innov. Res. Sci. Eng. Technol.*, vol. 2, no. 6, pp. 2000–2007, 2013.

[10] O. Oluwole, J. Joshua, and H. Nwagwo, “Finite Element Modeling of Low Heat Conducting Building Bricks,” vol. 2012, no. August, pp. 800–806, 2012.

[11] K. S. Al-Jabri, A. W. Hago, A. S. Al-Nuaimi, and A. H. Al-Saidy, “Concrete Blocks for Thermal Insulation in Hot Climate,” *Cem. Concr. Res.*, vol. 35, no. 8, pp. 1472–1479, 2005.

[12] V. Corinaldesi, A. Mazzoli, and R. Siddique, “Characterization of Lightweight Mortars Containing Wood Processing By-products Waste,” *Constr. Build. Mater.*, vol. 123, pp. 281–289, 2016.

[13] A. M. Papadopoulos, “State of the Art in Thermal Insulation Materials and Aims

for Future Developments," *Energy Build.*, vol. 37, no. 1, pp. 77–86, 2005.

[14] F. H. bin M. Zulkifeli and H. binti M. Saman, "Compressive and Flexural Strength of Expanded Perlite Aggregate Mortar Subjected to High Temperatures," in *in the American Institute of Physics conference*, 2017, pp. 1–8.

[15] C. Tsai, M. Tsai, J. Yeh, and C. Yang, "Effect of Temperature on Mechanical Properties of Al0.5CoCrCuFeNi Wrought Alloy," *J. ofAlloys Compd.*, vol. 490, pp. 160–165, 2010.

[16] M. Lanzón and P. A. García-Ruiz, "Lightweight Cement Mortars: Advantages and Inconveniences of Expanded Perlite and Its Influence on Fresh and Hardened State and Durability," *Constr. Build. Mater.*, vol. 22, no. 8, pp. 1798–1806, 2008.

[17] F. Xu, C. Peng, J. Zhu, and J. Chen, "Design and Evaluation of Polyester Fiber and SBR Latex Compound-Modified Perlite Mortar with Rubber Powder," *Constr. Build. Mater.*, vol. 127, pp. 751–761, 2016.

[18] P. Meshgin, Y. Xi, and Y. Li, "Utilization of Phase Change Materials and Rubber Particles to Improve Thermal and Mechanical Properties of Mortar," *Constr. Build. Mater.*, vol. 28, no. 1, pp. 713–721, 2012.

[19] P. Turgut and B. Yesilata, "Physico-Mechanical and Thermal Performances of Newly Developed Rubber-Added Bricks," *Energy Build.*, vol. 40, pp. 679–688, 2008.

[20] M. Zukowski and G. Haese, "Experimental and Numerical Investigation of a Hollow Brick Filled with Perlite Insulation," *Energy Build.*, vol. 42, no. 9, pp. 1402–1408, 2010.

[21] I. Budaiwi and A. Abdou, "Variations of Thermal Conductivity of Insulation Materials Under Different Operating Temperatures : Impact on Envelope-Induced Cooling Load," *J. Archit. Eng.*, vol. 8, no. 4, pp. 125–132, 2002.

[22] J. Diaz, P. Nieto, C. Biempica, and M. Gero, "Analysis and Optimization of the Heat-Insulating Light Concrete Hollow Brick Walls Design by the Finite Element Method," *Appl. Therm. Eng.*, vol. 27, no. 7, pp. 1445–1456, 2007.

[23] M. R. Moufti, A. A. Sabtan, and W. M. Shehata, "Assessment of the Industrial Utilization of Scoria Materials in Central Harrat Rahat, Saudi Arabia," *Eng. Geol.*, vol. 57, pp. 155–162, 2000.

[24] I. H. Ling and D. C. L. Teo, "Properties of EPS RHA Lightweight Concrete Bricks under Different Curing Conditions," *Constr. Build. Mater.*, vol. 25, no. 8, pp. 3648–3655, 2011.

[25] M. M. Al-Hazmy, "Analysis of Coupled Natural Convection-Conduction Effects on the Heat Transport Through Hollow Building Blocks," *Energy Build.*, vol. 38, no. 5, pp. 515–521, 2006.

[26] L. M. Al-Hadhrami and A. Ahmad, “Assessment of Thermal Performance of Different Types of Masonry Bricks Used in Saudi Arabia,” *Appl. Therm. Eng.*, vol. 29, no. 5–6, pp. 1123–1130, 2009.

[27] S. G. Park and P. D. H. Chilsholm, “Polystyrene Aggregate Concrete,” *Branz Resour. Cent. Build. Excell.*, vol. 85, no. 85, 1999.

[28] D. Yang, W. Sun, Z. Liu, and K. Zheng, “Research on Improving the Heat Insulation and Preservation Properties of Small-Size Concrete Hollow Blocks,” *Cem. Concr. Res.*, vol. 33, no. 9, pp. 1357–1361, 2003.

[29] K. S. Al-Jabri, A. W. Hago, R. Taha, A. S. Alnuaimi, and A. H. Al-Saidy, “Strength and Insulating Properties of Building Blocks Made from Waste Materials,” *J. Mater. Civ. Eng.*, vol. 21, pp. 191–197, 2009.

[30] O. Ünal, T. Uygunoğlu, and A. Yildiz, “Investigation of Properties of Low-Strength Lightweight Concrete for Thermal Insulation,” *Build. Environ.*, vol. 42, no. 2, pp. 584–590, 2007.

[31] K. M. A. Hossain, “Blended Cement and Lightweight Concrete Using Scoria: Mix Design, Strength, Durability and Heat Insulation Characteristics,” *Int. J. Phys. Sci.*, vol. 1, no. 1, pp. 5–16, 2006.

[32] A. G. Celik, T. Depci, and A. M. Kılıc, “New lightweight colemanite-added perlite brick and comparison of its physicomechanical properties with other commercial lightweight materials,” *Constr. Build. Mater.*, vol. 62, no. March 2016, pp. 59–66, 2014.

[33] A. G. Çelik, “Investigation on Characteristic Properties of Potassium Borate and Sodium Borate Blended Perlite Bricks,” *J. Clean. Prod.*, vol. 102, pp. 88–95, 2015.

[34] Y. Xu, L. Jiang, J. Xu, and Y. Li, “Mechanical Properties of Expanded Polystyrene Lightweight Aggregate Concrete and Brick,” *Constr. Build. Mater.*, vol. 27, no. 1, pp. 32–38, 2012.

[35] A. A. Sayadi, J. V. Tapia, T. R. Neitzert, and G. C. Clifton, “Effects of Expanded Polystyrene (EPS) Particles on Fire Resistance, Thermal Conductivity and Compressive Strength of Foamed Concrete,” *Constr. Build. Mater.*, vol. 112, pp. 716–724, 2016.

[36] M. Singh and M. Garg, “Activation of Fluorogypsum for Building Materials,” *J. Sci. Ind. Res. (India).*, vol. 68, no. 2, pp. 130–134, 2009.

[37] K. Arendt, M. Krzaczek, and J. Florczuk, “Numerical Analysis by FEM and Analytical Study of the Dynamic Thermal Behavior of Hollow Bricks with Different Cavity Concentration,” *Int. J. Therm. Sci.*, vol. 50, no. 8, pp. 1543–1553, 2011.

[38] J. Diaz, P. Nieto, J. Sierra, and C. Biempica, “Nonlinear Thermal Optimization of

External Light Concrete Multi-Holed Brick Walls by the Finite Element Method," *Int. J. Heat Mass Transf.*, vol. 51, no. 7–8, pp. 1530–1541, 2008.

[39] H. Baig and M. Antar, "Conduction/Natural Convection Analysis of Heat Transfer Across Multi-Layer Building Blocks," in *Proc. 5th European Thermal-Sciences …*, 2008, no. 1982, pp. 1–8.

[40] J. J. Coz, P. J. G. Nieto, F. P. A. Rabanal, and J. D. Hernández, "Non-Linear Thermal Analysis of the Efficiency of Light Concrete Multi-Holed Bricks With Large Recesses by FEM," *Appl. Math. Comput.*, vol. 218, no. 20, pp. 10040–10049, 2012.

[41] J. J. C. Díaz *et al.*, "Non-linear Thermal Analysis of the Efficiency of Light Concrete Big-holed Bricks by FEM," *Am. Inst. Phys.*, vol. 1178, pp. 1–5, 2012.

[42] A. S. Al-tamimi, M. A. Al-osta, and O. S. B. Al-amoudi, "Thermal Simulation for a Wall of Hollow Concrete Brick with Different Insulation Materials and Mortars," in *The International Conference on Water, Informatics, Sustainability, and Environment (iWISE2017), At Carleton University, Ottawa, Canada*, 2017, vol. 8.

[43] J. Li, X. Meng, Y. Gao, W. Mao, T. Luo, and L. Zhang, "Effect of the Insulation Materials Filling on the Thermal Performance of Sintered Hollow Bricks," *Case Stud. Therm. Eng.*, vol. 11, pp. 62–70, 2018.

[44] K. Kant, A. Shukla, and A. Sharma, "Heat Transfer Studies of Building Brick Containing Phase Change Materials," *Sol. Energy*, vol. 155, pp. 1233–1242, 2017.

[45] M. Martínez, N. Huygen, J. Sanders, and S. Atamturktur, "Thermo- Fluid Dynamic Analysis of Concrete Masonry Units via Experimental Testing and Numerical Modeling," *J. Build. Eng.*, vol. 19, no. February, pp. 80–90, 2018.

[46] Z. Hongxia, P. Kang, C. Baoquan, and L. Xuanyi, "Numerical Simulation of Thermal Theory of Sintered Coal Gangue Self-Insulation Block and Wall," in *Conference on Anhui Jianzhu University, Civil Engineering- Anhui Province, China*, 2018, vol. 01021, pp. 1–4.

[47] V. Corinaldesi, J. Donnini, and A. Nardinocchi, "Lightweight Plasters Containing Plastic Waste for Sustainable and Energy-efficient Building," *Constr. Build. Mater.*, vol. 94, pp. 337–345, 2015.

[48] A. S. B. Al-tamimi, "Thermal Insulation of Concrete and Masonry Hollow Concrete Bricks Experimentally and Analytically," King Fahd University of Petroleum & Minerals, KSA, 2017.

[49] S. Abidi, B. Nait-ali, Y. Joliff, and C. Favotto, "Impact of Perlite , Vermiculite and Cement on the Thermal Conductivity of a Plaster Composite Material : Experimental and Numerical Approaches," *Compos. PART B*, vol. 68, pp. 392–400, 2015.

[50] ASTM International, "Standard Specification for Portland Cement," *C 150 – 04*,

Annu. B. ASTM Stand., pp. 1–8, 2004.

[51] J. Smialek, “The Chemistry of Saudi Arabian Sand - A Deposition Problem on Helicopter Turbine Airfoils,” in *Gordon Conference on Corrosion, United States*, 1991, pp. 1–12.

[52] M. Hago, A. W., Al-Jabri, K., Al-Harthy, A., & Qamaruddin, “Development of Lightweight Concrete Blocks for Thermal Insulation,” in *Proc. Brit. Mason. Soc.(UK)*, 2002, vol. 9, pp. 213–216.

[53] B. Vakhshouri and S. Nejadi, “Review on the Mixture Design and Mechanical Properties of the Lightweight Concrete Containing Expanded Polystyrene Beads,” *Aust. J. Struct. Eng.*, vol. 7982, no. July, pp. 1–23, 2017.

[54] M. D. Smoluk, M. D. Smoluk, and R. U. S. A. Data, “(2) Patent Application Publication (10) Pub. No.: US 2015/0140147 A1,” vol. 1, no. 19, 2015.

[55] R. Siddique, J. M. Khatib, and I. K. Guru, “Use of Recycled Plastic in Concrete : A review,” *Waste Manag.*, vol. 28, no. December, pp. 1835–1852, 2007.

[56] J. Carlos, A. Galvão, K. Franke, A. Joukoski, and R. Mendes, “Use of Waste Polymers in Concrete for Repair of Dam Hydraulic Surfaces,” *Constr. Build. Mater.*, vol. 25, pp. 1049–1055, 2011.

[57] A. M. Rashad, “Vermiculite as a Construction Material – A Short Guide for Civil Engineer,” *Constr. Build. Mater.*, vol. 125, pp. 53–62, 2016.

[58] A. Dinesh, I. Padmanaban, and M. Maruthachalam, “Study on Mechanical Properties of Low Density Concrete with Partial Replacement of Coarse Aggregate,” *Int. J. Earth Sci. Eng.*, vol. 09, no. June, pp. 471–475, 2016.

[59] W. M. Aljaaidi, H. M. Almohanna, A. Zaid, and B. Jumah, “Used Tires Recycling and Utilization in Saudi Arabia,” in *Design Project, King Saud University, KSA*, 2014.

[60] Z. K. Khatib and F. M. Bayomy, “Rubberized Portland Cement Concrete,” *J. Mater. Civ. Eng.*, no. August, pp. 206–213, 1999.

[61] “Thermtest Thermophysical Instruments,” *Materials Thermal Properties Database*, 2017. .

[62] I. Topc u and B. Iskdag, “Manufacture of high heat conductivity resistant clay bricks containing perlite,” *Build. Environ.*, vol. 42, pp. 3540–3546, 2007.

[63] “Perlite Lightweight Insulating Concrete Insuperl- INSUPERL LWC,” *Ind. Arab. Vermiculite*.

[64] ASTM International, “Standard Test Methods for Sampling and Testing Concrete Masonry Units and Related Units,” in *C 140 – 03, Annual Book of ASTM Standards*, vol. 04, 2003, pp. 1–11.

[65] ASTM International, “Standard Practice for Calculating Thermal Transmission Properties under Steady-State Conditions,” in *C 1045 – 97, Annual Book of ASTM Standards*, vol. 14, no. June, 2012, pp. 1–13.

[66] Abdul-Mohsen Al-Hammad, M. A. Abdelrahman, W. Grondzik, and A. Hawari, “A Comparison Between Actual and Published K-Values for Saudi Insulation Materials,” *Therm. Insul. BLDG. ENVS.*, vol. 17, pp. 379–385, 1994.

[67] ASTM International, “Standard Specification for Mortar for Unit Masonry,” in *C270–04, Annual Book of ASTM Standards*, 2004, pp. 1–13.

[68] I. Manual, I. To, and P. Terephthalate, “Thermal Conductivity Tests of Liquids Using Fox50 Heat Flow Meter Instrument,” pp. 1–7, 2003.

[69] ASTM International, “Standard Specification for Nonloadbearing Concrete Masonry Units,” in *C 129 – 01, Annual Book of ASTM Standards*, vol. 04, 2015, pp. 1–3.

[70] H. F. Li, M. Q. Chen, B. A. Fu, and B. Liang, “Evaluation on the Thermal and Moisture Diffusion Behavior of Sand / Bentonite,” *Appl. Therm. Eng.*, vol. 151, no. January, pp. 55–65, 2019.

[71] ASTM International, “Standard Specification for Loadbearing Concrete Masonry Units,” in *C 90 – 03, Annual Book of ASTM Standards*, vol. 04, 2002, pp. 1–4.

[72] K. Leet, C. M. Uang, and A. M. Gilbert, *Fundamentals of Structural Analysis*. 2002.

[73] L. Yu, H. Ou, and L. Lee, “Investigation on Pozzolanic Effect of Perlite Powder in Concrete,” *Cem. Concr. Res.*, vol. 33, no. April, pp. 73–76, 2003.

[74] H. Xiao, F. Zhang, R. Liu, R. Zhang, Z. Liu, and H. Liu, “Effects of Pozzolanic and Non-Pozzolanic Nanomaterials on Cement-Based Materials,” *Constr. Build. Mater.*, vol. 213, pp. 1–9, 2019.

[75] N. Zhou, M. D. Levine, and L. Price, “Overview of Current Energy-efficiency Policies in China,” *Energy Policy*, vol. 38, no. 11, pp. 6439–6452, 2010.

[76] J. J. Del Coz Diaz, P. J. Garca Nieto, a. M. Rodriguez, a. L. Martinez-Luengas, and C. B. Biempica, “Non-Linear Thermal Analysis of Light Concrete Hollow Brick Walls by the Finite Element Method and Experimental Validation,” *Appl. Therm. Eng.*, vol. 26, no. 8–9, pp. 777–786, 2006.

[77] S. Whitaker, *Fundamental Principles of Heat Transfer*. 1977.

[78] A. S. Al-Tamimi, M. A. Al-osta, O. S. B. Al-amoudi, and R. Ben-mansour, “Effect of Geometry of Holes on Heat Transfer of Concrete Masonry Bricks Using Numerical Analysis,” *Arab. J. Sci. Eng.*, vol. 42, no. 9, pp. 3733–3749, 2017.

[79] K. H. Solangi *et al.*, “A Comprehensive Review of Thermo-Physical Properties

and Convective Heat Transfer to Nano Fluids," *Energy*, vol. 89, pp. 1065–1086, 2015.

[80] A. Falahat, "Effect of Aspect Ratio on Laminar Natural Convection in Partially Heated Enclosure," *Univers. J. Mech. Eng.*, vol. 2, no. 1, pp. 28–33, 2014.

[81] A. Carozza, "Numerical Study on Mixed Convection in Ventilated Cavities with Different Aspect Ratios," *Fluids*, vol. 3, no. 11, pp. 1–18, 2018.

[82] M. Arici, M. Kan, and H. Karabay, "Effect of Aspect Ratio on Natural Convection in a Cavity with Wavy Walls," *Int. Conf. Comput. Exp. Sci. Eng.*, vol. 128, no. 2, pp. 197–200, 2015.

[83] M. Bhuvaneswari, S. Sivasankaran, and Y. J. Kim, "Effect of Aspect Ratio on Convection in a Porous Enclosure with Partially Active Thermal Walls," *Comput. Math. with Appl.*, vol. 62, no. 10, pp. 3844–3856, 2011.

[84] A. S. Al-Tamimi, M. A. Al-Osta, O. S. B. Al-Amoudi, and R. Ben-mansour, "Thermal Simulation for a Room with Solid and One-way Ribbed Slab Using FEM," vol. 8, pp. 1–10, 2017.

[85] A. Ahmad, M. Maslehuddin, and L. M. Al-hadhrami, "In Situ Measurement of Thermal Transmittance and Thermal Resistance of Hollow Reinforced Precast Concrete Walls," *Energy Build.*, vol. 84, pp. 132–141, 2014.

[86] ASTM International, "Standard Specification for Application of Portland Cement-Based Plaster," *C 926 – 98, Annu. B. ASTM Stand.*, vol. 04.01, pp. 1–10, 1998.

[87] M. U. P. Hafiz M. Abd-ur-Rehman, Fahad A. Al-Sulaiman, Aamir Mehmood, Sehar Shakir, "The Potential of Energy Savings and the Prospects of Cleaner Energy Production by Solar Energy Integration in the Residential Buildings of Saudi Arabia," *J. Clean. Prod.*, pp. 1–23, 2018.

[88] A. Ahmad and L. M. Al-hadhrami, "Thermal Performance and Economic Assessment of Masonry Bricks," *Therm. Sci.*, vol. 13, no. 4, pp. 221–232, 2009.

VITAE

Name		Waleed Ahmed Yaslam Al-Awsh
Nationality		Yemeni
Date of Birth		15 October 1987
Emil		waleed262010@gmail.com
Address		Dhahran, Eastern Province, Saudi Arabia/ Zip code 31261
Education	**M.S**	**(Civil Engineering-Structures)**
		King Fahd University of Petroleum and Minerals
		Dhahran, Saudi Arabia, April 2019
	B.S	**(Civil Engineering-Structures)**
		Hadhramout University of Science and Technology
		Hadhramout, Yemen, November 2012
Publications		Waleed Ahmed Al-Awsh, Ahmed Salem Al-Tamimi, Mohammed Ali Al-Osta, and Omar S. Baghabra Al-Amoudi "Mechanical and Thermal Properties of Perlite and Rubber Insulation Cement Mortar" International Journal of Environment and Sustainability Vol. 7 No. 2, pp. 1-7 (2018)